Structural variations in catalytic and ubiquitin –associated domains of Human protein kinase MARK1 and MARK3

Thesis submitted to the University of Hamburg in partial fulfillment of the requirements for the degree of Ph.D.

Presented by

Chanakya Nugoor

from Hyderabad, India

January, 2008

Hamburg

Genehmigt vom Department Biologie
der Fakultät für Mathematik, Informatik und Naturwissenschaften
an der Universität Hamburg
auf Antrag von Herr Professor Dr. E. MANDELKOW
Weiterer Gutachter der Dissertation:
Herr Priv.-Doz. Dr. H. QUADER
Tag der Disputation: 11. April 2008

Hamburg, den   24. März 2008

Professor Dr. Jörg Ganzhorn
Leiter des Departments Biologie

1 Introduction

1.1 Introduction to kinase superfamily

Protein kinases are the largest family of proteins in the eukaryotic genome. They are of immense interest due to involvement in several diseases and thus targets of drug therapy. A comprehensive study by Manning and co-workers (Manning et al., 2002) has concluded that the human genome contains about 518 kinases. These kinases were classified into groups, families and subfamilies based on the sequence comparison of the catalytic domains, domain structure outside the catalytic domains, known biological function and similar classification in lower organisms (Fig. 1.1).

The major groups are as follows:

AGC group - includes the cyclic-nucleotide-dependent protein kinase families, BARK and ribosomal S6 kinase families,

CAMK group - includes the families of protein kinases regulated by Ca^{2+}/calmodulin, the Snf1/AMPK families and other close relatives,

TK group - largest of the kinase superfamily, consists of conventional protein tyrosine kinases,

CMGC group - includes the CDK, MAPK, GSK3 and CLK protein kinase families,

STE group - includes homologues of Ste7/MAP2K, Ste11/MAP3K and Ste20/MAP4K protein kinases,

CK1 group - includes the CK1, TTBK and VRK protein kinase families,

TKL group - Tyrosine kinase like kinases, includes kinase families that resemble both tyrosine and serine/threonine kinases like MLK, LISK, IRAK and STRK families,

Atypical protein kinases group - have protein kinase activity but lack sequence similarity with other protein kinases.

Figure 1.1: The Human kinome. The MARK kinases encircled in red belong to the branch of the CAMK group and AMPK subfamily. Figure reproduced from http://www.cellsignal.com/reference/kinase (Manning et al., 2002).

1.2 Identification of MARK

Tau is a microtubule associated protein whose major function is to stabilize the microtubules (MT). MTs are the major tracks for cellular transport and form the part of cytoskeleton. A prominent feature in Alzheimer disease is the presence of intracellular neurofibrillary tangles

(NFTs) and extracellular amyloid plaques. NFTs are formed by tau filaments called as Paired Helical Filaments (PHFs),   and the extracellular amyloid plaques are composed of aggregated, fibrillar β-amyloid peptide (Aβ) (Lee et al., 2001). Tau consists of two main domains, an acidic N-terminal 'projection domain' and a C-terminal 'assembly domain' (Gustke et al., 1994). The C–terminal assembly domain consists of microtubule binding region with four repeats of approximately 33 residues that mediate MT binding.

Tau can be phosphorylated by multiple kinases at multiple sites (Fig. 1.2) (Johnson and Stoothoff, 2004). Of the many different phosphorylation sites, phosphorylation of tau at or in KXGS motif (Ser262) results in strong reduction of tau's ability to bind microtubules (Drewes et al., 1997).   Hyperphosphorylated tau can no longer bind to MTs and can aggregate to form PHFs (Mandelkow and Mandelkow, 1998). Hyperphosphorylation at Ser214 or Ser262 are major features of Alzheimer disease (Gustke et al., 1992; Mandelkow et al., 1995; Mandelkow and Mandelkow, 1998).
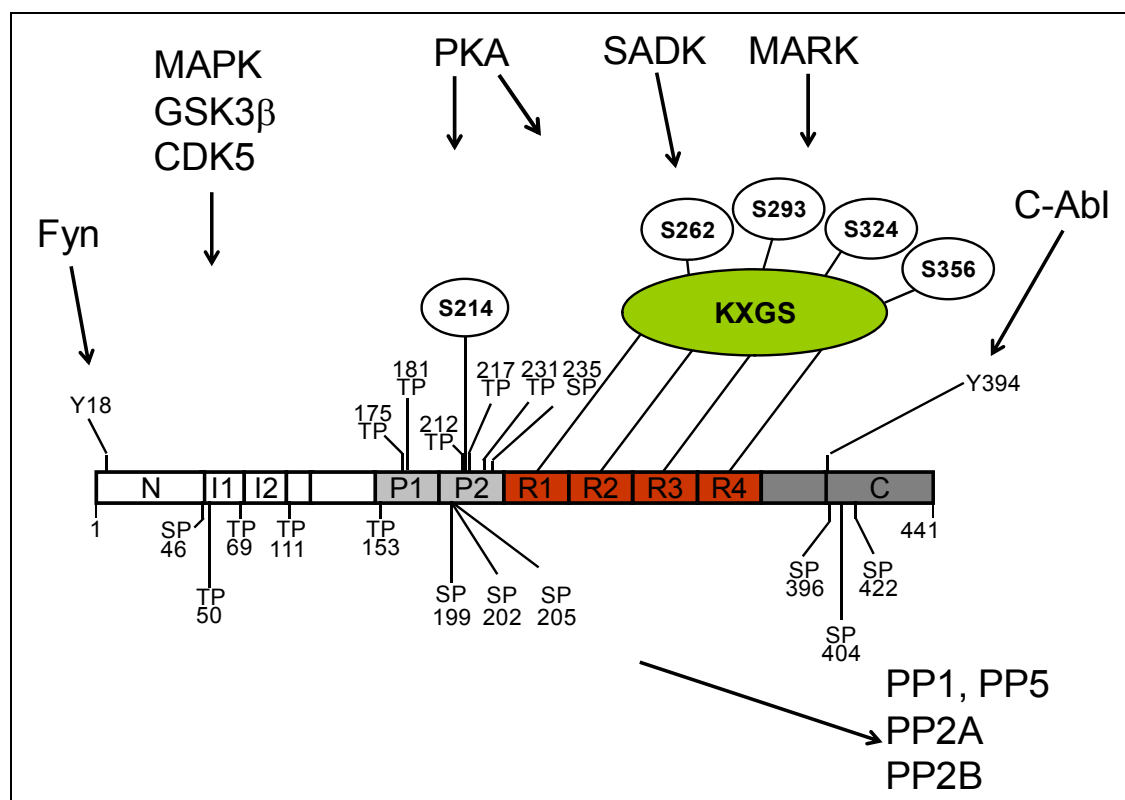
Figure 1.2: Phosphorylation sites of tau. htau40 isoform of full length tau protein is shown with phosphorylation targets of many different kinases. The SP/TP motifs are the main targets for proline directed kinases such as GSK3β, CDK5 and MAPK. S214 and KXGS motifs are targets of non-proline directed kinases such as PKA, MARK and SADK. Tyrosine residues at position 18 and 394 are targets of Src family kinases such as fyn and c-Abl.

A search for kinase responsible for phosphorylation of tau at Ser262 led to discovery of MAP/ Microtubule Affinity Regulating Kinase (MARK) (Drewes et al., 1997).   MARK

kinases are also known as PAR-1 (partitioning-defective) and belong to the family of Ca/calmodulin dependent kinases (Manning et al., 2002). MARK proteins are conserved from yeast to humans are involved in diverse cellular functions and physiological processes such as polarity and cell cycle control (Drewes, 2004; Tassan and Le Goff, 2004). They are also shown to be involved in various physiological process such as metabolism (Hurov and Piwnica-Worms, 2007; Hurov et al., 2007), fertility (Bessone et al., 1999), immune system (Hurov et al., 2001), learning and memory (Segu et al., 2006), intracellular signaling (Elbert et al., 2006; Ossipova et al., 2005) and regulation of microtubule dependent transport (Mandelkow et al., 2004).

PAR-1 was first described in *C.elegans* as one of the six par genes required for the formation of anterior-posterior asymmetry of the nematode embryo (Guo and Kemphues, 1995; Kemphues et al., 1988; Pellettieri and Seydoux, 2002). PAR-1 homologues have been identified and studied in a number of organisms, including yeast, *Drosophila* and mammals (Drewes et al., 1997; Elbert et al., 2005; Shulman et al., 2000; Trinczek et al., 2004). These studies have further implicated the role of PAR-1 in regulating cell polarity, mitogenic signaling and cell cycle control.

In humans, PAR-1 is encoded by four genes, giving rise to four isoforms and several splice variants, namely MARK1 (PAR-1c), MARK2 (PAR-1b/EMK), MARK3 (PAR-1a/P78/C-TAK1) and MARK4 (PAR-1d/MARKL1). As in *C.elegans*, human isoforms are asymmetrically localized in epithelial cells (Bohm et al., 1997). MARK1 and MARK2 are required for polarity of MDCK cells (Bohm et al., 1997; Cohen et al., 2004a; Cohen et al., 2004b) and neurite outgrowth (Biernat et al., 2002). MARK4 is upregulated in glioblastomas and hepatocellular carcinomas thus suggesting a role in tumerogenesis (Beghini et al., 2003; Kato et al., 2001).

The general organization of MARK proteins consists of five domains (Fig. 1.3):

1.   N-terminal header
2.   Catalytic domain
3.   Ubiquitin Associated (UBA) domain
4.   Spacer domain
5.   Tail domain which includes the Kinase Associated 1 (KA 1) domain
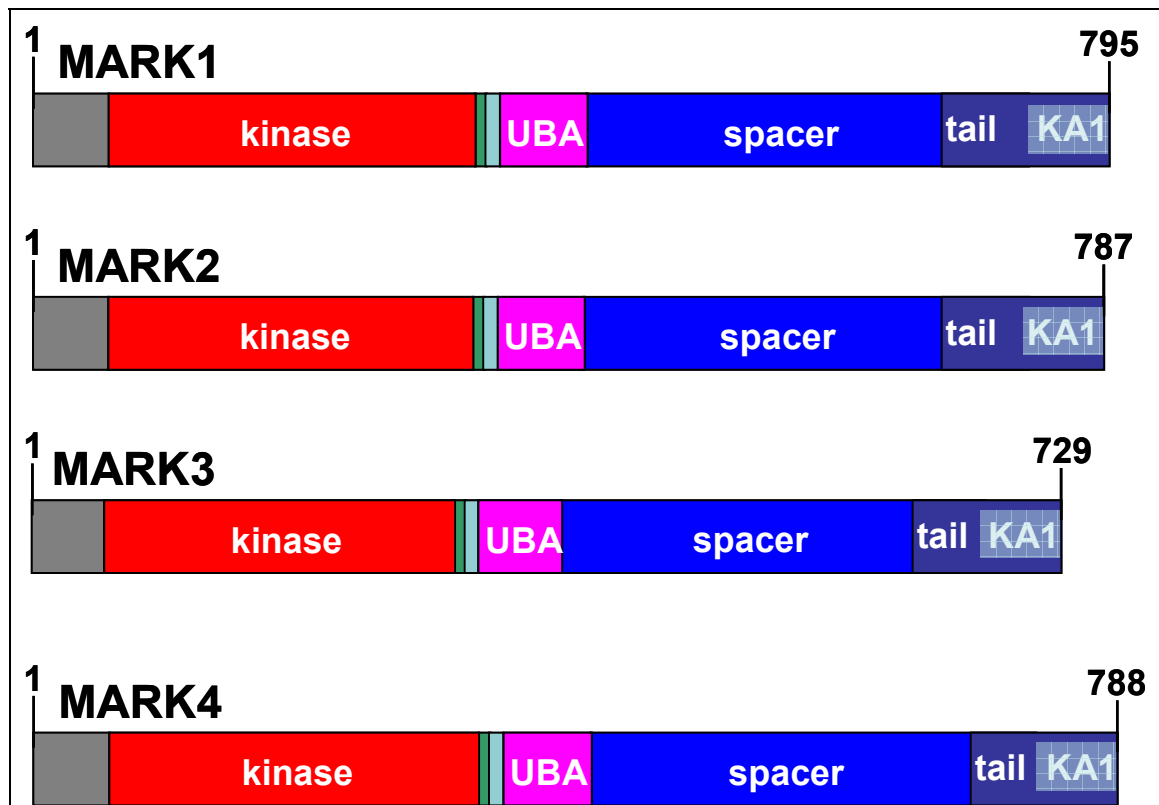
Figure 1.3: Domain organization of MARK kinases. One representative of each isoforms is shown here. All the MARKs have a unique and similar domain arrangement: the N-terminal header, shown in grey consists of variable sequences, the kinase domain consists of typical Serine/Threonine kinase domain architecture shown in red. The UBA domain, the functions of which are largely in speculation are shown in pink. The spacer domain is shown to be required for localization is shown in blue, and the tail domain which includes the KA1 domain colored in navy blue, might help in binding to cytoskeletal proteins.

The N-terminal header consists of 40-50 residues, the sequences of which are diverse and with no known function. Adjacent to the header is a conserved kinase domain consisting of Ser/Thr kinase domain architecture. The kinase has two characteristic lobes. The N-terminal lobe is mostly made of β-sheets and contains a lysine residue and a P-loop which aids in coordinating the ATP. The C-terminal lobe is more alpha helical. The central part of the catalytic domain contains a conserved aspartic acid residue which is important for the catalytic activity of the enzyme. The activation segment contains the activation loop and has Thr and Ser residues which can be phosphorylated by the up-stream kinases thereby activating or inactivating the kinase (Thr208 and Ser212 in MARK2 (Kosuga et al., 2005; Timm et al., 2003)).

The UBA domain consists of approximately 45 residues found in proteins involved in ubiquitin proteasome pathway (Chen and Madura, 2002). The UBA domains are

characterized as polypeptides binding to mono- and poly-ubiquitin (Raasi et al., 2005; Varadan et al., 2005). A study on 30 yeast and mammalian UBA domain containing proteins indicated that 30% of them do not bind mono- or poly-ubiquitin (Raasi et al., 2005). The sequence comparison of UBA domains which bind or do not bind ubiquitin did not show any significant differences in their primary sequence. According to a classification by Raasi and co workers (Raasi et al., 2005), the UBA domains of MARK belong to the class which does not bind to ubiquitin. It has been shown that the UBA domains of the AMPK family do not bind to ubiquitin (Jaleel et al., 2006). A recent NMR characterization of the MARK3 UBA domain has demonstrated that the isolated UBA domain is unfolded and binds to ubiquitin with extremely low affinity (Murphy et al., 2007).

The spacer domain next to the UBA domain consists of about 300 residues and is predicted to contain little secondary structure. This domain is shown to be required for the localization of PAR-1 in polarizing follicular epithelial cells (Vaccari et al., 2005). The spacer domain contains conserved a threonine residue (Thr595 in MARK2) which is phosphorylatd by atypical PKC and negatively regulates MARK activity (Chen et al., 2006; Hurov et al., 2004).

The tail domain is the last part of the kinase which includes the Kinase Associated domain 1 (KA1). The KA1 domain consists of about 100 residues at the C-terminus of the kinase domain ending with the characteristic ELKL motif (Espinosa and Navarro, 1998). The KA1 domain is also found in other kinases like MELK (Maternal Embryonic Leucine Zipper kinase), pEg3 and Snf1-related kinase (Tochio et al., 2006). The function of the KA1 domain is not known. In *C.elegans* PAR-1, it was reported that a region in the KA1 domain interacts with non-muscle myosin II heavy chain (Guo and Kemphues, 1996). In *Saccharomyces cerevisiae*, this region acts as autoinhibitory domain (Elbert et al., 2005). In case of human MARK3, the KA1 domain is shown to be required for membrane localization (Goransson et al., 2006). The structure of the KA1 domain of MARK3 was elucidated using NMR techniques (Tochio et al., 2006). The NMR structure shows that the KA1 domain has an α + β sandwich fold with a characteristic concave surface formed by hydrophobic and positively charged residues. This surface is predicted as possible binding site to cytoskeletal proteins.

1.3 Substrates of MARK

MARK has several substrates and is involved in many different cellular functions. One of the main functions of MARK is to regulate cell polarity of various cell types. MARK regulates

polarity through the conserved polarity cassette consisting of PAR-3, PAR-6 and atypical Protein Kinase C (PKC) (Ohno, 2001). In hippocampal neuronal cells, MARK functions downstream of the polarity complex, augmenting axon formation (Chen et al., 2006) and inhibiting the dendrite formation (Terabayashi et al., 2007) by phosphorylating tau. Similarly in N2a cells, MARK effects neurite outgrowth and polarity (Biernat et al., 2002).

MARK phosphorylates MAP2 and MAP4 similar to tau in their KXGS motifs leading to loss of microtubule binding and disassembly of microtubules (Bessone et al., 1999; Drewes et al., 1997; Illenberger et al., 1998).

MARK associates with dishevelled to regulate both the canonical and non-canonical branches of wnt signaling pathway (Ossipova et al., 2005; Sun et al., 2001).

In MDCK cells, MARK regulates cell to cell adhesion by phosphorylating dishevelled through wnt signaling pathway (Elbert et al., 2006).

Several substrates are phosphorylated by MARK to generate 14-3-3 binding sites. MARK phosphorylates Cdc25C which results in inactive Cdc25C that is excluded from the nucleus to bind 14-3-3 (Peng et al., 1998) and thereby acts as G2/M checkpoint in cell cycle (Bachmann et al., 2006). Similarly, MARK phosphorylates Kinase Suppressor of Ras 1 (KSR1) involved in ras signaling (Muller et al., 2001) and plakophilin 2 (PKP) (Muller et al., 2003) leading to 14-3-3 binding.

MARK phosphorylates other proteins like doublecortin which is essential for microtubule dynamics in growth cones of neurons (Schaar et al., 2004), exuperantia regulating bicoid mRNA localization (Riechmann and Ephrussi, 2004) and Rab11-FIP (Bjorbaek and Kahn, 2004).

Class IIa histone deacetylases (HDACs) are the new substrates phosphorylated at the N-terminal region by MARK to regulate their localization (Dequiedt et al., 2006).

1.4 Regulation of MARK

MARK kinases are regulated by various methods, the most prominent being phosphorylation (Fig. 1.4).

  1. Phosphorylation of the activation loop threonine by LKB1 (Lizcano et al., 2004) or
  MARKK (Timm et al., 2003) leads to activation of MARK. Phosphorylation of the serine
  downstream to the phosphorylable threonine is probably inhibitory as judged by the
  mutational analysis (Timm et al., 2003). However, a study by Kosuga and co-workers

(Kosuga et al., 2005) claims that phosphorylation of this serine leads to activation of the kinase. Thus the exact function and role of this residue is still not well understood.

2. Phosphorylation at several residues near the P-loop and helix C region of MARK3 by Pim-1 is shown to be inhibitory (Bachmann et al., 2004). The residues phosphorylated by Pim-1 are not concluded from this study since MARK was phosphorylated both at the kinase and the spacer domain region at several residues. Similarly, it was recently shown for the case of MARK2 that phosphorylation of similar residues by CamKI kinase also leads to inhibition of the kinase activity. A new phosphorylation site Thr294 near the CD domain was found in the MARK, but it was not clearly demonstrated what was the effect of phosphorylation of this residue (Uboha et al., 2007).

3. Spatial localization represents one of the methods of regulating a protein. This occurs in MARK mainly through the spacer domain by two methods. Phosphorylation in the spacer domain by atypical PKC (Suzuki et al., 2004) not only leads to inhibition of MARK kinase activity but also to a change in the localization from plasma membrane to
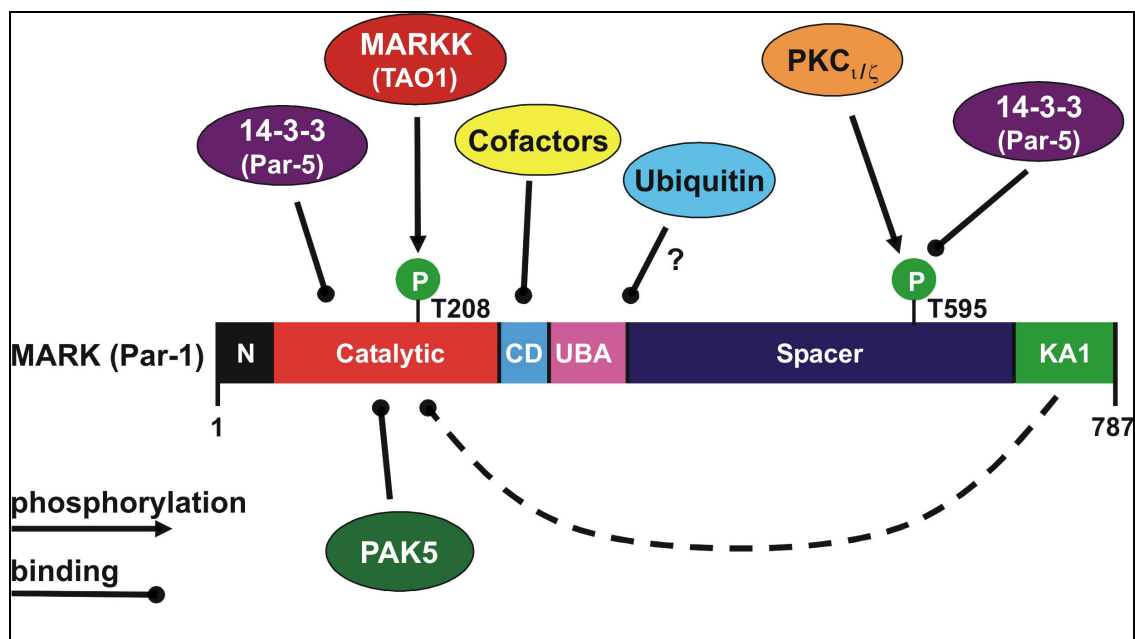
Figure 1.4: Different modes of regulation of MARK. Activation via phosphorylation by MARKK or LKB1 at the activation loop (red). Possible regulation by interaction of the UBA domain with ubiquitin (aqua) and regulation by interaction of the CD motif with a cofactor, in analogy with MAP kinases where upstream or downstream kinases can be bound (yellow). Localization by interaction of the catalytic domain with the 14-3-3 (purple). Localization and inhibition by interaction of the spacer domain with 14-3-3, after phosphorylation by aPKC (orange). Auto inhibition by interaction between the C-terminal tail and the N-terminal header or catalytic domain (dotted line). Inhibition by binding of PAK5 to the catalytic domain (green). (Figure reproduced from Timm et al., 2006).

cytoplasm (Hurov et al., 2004). In the same line, deletion of the spacer domain leads to mislocalization of PAR-1 (Vaccari et al., 2005).

4. The exact role of the UBA domain in MARK is not well understood. However, a study on the UBA domains of the AMPK family by Jaleel and co workers (Jaleel et al., 2006) has concluded that the UBA domain is required for the activation of the kinase. Other studies have shown a role of the UBA domain in dimerization (Bertolaet et al., 2001a) and proteasome degradation of the target protein it binds (Bertolaet et al., 2001b).

5. Other ways of regulation include an interaction between catalytic domain of MARK and 14-3-3 (Angrand et al., 2006; Benton et al., 2002; Brajenovic et al., 2004; Goransson et al., 2006). MARK phosphorylates several substrates to generate 14-3-3 binding sites and it can also bind 14-3-3 proteins.

6. The N- and C-terminal regions are shown to be interacting in the case of yeast homologue of PAR-1, leading to autoinhibition (Elbert et al., 2005).

7. Inhibition of MARK by direct binding of the kinase domains of MARK and PAK5 was demonstrated from our lab (Matenia et al., 2005; Timm et al., 2006). This binding is does not involve any phosphorylation of MARK and does not affect the activity of PAK5, a kinase targeting the actin cytoskeleton.

1.5 Structure of MARK2

1.5.1 Structure of the catalytic domain

Structure of MARK2 was determined in our lab using X-ray crystallography (Panneerselvam et al., 2006). The structures of wild type and two mutants had shown that the MARK2 kinase domain possesses a bi-lobe structure like most protein kinases. The smaller, N-terminal lobe mainly consists of five β-strands and a long α-helix whereas the large, C-terminal lobe mainly consists of helices.

The activation segment (Asp193-Cys210) was mostly disordered, thus the important DFG motif and other parts important of the activation segment were invisible. Only in the case of the Thr208/Ser212Ala mutant, five residues of the C-terminus of the activation loop (Leu206-Cys210) were visible. The activation loop along with the P+1 loop is thought to recognize the substrate by specific interaction with the residue following the phosphorylation site. The conformation of the structured parts of the activation segment indicates that it folds away from the helix C, opposite to the direction found in most active kinases and thus the MARK2 kinase structure represents an open and inactive conformation.

1.5.2 UBA domain

The UBA domain is a small, globular domain that consists of three short helices (α1-α3). Helices α1 and α3 are roughly antiparallel (folding in a form of a "U"). This conformation was non-canonical since the helices of UBA domains of HHR23A, a representative for the UBA domains, show α1 and α3 helices almost parallel to each other (as in an "N") (Mueller and Feigon, 2002) (Fig. 1.5). The UBA domain of MARK2 binds to the N-lobe of the catalytic domain at the distal side. The interaction is predominantly hydrophobic and mainly due to helix α3 and involves residues Tyr351, Met335, Ala356, Leu359, Leu360, and Leu361 of the UBA domain and residues Leu115, Phe116 at the beginning of β4 in the catalytic domain. The UBA domain contains three leucines near the end of α3 (Leu359-Leu361). Leu359 is highly conserved and is important for the internal cohesion of the UBA domain by fitting into a hydrophobic pocket formed by residues of α1-α2 and the MGF/Y motif.
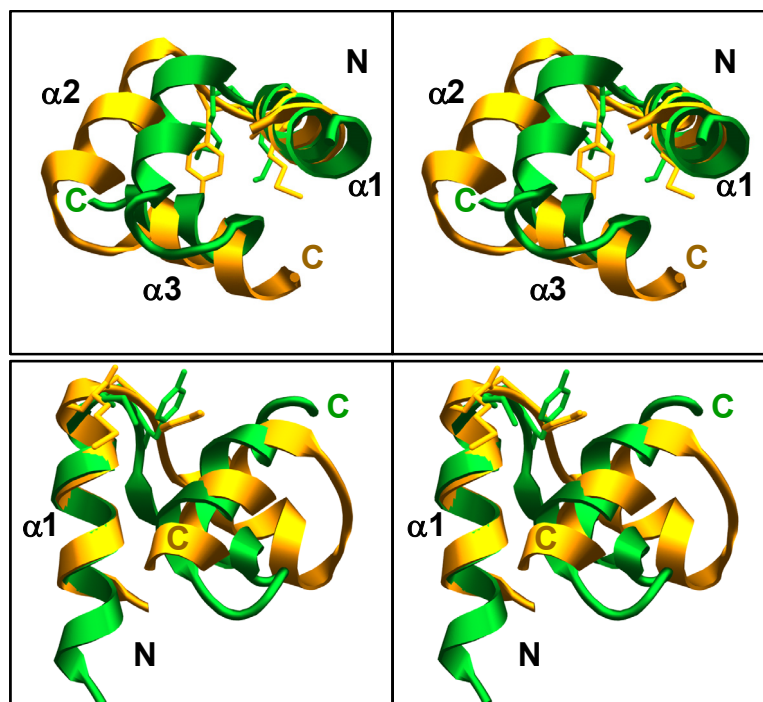
Figure 1.5: Overlay of the MARK2 UBA domain with UBA of HHR23A (stereo view). The MARK2 UBA domain (yellow) is overlaid with UBA of HHR23A (green; PDB-ID: 1IFY; (Mueller and Feigon, 2002)) after least-squares superposition of 9 residues in helix α1. Residues M335 and Y337 of the MGY motif are shown in stick model representation., The peptide chains at the end of helix α2 bend in different directions, in such a way that helix α3 ends up at almost the same position but with reversed orientation (Panneerselvam et al., 2006).

1.5.3 UBA linker and common docking domain

The UBA domain is linked to the catalytic domain by approximately 20 residues. The first half contains a motif similar to the "common docking" motif (CD) of MAP kinases, characterized by a cluster of negative surface charges (DxxD/E, (Tanoue et al., 2000). The motif EDDE and surrounding residues folds into a loop which is similar to the CD domain of MAP kinases (Fig.1.6) (Panneerselvam et al., 2006). The ED site (residues Ala185-Asp186) at the $\beta7$-$\beta8$ turn along with the CD domain seems to form a docking groove on the back surface of the catalytic domain opposite to the active site (Tanoue and Nishida, 2003). The presence of these features in MARK2 (Fig. 1.6) suggests a similar function, but the putative docking partners of MARK are not known.
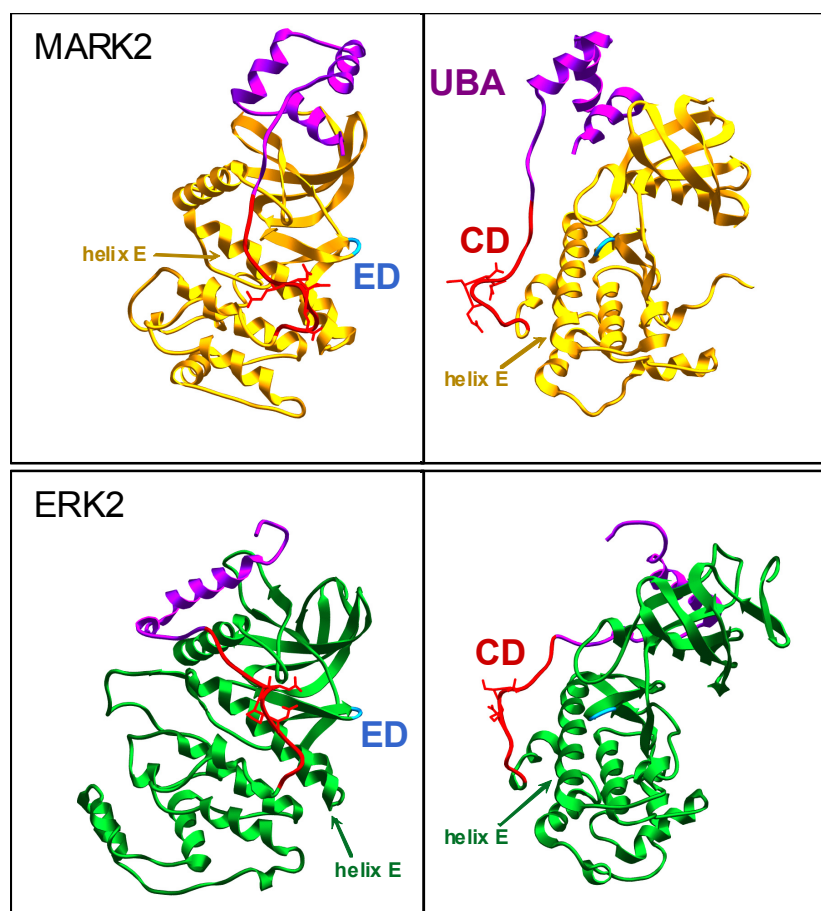
Figure 1.6: Common docking domain and ED site of MAP kinases compared to MARK2. The structures of MARK2 and ERK2 are shown in the same orientations after least-squares superposition of helix E to the catalytic loop. The common docking domain (CD, in red) is C-terminal to the kinase domain and corresponds in MARK to the first half of the tether connecting the kinase domain to the UBA domain (residues ~305-315). The C-terminal extensions following the CD domain (linker and UBA domain in MARK2) are shown in purple. Characteristic for the CD domain is a cluster of negatively charged residues exposed to the surface, located in a bulge at the end of the catalytic domain (stick model representation) (Panneerselvam et al., 2006).

The second half of the stretch tethering the UBA and catalytic domain ("linker", residues 315-322) assumes an extended conformation and has less contact to the lobes of the catalytic domain. The loose attachment suggested the possibility that the linker and the UBA domain could swing away from the catalytic domain and alter the regulatory state of the domains.

1.5.4 Disulphide bridge and dimerization

One of the important features of the MARK2 structure was that the two molecules of the MARK2 structure were covalently linked by a disulfide bridge and these molecules of the asymmetric unit (A and B), interact through multiple contacts and form a dimer with proper two-fold non-crystallographic symmetry (NCS) (Fig. 1.7). The catalytic domains in a dimer face each other with their active sites. The dimer interactions between the monomers are concentrated in three zones. Zone 1 in the C-lobe and zone 3 in the N-lobe of one molecule form a wide-open entrance to the catalytic cleft. Helix G of the other molecule (zone 2) plugs into the cleft formed by zone 1 and 2 making contacts with the rims.
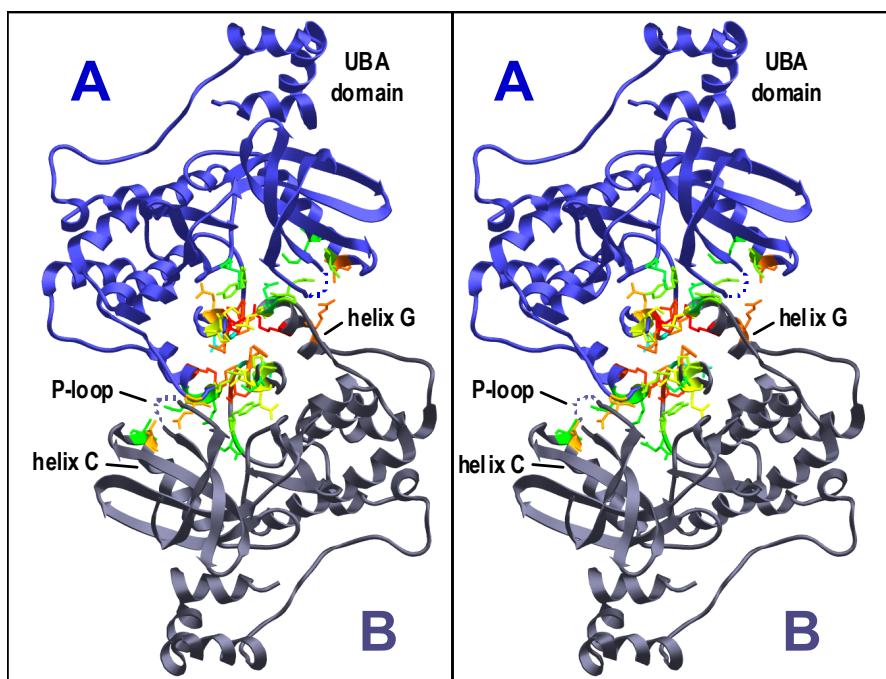
Figure 1.7: Intermolecular contacts in MARK2 dimers (stereo view). Ribbon diagrams of the double mutant dimer viewed along the non-crystallographic two-fold symmetry axis. Residues involved in intermolecular contacts are in stick model representation. The cysteines form an interchain disulfide bridge. Contact zones consists of zone 1 comprising 15 contact residues in the range from D207 to D227, zone 2 all but one residue in the range D251-R261. Residues S92, S93, and K96 at the N-terminus of helix C form another cluster of contact residues (zone 3). Helix G and the preceding loop (zone 2) in one molecule insert into the space between zones 1 and 3 of the other molecule (Panneerselvam et al., 2006).

1.6 Aim of the work

MARK is an important kinase phosphorylating tau and other MAPs in their KXGS motifs. One of the prominent features of tau in Alzheimer disease is the phosphorylation of Ser262 by MARK (Mandelkow and Mandelkow, 1998). This phosphorylation detaches tau from the microtubule which then aggregates into PHFs. One way to inhibit such pathological phosphorylation is through inhibition of MARK. This is possible through structure based drug design of specific inhibitors of MARK, thus it is important to determine the structure of MARK.

In gastric cells, disruption of MARK activities by *Helicobactor pylori* leads to junctional and polarity defects and adenocarcinoma (Saadat et al., 2007). Recently, involvement of MARK kinases in type 2 diabetes has been demonstrated (Hurov and Piwnica-Worms, 2007; Hurov et al., 2007). MARK is one of the downstream targets of the LKB1, which is inactivated in the case of cancer-prone Peutz-Jeghers Syndrome (de Leng et al., 2007; Jenne et al., 1998). Considering the fact that the MARK is involved in several pathways, it would be interesting to know the structure of MARK and its associated domains involved in interactions.

MARK consists of four isoforms and several different splice variants. It has been clearly shown that some of the isoforms of MARK function in diverse roles such as regulating polarity, cell signaling, regulation of metabolism and cell cycle etc. How this functional diversity is achieved is not known. Thus it is important to determine the structure of different isoforms of MARK to understand their functional specificity.

Many members of the AMPK family of kinases have the UBA domains adjacent to the kinase domain (Jaleel et al., 2006). Crystal structures of MARK2 constructs which consisted of the catalytic domain and the UBA domain showed that the UBA domain was made of three helices and strongly interacted with the N-terminal lobe of the kinase by strong hydrophobic interaction through several residues. As a result, the last helix of the UBA domain was inverted compared to the structures of conventional UBA domains. On the contrary, a study by Jaleel and co-workers (Jaleel et al., 2006) had concluded through low resolution small angle scattering studies that in solution, the MARK UBA domain was binding at the C-lobe of the kinase domain and this position of the UBA domain was shown to be enhancing the kinase activity. The position of UBA domain concluded from this study was diametrically opposite to what is present in the MARK2 crystal structure.

Thus, the aim of the project was

1. To crystallize different isoforms of MARK kinases.

2. To crystallize MARK proteins in both active and inactive conformations.

3. To compare the conformation of MARK UBA observed in the crystal structure with that of the solution state.

4. To test whether the unusual conformation of the MARK UBA domain, is also present in the UBA domains of other isoforms.

5. To determine the position and role of UBA domain in MARK kinases.

6. To determine the possible role of the dimerization of the kinase, as observed in the crystal structure.

2 Materials and methods

2.1 Materials

2.1.1 Chemicals

All chemicals used were of the highest purity available (ACS grade) and were purchased

from the following companies:

Amersham Pharmacia Biotech (GE Health Care Europe, Freiburg, Germany)

AppliChem (Darmstadt, Germany)

Fluka (Taufkirchen, Germany)

Merck (Beeston Nottingham, United Kingdom)

New England Biolabs (Frankfurt, Germany)

Qiagen (Hilden, Germany)

Sigma (Taufkirchen, Germany)

Novagen (Beeston Nottingham, United Kingdom)

In addition, the chemicals for crystallization were purchased from the following companies
as pre-formulated screens or separate reagents:

Hampton Research (Aliso Viejo, CA, USA)

Jena Biosciences (Jena, Germany)

Molecular Dimensions (Cambridgeshire, United Kingdom)

Qiagen (Hilden, Germany)

Sigma (Munich, Germany)

2.1.2 Enzymes

All restriction enzymes used for DNA engineering and the T4 DNA ligases were purchased

from **New England Biolabs**, United States Biochemical and Stratagene.

2.1.3 Cloning vectors

Most cloning fragments used in this study were amplified through PCR and cloned initially into the Topo Zero Blunt vector of Invitrogen and then recloned into the final destination or expression vector (pET or pGEX) (Table 2.1).

Vector	Expression System	Features
pTopo Zero Blunt	Used for cloning of PCR fragments	KanR
pET16b	*E. coli*	AmpR, N-terminal His 9 tag
pGEX	*E. coli*	AmpR, N-terminal GST tag

Table 2.1: Summary of the vectors used in this study.

2.1.4 Expression vectors

The expression vectors used in this study for the high-yield expression of recombinant proteins carry cloned inserts under the control of the T7 promoter. Thus, only *E. coli* strains engineered to express the T7 RNA polymerase upon arabinose induction can be used for expression, e.g. BL21 (AI) which has an arabinose inducible (araBAD promoter) (Table 2.2).

Bacterial strains

Strain	Genotype	Features
XL2-Blue	recA1 endA1 gyrA96 thi-1 hsdR17 supE44 ReIA1 lac[F' proAB laclqZΔM15 Tn10 (Tetr) Amy Camr]α	Host for cloning and plasmid propagation (Stratagene).
DH5α Library Efficiency	F-φ80lacZ ΔM15 Δ(lacZYA-argF)U169 recA1endA1 hsdR17 (rkmk+)phoA supE44 thi-1gyr A96 relA1 λ	Host for cloning and propagation of Topo (Invitrogen) and pET (Novagen) vectors.
BL21-AI	F- ompT hsdS(rB -, mB-) dcm araB:T7RNAP-tetA	The T7 RNA polymerase gene is contained in the araB locus of the araBAD operon, allowing the regulation of the expression of the T7 RNA polymerase by L-arabinose (Invitrogen).

TOP10	F- mcrA Δ(mrr-hsdRMS-mcrBC) Φ80lacZΔM15 ΔlacX74 recA1 araD139Δ(ara-leu)7697 galU galK rpsL (StrR) endA1 nupG	Host for cloning and propagation of Topo (Invitrogen) and pET (Novagen) vectors.

Table 2.2: Cell strains and feature list. XL2-Blue and TOP10 cells were used as cloning hosts. BL21 AI (Studier and Moffatt, 1986) was used for protein expression.

2.1.5 Media

Antibiotics: All antibiotic solutions were dissolved either in water or ethanol depending on the solubility of the corresponding antibiotic. The water soluble antibiotics were sterilized by filtering through a 0.22 µM sterile filter. The stock solutions were prepared with the following concentrations: Ampicillin-15 mg/ml in ddH2O, Kanamycin-25 mg/ml in ddH2O, Chloramphenicol-34 mg/ml in ethanol and Carbenicillin-15 mg/ml in ddH2O.

Luria-Bertani (LB) medium: 1% (w/v) bacto-tryptone, 0.5% (w/v) bacto-yeast extract, 1% (w/v) NaCl; sterilized by autoclaving, purchased from Life Technologies as dried powder.

LB agar plates: LB medium and 1.5 % (w/v) bacteriological agar, sterilized by autoclaving. Plates were poured when the temperature dropped to 50°C.

SOB medium: 2% (w/v) bacto-tryptone, 0.5% (w/v) bacto-yeast extract, 0.5 % (w/v) NaCl. A solution of KCl was added to a final concentration of 25 mM. The pH was adjusted to 7 with NaOH and the solution sterilized by autoclaving. Before use a sterile solution of MgCl2 was added to a final concentration of 0.1 M.

SOC medium: SOB medium supplemented with 1.8 % glucose.

2.2 Crystallization

2.2.1 Crystallization supplies and tools

Crystallization supplies and tools including crystallization plates, siliconised cover slides (round and square slides of different thickness), sealing tape, forceps and tools for crystal manipulation were purchased from Hampton Research or Jena Biosciences.

2.2.2 Crystallization solutions

Crystallization screens purchased from Hampton Research:

Crystal screen 1	**Additive screen 1**
Crystal screen 2	**Additive screen 2**
PEG/Ion screen	**Additive screen 3**
Grid screen Na-Malonate	**Crystal screen Index**
Grid screen PEG6000	**Grid screen Ammonium sulfate**
SaltRx screen	**Crystal screen Lite**

Crystallization screens purchased from Jena Biosciences:

JB High throughput Screen I and II

Crystallization Additive Screen were purchased from Sigma

2.2.3 Equipment and accessories

Centrifuges:

Cold centrifuge J2-21 M/E	Beckman (Krefeld, Germany)
Ultracentrifuge	Beckman
Table centrifuge 5402	Eppendorf (Hamburg, Germany)

Rotors:

JA-10, JA-20 Beckman

45Ti   Beckman

2.2.4 Äkta purification system and corresponding accessories

Mono-S column HR10/10	Pharmacia
HiLoadTM 16/60	Pharmacia
SuperdexTM 200	Pharmacia
Ni-NTA Superflow	Sigma
Sample loops 1ml, 2ml, 50ml	Pharmacia

2.2.5 Other equipments and accessories:

French press cell	Amnico
Gel dryer model 583	Bio-Rad (Munich, Germany)
Incubator shaker model Innova 4330	New Brunswick Scientific

	(Nurtingen, Germany)
UV/visible spectrophotometer	Pharmacia
Dynamic light scattering	Dierks and Partner
	(Hamburg, Germany)
Scintillation counter	Tricarb 1900 CA, Packard
Gel documentation system	Bio-Rad (Munich, Germany)

2.3 Molecular biology and microbiological methods

2.3.1 Culture and storage of E. coli

Bacteria cells were grown on LB agar plates or in liquid LB medium at 37°C unless stated otherwise. For positive selection, media and plates were supplemented with the appropriate antibiotics in the following concentrations: 50 μg/ml ampicillin, 50 μg/ml carbenicillin, 25 μg/ml kanamycin. All media and manipulation tools were sterilized by autoclaving, or if heat-labile, by filtration through a 0.22 μm filter. For permanent storage at -80°C, cell strains were flash-frozen in liquid nitrogen after mixing with glycerol for cryoprotection. BL21 and XL2 blue strains were preserved in 30% (v/v) glycerol in LB.

2.3.2 Transformation of E. coli strains

E. coli cells competent for transformation were either purchased from the commercial companies or prepared in the laboratory. XL2-Blue, and BL21 AI cells were transformed by the heat-shock method: 20-100 ng of DNA was added to an aliquot of competent cells (~20-50 μl) previously thawed on ice for approximately 10 minutes. The mixture of DNA and competent cells was incubated on ice for 2 minutes. After the heat-shock at 42°C for 30 seconds, 200-400 μl of SOC medium was added and the cells were incubated at 37°C for 1 hour with shaking. Finally, 100-200 μl cells were plated on a selective medium plate and incubated overnight at 37°C.

2.3.3 Isolation of plasmid DNA

All plasmid mini-preparations were carried out with the Invisorb Spin Plasmid Mini Kit (Invitek) following the user manual. All midi-preparations were carried out with the Nucleobond AX Kit (Macherey-Nagel) according to the manual.

2.3.4 Determination of DNA concentration and purity

The concentration and the degree of purity of double stranded plasmid DNA was determined based on the Beer-Lambert Law by measuring the absorbance at 260 nm and 280 nm:

$$A_{260} = \varepsilon_{260} \text{ x c x } l \text{ and } A_{260} \text{ x 50} = \mu g/ml \text{ (when } l = 1 \text{ cm)}$$

A260 is the absorbance at 260 nm, ε_{260} is the molar absorption coefficient, c is the molar concentration and l is the optical path. For a protein-free and RNA-free solution of DNA the ratio of A_{260}/A_{280} should be close to 2. Protein contaminants would decrease this ratio, whereas RNA contamination would increase it.

2.3.5 DNA agarose gel electrophoresis and staining:

DNA Marker (Smart Ladder, Eurogentec) and DNA samples with loading buffer were applied to 0.8-1% agarose gel (according to the size of the DNA fragment). The electrophoresis was performed horizontally in Tris-acetate (TAE) buffer (40 mM Tris-acetate, 1mM EDTA, pH 8.0) at 100 mA for 30-90 minutes. After electrophoresis, the agarose gel was stained in ethidiumbromide solution (4 $\mu g/ml$ in H2O) for 15 minutes, then destained in H2O for 10 minutes. Photos of DNA bands were taken with the gel documentation system.

2.3.6 Isolation of DNA fragments from agarose gels:

Correct DNA fragments were excised under a UV light and DNA fragments were extracted with UltraClean 15 DNA Purification Kit (MO BIO Laboratories Inc.) according to the manufacturer's instruction.

2.3.7 Screening for a positive clone:

LB-medium dishes were incubated at 37°C for 16-20 hours. 5-10 single colonies were picked and incubated overnight separately in 5ml LB medium containing selective antibiotic. Mini plasmid DNA preparation was done according to the manufacturer's instructions (Invitek). Analysis of the clones was carried out by restriction endonuclease digestion and DNA sequencing. One positive clone was inoculated to 50ml LB medium containing selective antibiotic, and cultured at 37°C and 200 rpm overnight. Midi plasmid DNA preparation was done according to the manufacturer's instructions with the Nucleobond plasmid kit

2.3.8 Ligation reaction

The components below were mixed in a 500µl Eppendorf tube. The mix was incubated at 16°C overnight. The molar ratio between the digested vector and the digested insert was around 1:5.

10x Buffer	1µl
Quick ligase (5U/µl)	1µl
Digested vector	200 ng

    Digested insert   200 ng

    Total volume   10 µl

2.3.9 Restriction digestion of DNA

DNA samples were analyzed with the use of restriction digestion enzymes (New England Biolabs). In each case the sample was mixed with the desired restriction enzyme (s) and the proper reaction buffer (New England Biolabs) in a final volume of 10 µl. The mixture was incubated for 60 min at 37°C. The digested DNA was loaded immediately onto an agarose gel to check the result of the restriction digestion analysis.

2.3.10 DNA sequencing

DNA sequencing reactions were performed to confirm the sequence of a construct and/or the existence of mutations, especially after PCR amplification steps. The reactions were performed using fluorescent dye labeling and the Sanger Method (Sanger et al., 1977) in a Robocycler Gradient 96 PCR machine. The protocol for the temperature cycle reaction was:

    Terminator ready reaction mix   8 µl

    dsDNA   0.5 -1 µg

    Primer (5pmol/ µl)   2 µl

    ddH2O to a final volume of   20 µl

    The PCR program for sequencing was
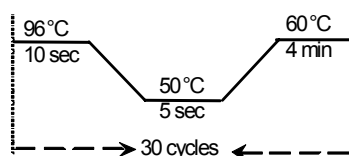
After the reaction, the DNA was precipitated by using the ethanol precipitation method. To the 20 µl reaction mixture, 80 µl of 100 % ethanol was added and the contents were mixed by vortexing, centrifuged at 13 krpm for 30 min at RT. The DNA pellet was then air dried and resuspended in 80 µl of HPLC-grade dd H2O.

30-40 µl was injected to the DNA ABI PRISM 310 Genetic Analyzer (PE Applied Biosystems) sequencer machine to sequence the DNA. The sequencing results were copied and analyzed with the Vector NTI software (Informax).

2.3.11 Mutagenesis of DNA

All mutations, deletions and additions were created by site-directed mutagenesis, which was performed using the Quick Change Site-Directed Mutagenesis kit (Stratagene) according to the manufacturer's protocol. The method utilizes the *Pfu* ultra high fidelity polymerase to replicate the parental plasmid by using two synthetic oligonucleotide primers containing the desired mutation. The primers were designed as follows

Forward primer (variable length, depends on amount of % GC content)

5'- coding sequence -mutation site- coding sequence -3'

Reverse primer (variable length, depends on amount of % CG content)

3'- coding sequence -mutation site- coding sequence -5'

The primers, each complementary to opposite strands of the vector, are extended during temperature cycling by the DNA polymerase. Temperature cycling generates copies of the plasmid by linear amplification, incorporating the mutation of interest. The cycling reaction was performed as follows:

Contents of the reaction:

10x Pfu Ultra high fidelity buffer	2 μl
ds DNA template (25ng/ μl)	5 μl
dNTPs (2.5 mM)	2 μl
Primer 1 (0.5 pmoles/μl)	1 μl
Primer 2 (0.5 pmoles/μl)	1 μl
Pfu polymerase (2.5 U/μl)	0,5 μl
ddH2O to a final volume of	20 μl

The mixture was temperature cycled using the program as:
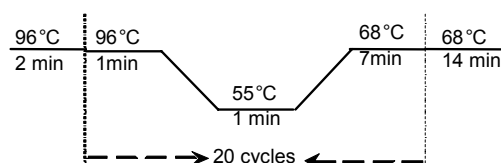
The primer annealing temperature was calculated according to the melting temperature (Tm) of the primers and the extension time was calculated according to the length of the plasmid. Next, a treatment with dpnI endonuclease was carried out to digest the parental methylated

DNA template, allowing the selection of the newly synthesized DNA containing the mutation (Fig. 2.1). 2-4 μl of this reaction mixture was used to transform XL2-Blue cells. Alternatively, some of the mutants were created by cutting and ligating the mutated DNA fragment from existing full length mutant clones.

Figure 2.1: Site directed mutagenesis. The principle of site-directed mutagenesis is that a mismatched oligonucleotide is extended, incorporating the "mutation" into a strand of DNA that can be cloned. The parental molecule is copied as a mutated version by a polymerase chain reaction. The parent molecule is then digested using the dpn I enzyme since it is methylated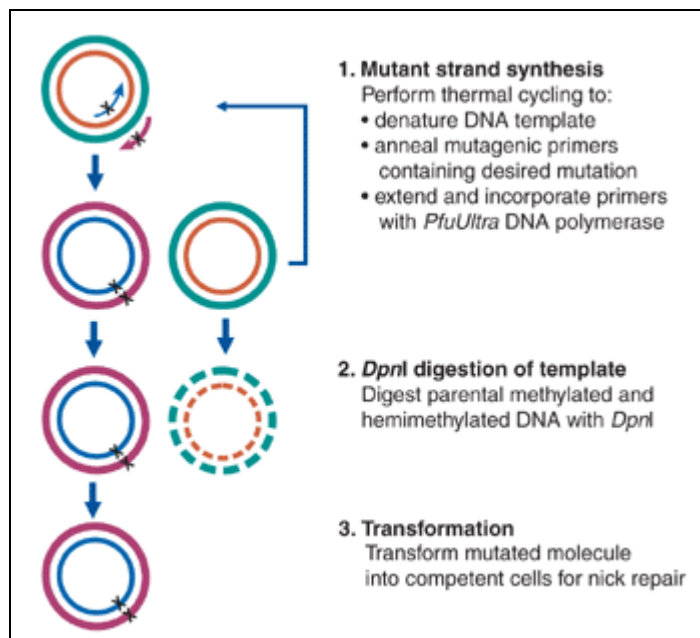 in the host from which it was prepared. The mutated PCR product is then transformed into bacteria for joining the ends of product and amplification. (Figure reproduced from Stratagene).

2.3.12 Cloning of human MARK genes using search primer method

New constructs of MARK were required since no clones encoding the full length MARK gene from humans were available. To clone human genes, a search primer method was employed. These search primers were designed, in such a way that would amplify human MARK genes excluding thousands of other cDNA's present in the human fetal cDNA library (Clontech, Palo Alto, CA). Several rounds of PCRs were done to search for MARK sequences. The MARK genes once found were cloned immediately into Topo vector as shown in the figure 2.2. These clones were further confirmed using restriction analysis and sequenced to exclude the possibility of errors and uncoded regions. These constructs were used as a starter constructs for the further sub cloning.
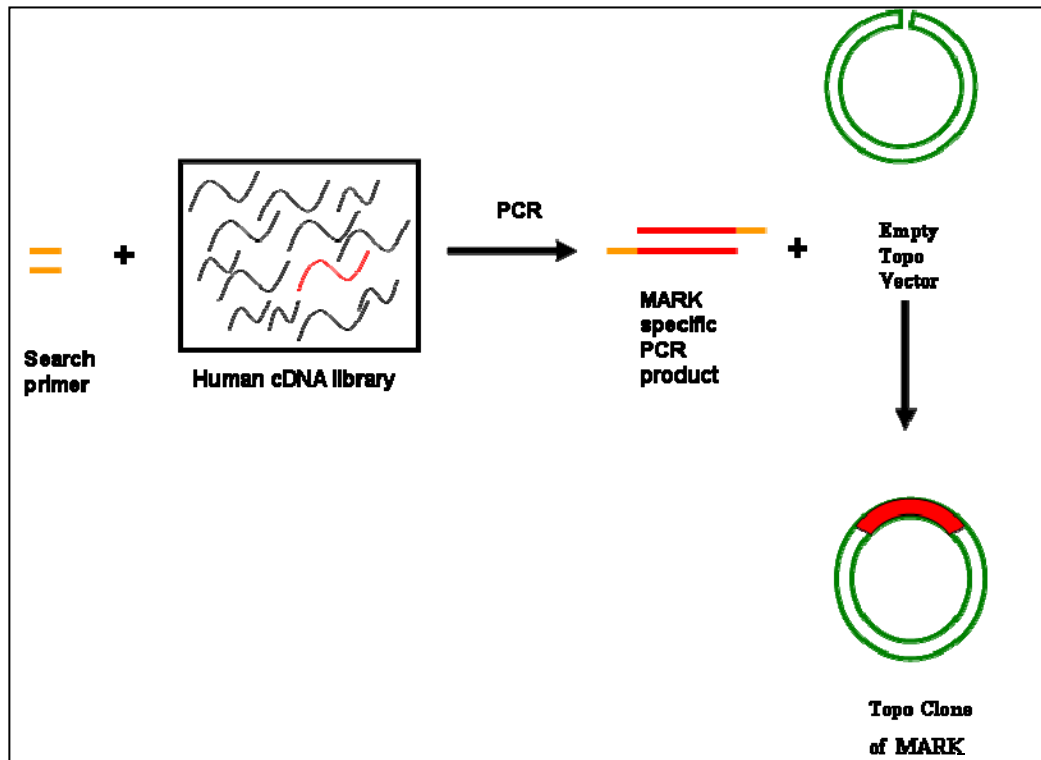
Figure 2.2: The search primer method. The search primer method involves screening cDNA library through high melting primers. These search primers contain complementary sequences from the start and end region of full length MARK gene. A high efficient PCR then amplifies only the MARK genes from the cDNA library. These human MARK genes were first cloned immediately into Topo vector after performing a topo reaction method to make a starter clone.

2.3.13 Sub cloning of MARK constructs into Topo vector and the expression vector

A general method of generating the constructs in Topo vector and expression vectors is described here. PCR's were repeated with a standard PCR reaction and new primers designed for each new construct in such a way that TEV protease cleavage site is incorporated in frame with the coding sequence of the protein. The simple way of representing these primers is shown.

Forward primer (variable length, depends on amount of % GC content)

5'- Restriction site –TEV protease sequence- coding sequence -3'

Reverse primer (variable length, depends on amount of % GC content)

3'-Restriction site–stop codon- coding sequence-5'

The PCR step was done with primers containing chosen restriction sites.

Contents of the reaction:

Template DNA	200 ng
2x reaction buffer	12.5 µl
Forward primer	30 picomoles
Reverse primer	30 picomoles
dNTPs Mix	5 mM
H2O	up to 25 µl

The mixture was temperature cycled as follows:
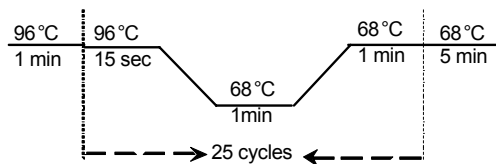
The PCR products were then analyzed by agarose gel electrophoresis. Then 100-200ng of the fresh PCR product was used to set a topo reaction as follows:

6x Buffer	1µl
Topo vector	1µl
PCR insert	1-4 µl
H2O	x µl
Total volume	6 µl

The reagents were incubated for 5-10 minutes at room temperature. 1-2 µl of mixture was transformed into XL-2 Blue/ DH5α or TOP10 cells.

2.4 Protein methods

2.4.1 SDS-Polyacrylamide gel electrophoresis (SDS-PAGE)

SDS-PAGE was performed in the lab following a modified protocol (Matsudaira and Burgess, 1978). The stacking gel was 4% acrylamide and the separating gel was 10% or 17% (Table 2.3). Protein samples were diluted 1:1 with 2x SDS-PAGE loading buffer and heated for 2 min at 95°C. Electrophoresis was carried out at 150V and maximal 35mA in SDS-PAGE running buffer (25 mM Tris-HCI, 190 mM Glycine, 0.1% (w/v) SDS). The gels were then stained in a 0.1% (w/v) solution of Coomassie brilliant blue R-250, 45% (v/v) methanol and 9% (v/v) acetic acid for 20 min on a shaking platform. Next, the gels were destained in an intensive destaining solution (50 % (v/v) methanol, 10% (v/v) acetic acid) for 20 min and for a minimum of 1 hour in a normal destaining solution (5% (v/v) methanol, 7.5% (v/v) acetic acid).

Components	Separating gel		Stacking gel (4 %) (ml)
	10 % (ml)	17 % (ml)	
40 % Acrylamide/ Bis acrylamide (37.5:1)	15.00	25.60	5.40
Tris HCl (1.0 M, pH 8.8)	22.00	22.00	-
Tris HCl (0.25 M, pH 6.8)	-	-	27.00
10 % SDS	0.60	0.60	0.54
TEMED	0.12	0.12	0.108
10 % APS	0.065	0.065	0.065
H_2O	22.00	11.50	20.90

Table 2.1: Solutions for preparing SDS-PAGE (volumes are in ml).

Molecular weight marker proteins (Biofermentas) were:

Protein name	Molecular weight (kDa)
β-Galactosidase	116.0
Bovine serum albumin	66.2
Lactate-dehydrogenase	45.0
Restriction endonuclease Bsp981	35.0
β -Lactoglobulin	18.0
Lysozyme	14.4

Table 2.2: Standard protein molecular weight markers. 1-2μg of the standard protein molecular weight markers were loaded on a mini gel.

2.4.2 Western blot

Western blotting was performed following a modified method of (Towbin et al., 1979). The proteins were electrophoresed on SDS gels and then electro-transferred to PVDF membranes (1mA/cm², for 1 hour). The membranes were blocked with 5% milk (5g milk powder in 100ml of 1xTBST) for 1 hour at RT and then treated with appropriate primary antibody (diluted in 1xTBST) at 37°C for 1 hour. The membranes were washed with 1xTBST (5 times). The secondary antibody (diluted in TBST) was added and the membranes were incubated at 37°C for 60 minutes followed by washing with 1xTBST (5 times). The substrate reaction was carried out with ECL detection reagents (GE, Healthcare). The ECL Western blotting system is a chemiluminescent, non-radioactive method to detect antigens that have been immobilized onto membranes. This system makes use of a horseradish peroxidase conjugated secondary antibody that, in conjugation with a chemiluminescent substrate, luminol generates a signal that can be captured on the film and the bands can be visualized using LAS 3000.

2.4.3 Protein expression and purification

The following strategy was applied for every new expression construct: First, 5 ml LB supplemented with the appropriate antibiotics was inoculated with the desired expression strain and grown at 37°C overnight. This pre-culture was used to inoculate a new 100 ml LB culture, which was left to grow at 37°C, shaking at 280 rpm until the optical density (at 600nm) reached to 0.6. A sample of 1 ml was centrifuged and kept as a un-induced control and the rest was induced with IPTG or arabinose to final concentration of 0.5 mM or 0.2 %, depending on the *E. coli* cell strain used for expression. The cultures were left to grow at lower temperature 25-30°C for overnight. Cells were then harvested by centrifugation at 8 krpm for 5 min (Eppendorf 5810R) and resuspended in lysis buffer.

2.4.4 Cell lysis and solubility test through spin columns

Cells were lysed using a French press (Aminco). First, cells were thoroughly resuspended in lysis buffer (2-4 ml of lysis buffer/100ml culture) and then they were transferred to a French press cell. Application of 15,000 PSI in two rounds ensured the lysis. Lysates were kept on ice and centrifuged at 40 krpm for 45 min at 4°C. After separating the supernatant and pellet, solubility was tested through Ni-NTA affinity spin columns from Sigma according to the manufacturer's protocol.

A sample of the elute of the spin columns, supernatant and the pellet resuspended in lysis buffer were loaded onto an SDS gel together with samples of before and after induction. In this way expression and solubility of the desired protein was tested in a first approach.

2.5 Chromatography

Purification of proteins was performed by Fast Performance Liquid Chromatography (FPLC) using Äkta purifier and Äkta explorer machines (Pharmacia). Most of the purification was done with described buffer without reducing agents unless otherwise described.

2.5.1 Ni-NTA affinity chromatography

Immobilized metal affinity chromatography (IMAC) makes use of the binding properties of metals towards proteins for purification purposes; nickel-nitriloacetic (Ni-NTA) resin (QIAGEN) contains chelated nickel, which is able to specifically bind to stretches of polyhistidine in proteins. Most expression systems include a tag of nine histidines either at the N- or at the C-terminus.

The resin was cast on a Pharmacia self-packed XK26 column or a batch protocol was performed with the use of Bio-Rad columns. The material was rinsed with ddH2O to remove the 20% (v/v) ethanol preservative and equilibrated with the appropriate equilibrium buffer. Once the column was equilibrated, the bacterial lysates containing the soluble protein was passed over the column. After loading, the column was washed with equilibration buffer (~10-20 column volumes) and finally, the protein was eluted with 3 volumes of elution buffer.

2.5.2 Anion and cation exchange chromatography

Protein separation by ion exchange chromatography depends on the reversible adsorption of charged molecules to an immobilized ion exchange group of opposite charge. Varying conditions such as ionic strength and pH can control these interactions. To ensure electrostatic binding, the total ionic strength needs to be low.

Generally, 100mM NaCl was included into the anion exchange buffers. The columns for anion exchange chromatography (AIEX) and cation exchange chromatography (CIEX) were MonoQ HR 10/10 and MonoS HR 10/10 (Pharmacia) respectively. After equilibration with 5 column volumes of the AIEX/CIEX buffer A, the sample was loaded and the washing step followed with 5-7 column volumes of AIEX/CIEX buffer A. The elution was performed with a linear gradient of AIEX/CIEX buffer B in two steps: first from 0 to 60% in 5-8 column volumes and then to 100% in 1-2 column volumes. Eluted fractions containing the protein of interest were pooled together.

2.5.3 Gel filtration chromatography

On a gel filtration (or size exclusion) column the molecules are separated according to differences in their sizes. The concentrated protein solution is injected into a 1 ml loop with a

injection needle (Pharmacia). Small molecules which can diffuse into the pores of the gel beads are delayed in their passage through the column in contrast to the larger molecules, which cannot diffuse into the gel beads. The larger molecules thus leave the column first, followed by the smaller ones in order of their sizes. Gel filtration was performed with a Superdex G-200 HR 16/60 column (Pharmacia).

2.5.4 Determination of the protein concentration

Protein concentrations were estimated by using the Bradford method (Bradford, 1976). The assay is based on the observation that the absorbance maximum for an acidic solution of Coomassie Brilliant Blue G-250 shifts from 465 nm to 595 nm when binding to the protein occurs. Bovine serum albumin solution is used as a standard. 1µg to 5 µg of BSA solution in 10µl were used to calculate a standard curve. The test proteins were measured in two different dilutions. To these samples 200µl of Bradford reagent (Bio-Rad) were added and mixed. The absorbance at 595 nm was measured in a Microtitre plate reader (BioLynx 2.2) and the protein concentrations were calculated from the standard curve.

2.5.5 Concentrating the protein solution

The protein solutions were concentrated using the Amicon (Millipore) device. In this device, a membrane with a molecular weight cut-off smaller than the protein of interest is placed at the bottom of a cell, which is filled with the protein solution. The cell is then placed in a 50 ml falcon tube and centrifuged at 3000g. The flow through contains only lower molecular weight components, while the protein is concentrated in the chamber.

2.5.6 Dynamic light scattering

Dynamic Light Scattering (DLS) was used to assess the quality of the protein solutions prior to crystallization trials. Laser light is scattered by the molecules in suspension. The scattered light forms an interference pattern which varies due to Brownian motion of the molecules. The autocorrelation function of the intensity of the scattered light depends on the rate of the diffusion of the molecules. Thus the recorded autocorrelation function is a direct indicator of the diffusion coefficients of the particles. Diffusion coefficients are converted to particle size using the Stokes-Einstein equation

$$D = k_b t / 6 \eta \pi r_h$$

where k_b is the Boltzmann constant, η is viscosity, t is temperature and r_h is radius. DLS experiments were conducted in a Dimingon-A machine (Firma Dierks and Partner, Hamburg). The data were processed with the software provided with the machine.

Before measuring the DLS, the samples were spun in a tabletop centrifuge to remove dust and other higher molecular weight aggregates. 5-10 µl of protein solution of concentration a 10-20 mg/ml in a pre-cooled 0.1 mm quartz cuvette were used.

2.6 Crystallographic methods

2.6.1 Crystallization techniques

A variety of methods exist to crystallize biological macromolecules. All the methods bring the protein solution into a supersaturated state. Among them, vapour diffusion is the most widely used method that also has been used in this study. A droplet containing the protein solution to be crystallized, buffer, crystallizing agent and additives is equilibrated against a reservoir containing a solution of the crystallizing agent at a higher concentration than in the droplet. Equilibration proceeds by diffusion of the volatile species (water or organic solvent) until the vapour pressure in the droplet is equal to the one in the reservoir. If equilibration occurs by water exchange (from the drop to the reservoir), it leads to a decreasing volume of the droplet. This method was used in this study in two variations, either as hanging or as sitting drops.

Crystallization solutions and supplies are described in the materials see section. Prior to each crystallization experiment, the highly concentrated protein solution (10-20 mg/ml) was centrifuged in an Eppendorf tabletop centrifuge at 13 krpm for 10 minutes at $4^{\circ}C$, in order to separate precipitates. First screens were set up in Crystal Quick 96 well sitting drop plates (Hampton Research) by mixing 1 µl of protein with 1µl of reservoir solution. During the optimization trials, the hanging drop method was preferred.

For each trial 1 µl of protein solution was mixed with 1 µl of reservoir. The plates were sealed with tape in the case of sitting drop and with a siliconised cover slip in the case of hanging drop trials and kept at 20°C and/or at 4°C. The plates were examined each day during the first week and 2 times a week during the first 2 months. The initial screens were performed by the use of the commercial screens as described before.

2.6.2 Crystallization robot screening

The crystallization robot from the EMBL, Hamburg was used to set up random crystallization screens (Mueller-Dieckmann, 2006). The Robotic arm of the crystallization facility prepares the crystallization set up by mixing equal amounts of protein and the crystallization cocktails available from the commercial screens. The experiments are set up as sitting drops with 96-well plates using a 500nl drop volume. After setting the crystallization mixtures, plates are stored at 5°C or 19°C. Only crystal plates at 19°C are automatically imaged and are made

available to the user to inspect through a web server. The inspection of the crystallization plates follows a default schedule. MARK1 and MARK3 proteins were screened for crystallization conditions through most of the available screens from the crystallization facility.

2.6.3 Cryoprotection of crystals

The high intensity of synchrotron radiation can lead to radiation damage of the protein crystals. The interaction between the beam and the crystal generates free radicals which damage the molecules bringing disorder and may even break bonds within the protein. A common method to reduce this radiation damage is freezing the crystals in a stream of cold nitrogen and collect the diffraction data at low temperature (Garman and Schneider, 1997). The high solvent content (~50%) of protein crystals can lead to ice crystal formation during freezing and these ice crystals will destroy the crystal integrity and disturb the protein diffraction. This problem can be overcome by soaking the crystal in a cryoprotectant solution which maintains the crystal quality and prevents the formation of ice crystals. MARK crystals were tested for different cryoprotecting agents like glycerol, MPD and ethylene glycol and tested for the diffraction quality.

2.6.4 Data collection

X-ray diffraction data were collected using synchrotron radiation at the beamline of the X13 Consortium for Protein Crystallography at HASYLAB and at the MPG beam line BW6 (DESY, Hamburg). The features of the beam line are summarized.

Beamline	**X13**
Institute	EMBL and University of Hamburg
Wavelength	0.802Å (fixed)
Optics	Triangular cut Si (111) monochromator crystal
Mirror	continuous bent Rh-coated focusing mirror
Detector	MAR300 CCD
Cooling device	Oxford-Cryosystem

Beam Line	**BW6**
Institute	MPG

Wavelength	Variable (0.6Å to 3.2Å), measurements were done at 1.05 Å
Optics	Double focusing X-ray optics
Detector	165mm MAR CCD
Cooling device	Oxford-Cryosystem

2.6.5 Data reduction and phase determination

The determination of the three-dimensional structure of macromolecules using X-ray crystal diffraction techniques requires the measurement of amplitudes and the calculation of phases for each diffraction point. Amplitudes $|F(h,k,l)|$ can be directly measured from diffracting crystals, phases $\alpha(h,k,l)$ have to be determined indirectly. Thus, methods were developed to calculate phases. These include molecular replacement (MR), multiple isomorphous replacement (MIR) and multi wavelength anomalous dispersion (MAD) method.

2.6.6 Molecular Replacement (MR)

Among all these techniques, MR is the most widely used with approximately 60 % of the structures in Protein Data Bank (PDB) solved using this technique. The molecular replacement method makes use of a known three-dimensional structure of a homologous protein as an appropriate starting model to provide initial phases for the unknown structure. The crystal structure of MARK2 (Panneerselvam et al., 2006) was used as search model for solving the structure of MARK1. For MARK3, structure of MARK1 (Marx et al., 2006) was used due to more close sequence similarity of MARK3 with MARK1.

2.6.7 Protein kinase assay

Kinase activities were assayed in 50 mM Tris-HCl pH 7.5, 5 mM MgCl2, 2 mM EGTA, 0.5 mM PMSF, 0.5 mM DTT and 0.5 mM benzamidine for 30 minutes at 30°C. Hot ATP was used at a concentration of $3.7*10^7$ MBq/mol (Amersham Biosciences) with a substrate peptide concentration of 100 μM. The substrates were TR1 peptide derived from the first repeat of tau protein containing Ser262 in the KXGS motif (TR1-peptide NVKSKIGSTENLK) (Drewes et al., 1997) or AMARA peptide (AMARAASAAALARRR) which is a common substrate peptide used for assaying AMPK family members (Dale et al., 1995). Reactions were quenched by addition of half the volume of 30 %(w/v) TCA. The reaction mixture was spun in a centrifuge and the supernatant was applied to phosphocellulose-paperdiscs, washed with phosphoric acid (0.1 M), dried by air and radioactivity was measured in a scintillation counter. The pellet was resuspended in 10μl of 1xSDS sample buffer, heated for 3 minutes at 95°C and loaded onto a 10% gel. The gel was stained with Roti-blue, destained, dried and autoradiogram was performed.

3 Results

3.1 Cloning of MARK1 and MARK3

The MARK proteins are relatively large proteins and consist of several domains. Crystallizing the entire protein is not possible due to a variable N-terminal header and large spacer domain that is predicted to be unstructured. The most important regions are the kinase domain, the UBA domain and the KA1 domain. The kinase and the UBA domain could be cloned together due to placing of these domains adjacent to each other in the sequence.

MARK2 crystallized in our lab (Panneerselvam et al., 2006) was cloned from rat, however the kinase and the UBA domain from rat are identical in sequence to human MARK2. Other MARK isoforms differ in this region. The first important step was to clone the human isoforms of MARK1 and MARK3 and then making suitable constructs for crystallization. To do so, a sequence alignment was made based on the construct used for crystallizing MARK2 (Fig. 3.1).

After that, a search for human MARK genes was made. One possible way to clone them was to search for the MARK genes in a human cDNA library. This problem was approached using the design of search primer method for fishing the MARK genes from the cDNA library. The search primers designed were of 50-60 residues in length and very high melting temperature. The large oligomeric length and high melting temperature assures that primers anneal specifically to MARK cDNA only in the large cDNA pool. A high efficiency PCR protocol was developed so as to avoid amplifying other MARK isoforms and non specific products during the PCR. Several rounds of the PCR were done in order to optimize the PCR product. In cases where multiple PCR products of MARK were obtained, the PCR products were separated on a gel, excised and sequenced to confirm the MARK genes. Using this effective search primer procedure, MARK genes were cloned from the several thousand cDNA's present in the human fetal brain cDNA library.

These genes were first cloned into Topo vector and immediately reconfirmed through restriction digestion. After that, the clones were completely sequenced to exclude the possibility of any errors and non coding regions present in it. Once the starter construct for specific isoform was made, they were further used to make all the sub cloning needed. Several constructs were cloned as mentioned in the protocols.
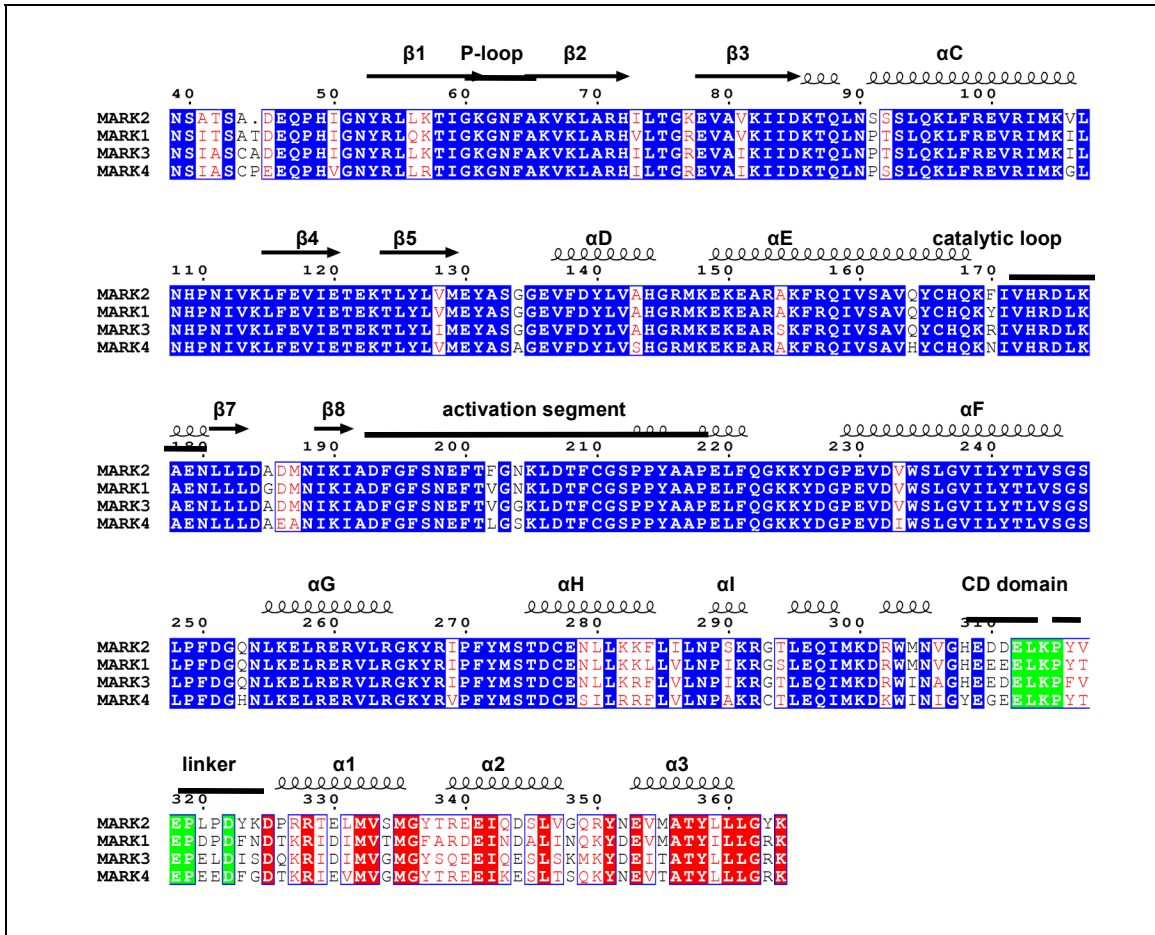
Figure 3.1: Sequence comparison of MARKs. Sequence comparison of the domain of MARK2 crystallized by Panneerselvam, (Panneerselvam et al., 2006) with the other MARKs. Amino acids with blue background belong to the kinase domain, green background shows the linker region and red background shows the UBA domain. The secondary structural elements present in crystal structure of MARK2 are indicated above. Figure was prepared using ESI pript of expasy webpage.

Further cloning was required to express the protein through the expression vector. After the boundaries or mutations of the constructs to be cloned were chosen, specific primers were designed to introduce appropriate restriction sites. These primers also contained DNA sequences which will introduce a 9X His tag fusion and a Tobacco Etch Virus (TEV) protease cleavage site in frame with the N-terminus of the protein. The incorporation of the restriction sites helps in taking the cloning product further into the expression vector while the tag will ease in protein purification. The protease cleavage site will help in cleaving the tag after purification. PCRs were repeated with the new primers the PCR fragment was cloned into the final expression vector using the ligation based cloning methods (Fig. 3.2).
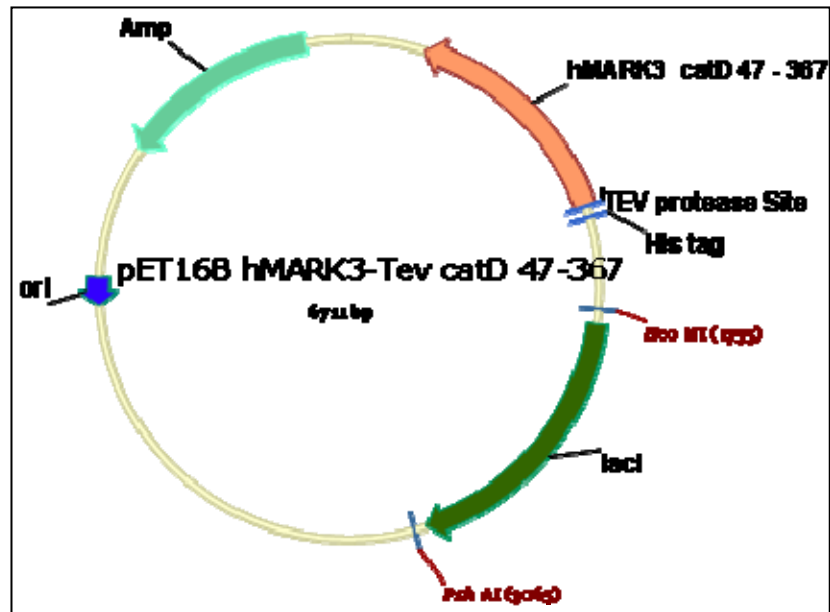
Figure 3.2: Vector map of the pET 16b MARK3 expression plasmid. The expression clone contains an N-terminal 9 x histidine tag for the affinity purification, TEV protease recognition site to remove the affinity tag after purification and ampicillin resistance gene for propagation and selection of the plasmid. Similar constructs were made for MARK1. This map was produced by using Vector NTI software V9.0 (Invitrogen).

Thus an initial wild type expression vector was first made. To make site specific mutations, deletions or additions, recombinant PCRs were made with the procedure of site directed mutagenesis. All clones were completely sequenced and verified once again for appropriate cloning sites, mutations or frame shifts which might have occurred during the cloning procedure. Several constructs were made based on the alignment analysis, domain regions and mutations, known to affect solubility, kinase activity of the proteins or improve the stability of the protein. Table 3.1 summarizes the list of constructs made.

3.1.1 Expression constructs

MARK isoform	start Amino	End Amino	Mutations	purpose of construct
MARK3	41N	367R	Wt	wild type for crystallization
MARK3	47A	367R	Wt	wild type for crystallization
MARK3	47A	370E	Wt	wild type for crystallization
MARK3	47A	367R	K85R	mutation of critical lysine for ATP co-ordination
MARK3	47A	367R	T90A	pim-1 active mutant
MARK3	47A	367R	T90D	pim-1 inactive mutant
MARK3	47A	367R	K85R,T211E	active mutant for crystallization
MARK3	47A	367R	T211A, S215A	inactive double mutant
MARK3	47A	367R	T215E	active mutant
MARK3	47A	367R	Y354A	critical UBA mutant
MARK3	47A	367R	K351A, K353A	surface entropy stabilized mutant for crystallization
MARK3	47A	367R	C213A,T211A, S215A	dimerization inhibition mutant
MARK3	47A	305R	Wt	catalytic domain only
MARK1	45N	371K	Wt	wild type for crystallization
MARK1	45N	371K	K89R	mutation of critical lysine for ATP co-ordination
MARK1	45N	371K	T215E	active mutant
MARK1	45N	371K	T215A, S219A	inactive double mutant
MARK1	45N	371K	V86R	UBA detachment mutant
MARK1	45N	371K	4GI	extension of UBA linker by four glycines
MARK1	45N	325D	Wt	catalytic domain only
MARK1	45N	325D	V86R,T215E	catalytic domain active mutant
MARK1	1M	795L	Wt	wild type full length

Table 3.1: List of expression constructs. All the constructs were cloned into the pET 16b vector of Novagen with a His tag at the C- or N-terminus. These constructs were made based on the known mutations which affect the activity, binding, solubility or stability by entropy reduction (Cooper et al., 2007) of the protein.

3.2 Expression and purification.

Protein expression test was performed in various bacterial cells like BL21 RIL and other strains but expression of MARK proved to be toxic to the cells and they could not be cultured. However BL21 AI cells grew better, had no toxic effects and expressed the MARK protein. These constructs were first tested for solubility as mentioned in the materials and methods section. Large scale cultures were done after confirming the solubility of the protein.

Protein purification was done essentially as in the case of MARK2 with four-step approach, which led to highest purity and crystallizibility. *E. coli* BL21 AI cells (Invitrogen) were transformed with the MARK expression plasmid by using the chemical transformation protocol. Transformed cells were initially grown at 37° C and induced overnight at 24° C by adding arabinose to a final concentration of 0.2% at $OD_{600} \approx 0.6$. The cells were harvested by centrifugation and lysed by passing two times through a French pressure cell. Purification of proteins was performed by fast performance liquid chromatography (FPLC) using Äkta purifier and Äkta explorer machines (Pharmacia). The expressed proteins were purified as follows.

3.2.1 Ni-NTA affinity chromatography

The bacterial lysates containing MARK protein were first partially purified using Ni-NTA affinity chromatography. All MARK constructs (unless specified) included a tag of nine Histidines at the N-terminus of the protein and thus binds to the Ni-NTA chelating resin.

3.2.2 TEV protease cleavage to remove the His-tag

Eluates from the IMAC column containing MARK protein were pooled and protein concentration was measured (Fig. 3.3). After that, His tagged TEV protease was added to the
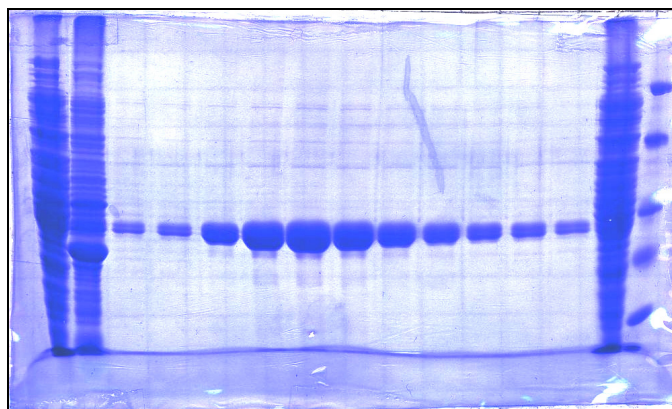
Figure 3.3: Nickel NTA column purification of MARK1 protein. The MARK1 protein eluted from the Ni-NTA column by imidazole gradient. 10µl of the sample was loaded on a 10% SDS –PAGE gel. The fractions containing the MARK1 protein were pooled and further purified.

pooled MARK protein at a ratio of 1:20 (w/w) and dialyzed overnight against the TEV protease buffer at 4°C. This results in efficient cleavage of the His tag from the MARK protein. Following which, a second Ni-NTA affinity chromatography was performed which removed the uncleaved His tagged protein and TEV protease from the cleaved ones.

3.2.3 Ion exchange chromatography

Ion exchange chromatography was regularly performed as it turned out that expressed MARK protein contained spurious extra peaks which could be separated on an ion exchange column. Thus this step was also important in removing contaminating bands and unknown peaks.

3.2.4 Gel filtration chromatography

Gel filtration was performed with a Superdex G-200 HR 16/60 column (Pharmacia) in appropriate gel filtration buffer.

The MARK1 protein eluted usually with broad peaks with the peak center at about 91 ml in the gel filtration column (Sephadex G200, HR16/60 Amersham Pharmacia). This indicates that the protein might be a mixture of monomer and dimer as calculated from a calibrated gel filtration column using standard molecular markers (Fig. 3.4).

MARK3 eluted similar to MARK1 with a peak centered at 91 ml in the gel filtration column. The solubility behavior of these proteins however differed. MARK1 was very stable and did not show any temperature dependent denaturation during the purification or crystallization. On the other hand, MARK3 was highly unstable and rapidly precipitated during the purification procedure. The best concentration of the protein which could be achieved was only 5 mg/ml. Thus the purification procedure was reoptimized by addition of reducing and stabilizing agents like DTT (5mM) and glycerol (20% w/v).

The pure peak fractions containing MARK protein were pooled and concentrated in appropriate gel filtration buffer to ~20 mg/ml using a Ultrafree-30 Centricon concentrators (Amicon). Dynamic light scattering was performed to asses the quality of the protein preparation (Fig. 3.5). The concentrated protein solution was then aliquoted in 0.2 ml PCR tubes and shock frozen in liquid nitrogen.

All procedures were carried out at 4ºC to minimize the protein degradation. After every step, purity was evaluated by SDS-PAGE (Laemmli, 1970).
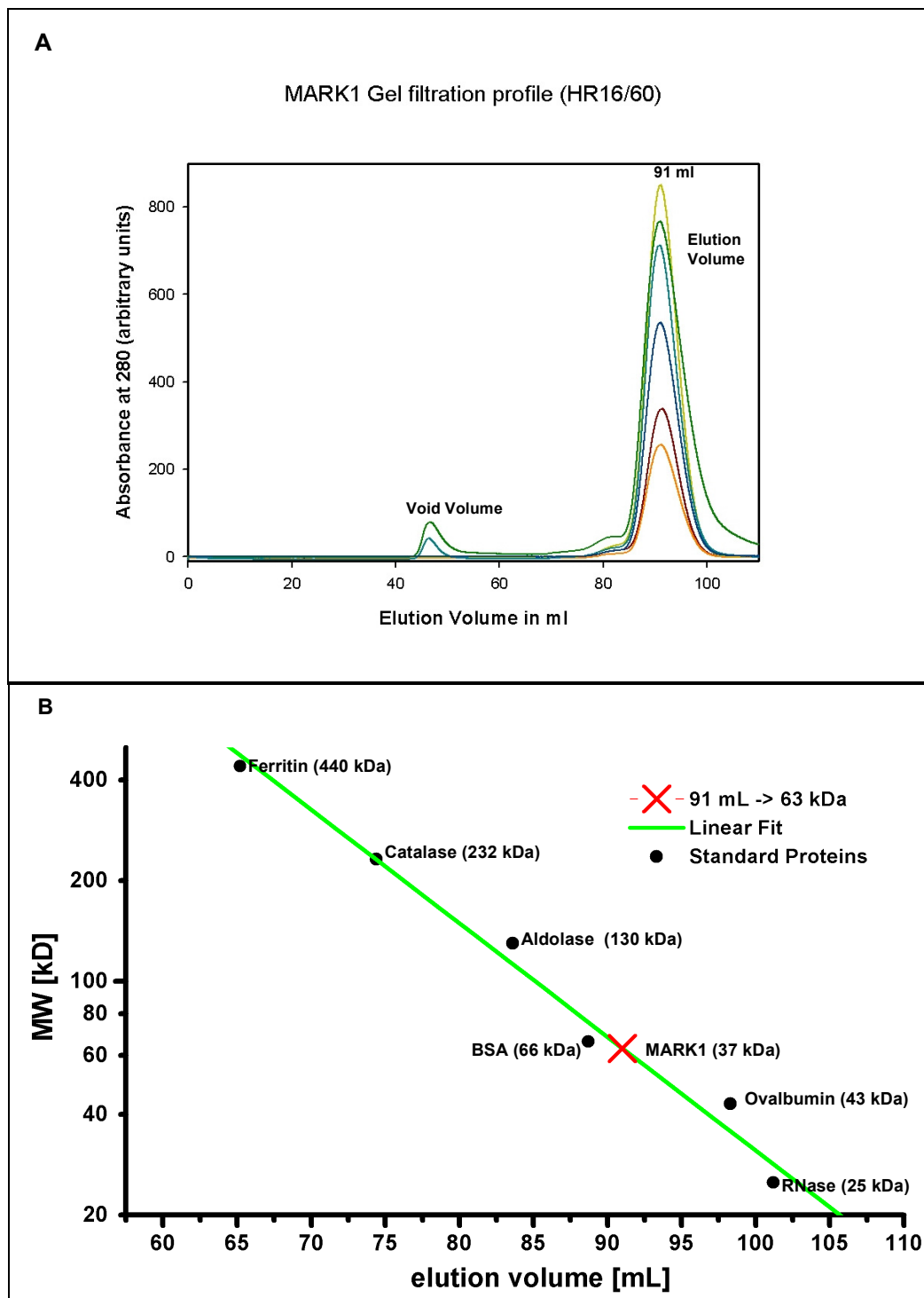
Figure 3.4: Gel filtration profile of MARK1 protein and the calibration curve. A. Gel filtration curves of six different wild type MARK1 protein preparations are shown are in the figure. The proteins were eluted in appropriate gel filtration buffer. The peak fractions from the gel filtration column eluted between 86-98 ml with the peak centered at 91 ml. **B.** The apparent molecular weight of MARK1 was calculated as 63 kDa for the 91ml peak from the calibrated gel filtration column (indicated by red X mark) using standard molecular weight markers. This indicates that the MARK1 protein is a mixture of monomers and dimers as the molecular weight of the monomer is 37kDa. MARK3 and MARK2 eluted similar to MARK1 profile shown here.
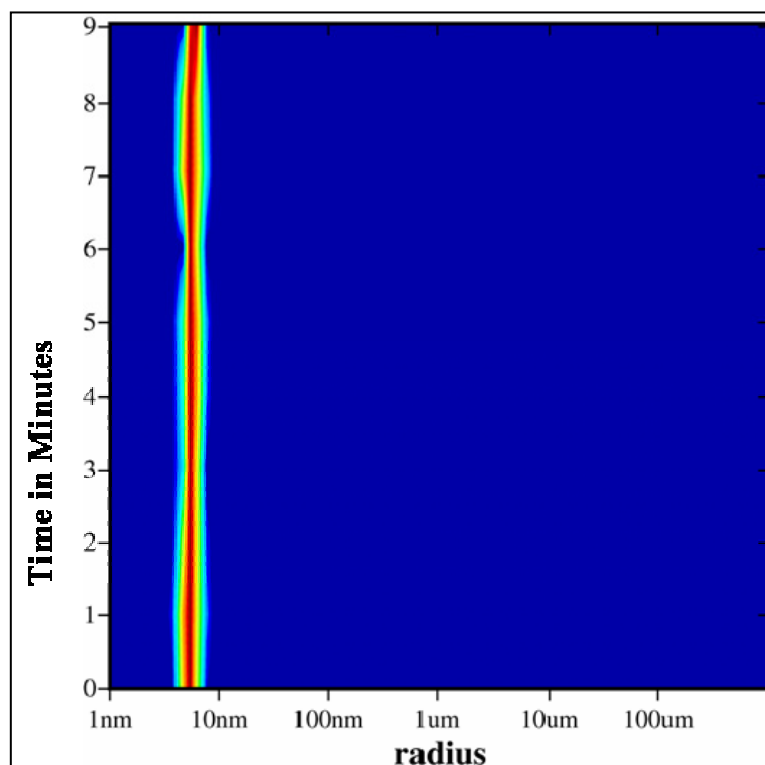
Figure 3.5: Dynamic light scattering of MARK3 sample. Samples at a concentration of 10-15 mg/ml were measured using a quartz cuvette in temperature controlled environment. The horizontal axis represents the size distribution of the particles and the vertical axis, the time. As seen from the figure, most particles have a radius distribution range of 6-8 nm indicating the protein was monodisperse and stable in the temperature controlled environment up to 10 minutes. A polydisperse sample would have broad distribution of the particle radii on the horizontal axis.

3.3 Crystallization

Crystal screening was done using two different approaches. One way was to crystallize with the regular conditions as in the case of MARK2. Second was to do a random search for the new crystallization conditions using the most popular screens available from the high throughput crystallization facility of EMBL, Hamburg.

The standard MARK2 crystallization conditions which crystallized MARK1 and MARK3 also were

Crystallization condition
0.1 M Bis Tris pH 6.5, 0.2 M ammonium sulphate,10-20% PEG3350
0.1 M Bis Tris pH 6.5, 5-10% tacsimate, 10-20% PEG5000 monomethylether

From the high throughput crystallization facility at the EMBL, several new crystallization conditions were identified.

3.3.1 MARK1 crystallization conditions

A. Index Screen

Screen Number	Crystallization condition
6	0.1M Tris pH 8.5, 2M ammonium sulphate
30	0.1 M BisTris pH 6.5, 1.5 M ammonium sulphate, 0.1M Nacl
33	0.1 M Hepes pH 7.0, 1.1 M sodium malonate pH 7.0, 0.5% Jeffamine ED-2001 (pH 7.0)
67	0.1 M Bis Tris pH 6.5, 0.2M ammonium sulphate, 25% PEG3350
68	0.1 M Hepes pH 7.5, 0.2M ammonium sulphate, 25% PEG3350
69	0.1 M Tris pH 8.5, 0.2M ammonium sulphate, 25% PEG3350
75	0.1 M Bis Tris pH 6.5, 0.2M lithium sulphate, 25% PEG3350
76	0.1 M Hepes pH 7.5, 0.2M lithium sulphate, 25% PEG3350
88	0.1 M Hepes pH 7.0, 0.2M ammonium citrate, 25% PEG3350
92	0.1M magnesium formate, 15% PEG3350
94	0.2M tri sodium citrate, 20% PEG3350

B. Crystal Screen

Screen Number	Crystallization condition
17	0.1M Tris pH 8.5, 0.2M lithium sulphate, 30% PEG 4000
30	0.1M Tris pH 8.5, 0.2M ammonium sulphate, 30% PEG 8000
31	0.1M Tris pH 8.5, 0.2M ammonium sulphate, 30% PEG 4000

C. PEG/Ion Screen

Screen Number	Screening condition
31	0.1 M Bis Tris pH 6.5, 0.2 M lithium sulphate, 18% PEG3350
33	0.1 M Bis Tris pH 6.5, 0.2 M sodium sulphate, 18% PEG3350
35	0.1 M Bis Tris pH 6.5, 0.2 M ammonium sulphate, 18% PEG3350
37	0.1 M Bis Tris pH 6.5, 0.2 M sodium potassium tartarate, 18% PEG3350
45	0.1 M Bis Tris pH 6.5, 0.2 M lithium citrate, 18% PEG3350
48	0.1 M Bis Tris pH 6.5, 0.2 M ammonium citrate, 18% PEG3350

3.3.2 MARK3 crystallization conditions

A. Index

Screen Number	Crystallization condition
44	0.1 M Hepes pH 7.5, 25% PEG 3350
46	0.1M Bis Tris pH 6.5, 20% PEG5000monomethylether
83	0.1 M Bis Tris pH 6.5, 0.2 M magnesium chloride 25% PEG 3350
84	0.1 M Hepes pH 7.5, 0.2 M magnesium chloride, 25% PEG 3350
85	0.1 M Tris pH 8.5, 0.2 M magnesium chloride 25% PEG 3350

B. Crystal screen

Screen Number	Crystallization condition
41	0.1M Hepes pH 7.5, 10% isoproponal, 20% PEG 4000
30	0.1M Tris pH 8.5, 20% ethanol

C. PEG/Ion Screen

Screen Number	Screening condition
5	0.1 M Tris pH 7.5, 0.2M magnesium chloride,18% PEG3350
7	0.1 M Tris pH 7.5,0.2M calcium chloride, 18% PEG3350
34	0.1 M Tris pH 7.5, 0.2 M potassium sulphate, 18% PEG3350
35	0.1 M Tris pH 7.5, 0.2 M ammonium sulphate, 18% PEG3350

Table 3.2: Crystallization conditions of MARK. MARK1 and MARK3 were screened with different crystallization cocktails as described in the protocols using the crystallization robot at EMBL, Hamburg. Many different crystallization conditions identified from the screen were reproduced. These were used as the starting condition for crystallization. The best reproducible conditions were optimized for growing crystals to test on a synchrotron beam line for diffraction.

Many conditions identified from the commercial screens were reproduced but only few most highly reproducible conditions were optimized first.

Other important parameters optimized for the crystallization were,

1. Reducing agents like DTT (5-10 mM) and TCEP (0.5-1 mM)

2. Stabilizing agents like glycerol (10-20 % w/v)

3. pH range from 6.5 to 9.0

4. Temperature 19°C and 4°C

5. Drop size and protein to reservoir ratio, various permutations and combinations

6. Cryo buffer conditions (MPD, glycerol and PEG400 used at 10-20 % w/v concentration).

MARK1 crystallized in similar conditions as MARK2 but the crystal shape and form were completely different being very irregular. However, a PEG/ion screen search led to identification of ammonium citrate, which yielded better shaped crystals. This salt led to quick optimization of the crystal trials. After optimization, crystals were grown by mixing 2 μl of protein with 2 μl of reservoir consisting of 7-10 % PEG 3350, 0.1 M Bis Tris pH 6.5, 0.2 M ammonium citrate at 4º C (Fig. 3.6).
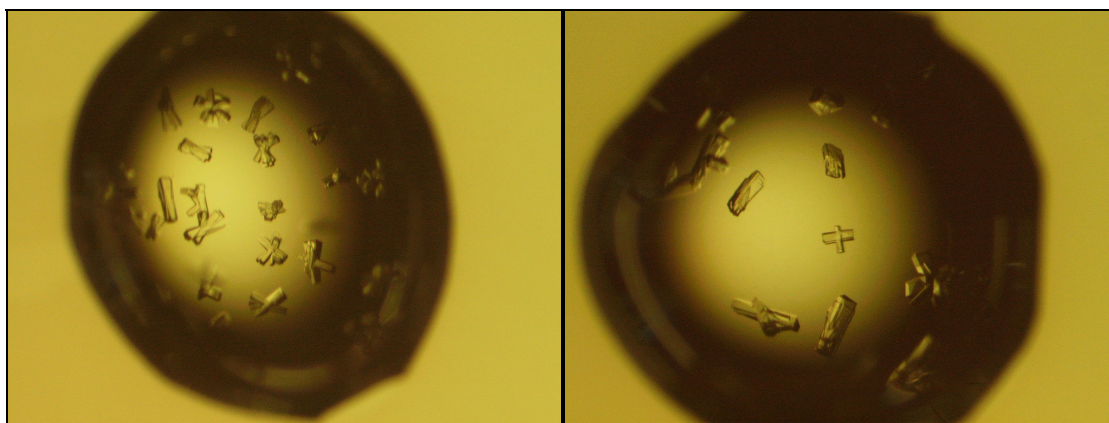
Figure 3.6: Crystals of MARK1. MARK1 crystals were grown from 7-10 % PEG 3350, 0.1 M Bis Tris pH 6.5, 0.2 M ammonium citrate at 4ºC. These crystals grow mostly as radiating clusters. A fragment of the cluster was used for data collection.

In the case of MARK3, crystals were growing mostly as thin platelets with very thin edges and were of extremely fragile nature. These crystals either had a weak diffraction or anisotropic diffraction where certain orientations of the crystal have a bad diffraction pattern. Diffraction data collected from these crystals were of poor quality and could not be used further for solving the MARK3 structure. Improving the diffraction quality involved reoptimizing the expression construct (inactive double mutant), the purification procedure (10-20 % w/v glycerol, 1 mM DTT) and crystal growth conditions (pre-cooled crystallization solutions and equipment etc). After optimization, crystals of MARK3 were grown by mixing

2 µl of protein with 2 µl of reservoir consisting of 7-10 % PEG 3350, 0.1 M Hepes pH 7.5, 0.2 M calcium chloride at 4ºC (Fig. 3.7).
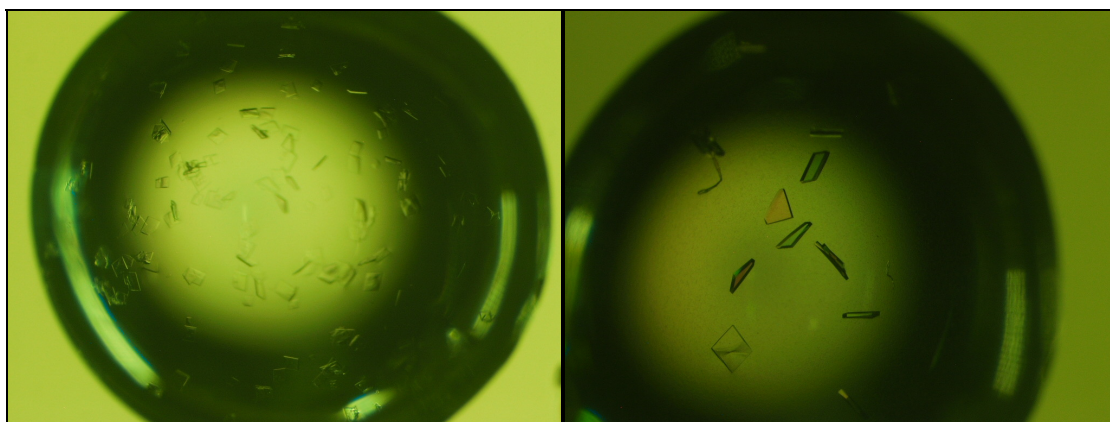
Figure 3.7: Crystals of MARK3. Crystals of MARK3 grown from 7-10 % PEG 3350, 0.1 M Hepes pH 7.5, 0.2 M calcium chloride at 4ºC. Wild type crystals mostly grew as thin platelets and were fragile. Crystals of double inactive mutant had more thick edges compared to the wild type crystals.

3.4 Data collection, data reduction and phase determination

X-ray diffraction data were collected with synchrotron radiation at the beam line of the X13 Consortium for Protein Crystallography at HASYLAB (DESY, Hamburg) and synchrotron radiation facility at the MPG beam line, BW6 (DESY, Hamburg). Diffraction images were recorded with a MAR165 CCD detector.

Before data collection, MARK1 crystals were soaked in cryoprotectant solution for a few minutes and rapidly cooled to 100K in a stream of cold nitrogen (Oxford Cryosystems). MARK3 crystals were pre-frozen in liquid nitrogen using standard procedures and stored in cryocans with liquid nitrogen until the time they were used on the beam line.

Diffraction data sets were collected using the strategies predicted from the BEST program (Bourenkov and Popov, 2006) (Fig. 3.8 and 3.9). Data were processed, integrated and scaled using HKL data processing system (Otwinowski et al., 1997).

Programs of the CCP4 package (Collaborative Computer Project Number 4, 1994) (http://www.ccp4.ac.uk/main.html) were used for phasing and calculation of electron density maps using its graphic user interface.The structure of MARK1 was solved by molecular replacement with the catalytic domain of MARK2 as search model, using Phaser Version 1.2 (Storoni et al., 2004). The structure of MARK3 was solved using similar methods by using the catalytic domain of MARK1.
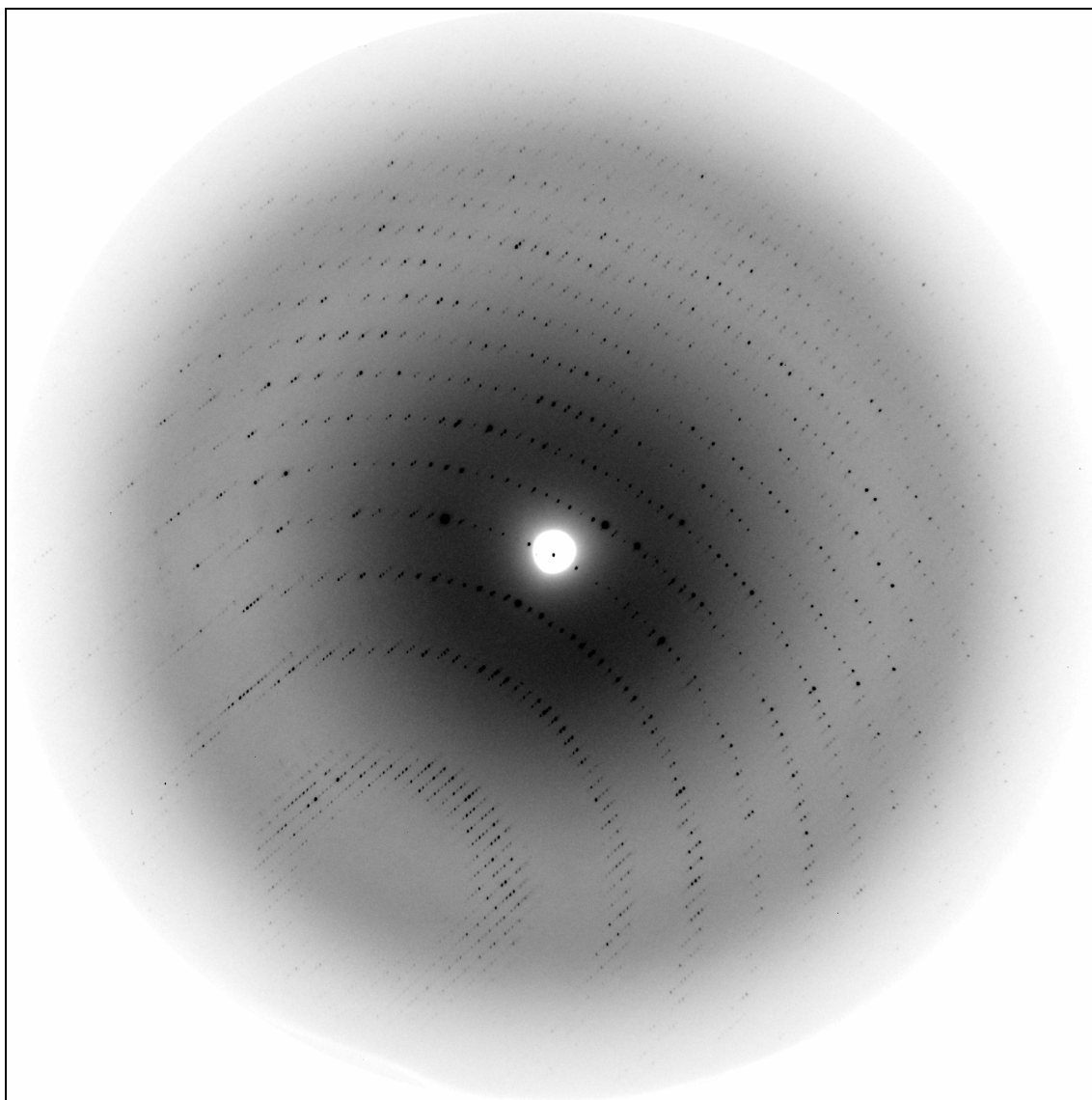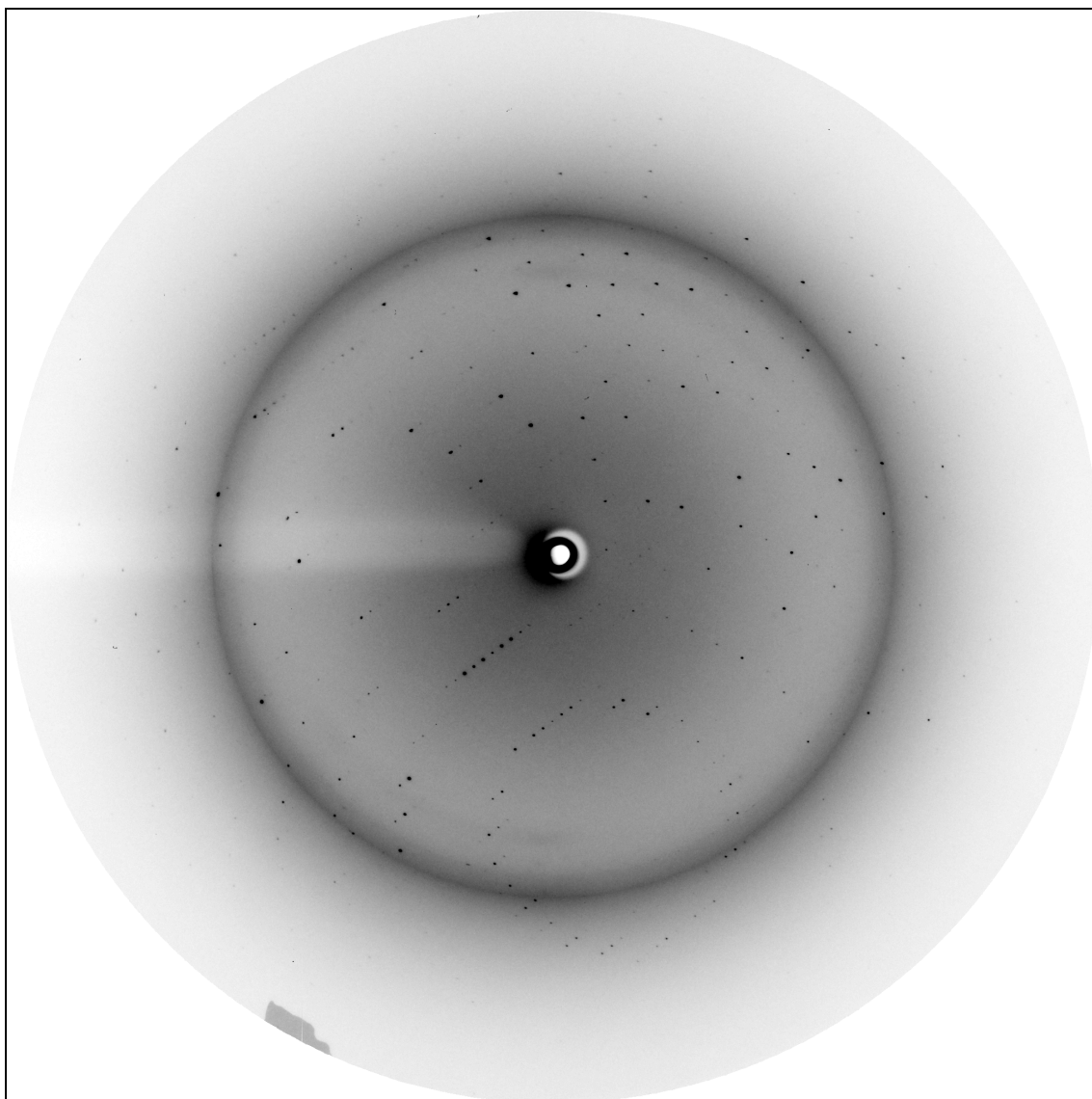
Figure 3.8: X-ray diffraction pattern from a MARK1 crystal. X-ray crystal diffraction measured at the beam line of the X13 consortium for protein crystallography (HASYLAB, DESY, Hamburg). Sample diffraction image of the MARK1 crystal. The bright spot in the centre indicates the beam stop and also the centre of the diffraction image. The outermost ring of diffraction image where the spots are detected defines the diffraction resolution of the crystal. The outer most ring of the diffraction image corresponds to 2.6 Å.

3.4.1 Model building and refinement

To reduce model bias, a composite omit map was calculated with CNS 1.1 (Brunger et al., 1998) before starting the cycles of manual model building with Coot (Emsley and Cowtan, 2004) and refinement with Refmac5 (Murshudov et al., 1997).

Figure 3.9: X-ray diffraction pattern from a MARK3 crystal. X-ray crystal diffraction measured at the MPG beam line BW6 (DESY, Hamburg). Sample diffraction image of the MARK3 crystal. The bright spot in the centre shows beam stopper and is the centre of the diffraction image. The prominent dark ring seen in the diffraction image here shows diffraction pattern of the ice crystals at about 3.7 Å. The outermost ring of diffraction where the spots are detected defines the diffraction resolution of the crystal. The outer most ring of the diffraction image corresponds to 2.4 Å.

Non crystallographic symmetry restraints were used until the R-factor dropped below 30%. TLS parameters were added during last stages of the refinement (Table 3.3). The final models structures were checked with PROCHECK (Laskowski et al., 1993) and WHAT_CHECK (Hooft et al., 1996) programs to asses the quality of the structure.

3.4.1.1 MARK data reduction and refinement statistics

	MARK1	MARK3
Parameters	Values	Values
Space group	$P2_12_12_1$	C2
Unit cell [Å]	$a = 110.7$, $b = 116.5$, $c = 285.7$	$a = 96.2$, $b = 95.4$, $c = 110.5$
Matthew's co-efficient	3.06	3.23
Data collection		
Resolution limits [Å] overall (last shell)	50 – 2.60 (2.64 – 2.60)	150-2.4 (2.39-2.46)
Number of observations > 1sigma	537334	138985
Number of unique reflections	112949	36849
Completeness, overall (last shell)	99.4% (98.5%)	98.2% (91.6%)
Rsym, overall (last shell)	8.2% (47.3%)	Null
$<I>/<s(I)>$, Overall (last shell)	15.4 (2.6)	14.2 (2.7)
Refinement		
Resolution limits [Å] overall (last shell)	10 – 2.60 (2.667 – 2.604)	66.37-2.4 (2.40-2.44)
Number of reflections, working set (test set)	107900 (2786)	36848 (2355)
Number of atoms	19579	5248
R, overall (last shell)	21.2 (28.9)	19.1 (24.8)
Rfree, overall (last shell)	29.0 (41.0)	23.6 (36.1)
Average B Factor [Å2]	48.6	42.14
Number of molecules /asu	8	2

Table 3.3: Summary of the data collection and structure refinement. MARK1 crystals belongs to space group $P2_12_12_1$ had large unit cell dimensions and eight molecules in asymmetric unit. MARK3 crystals belonged to space group C2 with two molecules in the asymmetric unit (asu).

3.5 Structure of MARK3

3.5.1 Organisation of MARK3 Crystals

MARK3 crystallized in space group C2 with two molecules in the asymmetric unit. These molecules are named A and B. A new feature seen in case of MARK3 crystals only is that two molecules of A form a continues β-sheet through their N termini. This results in additional stabilization of N-terminal region in molecules A (Fig. 3.10).
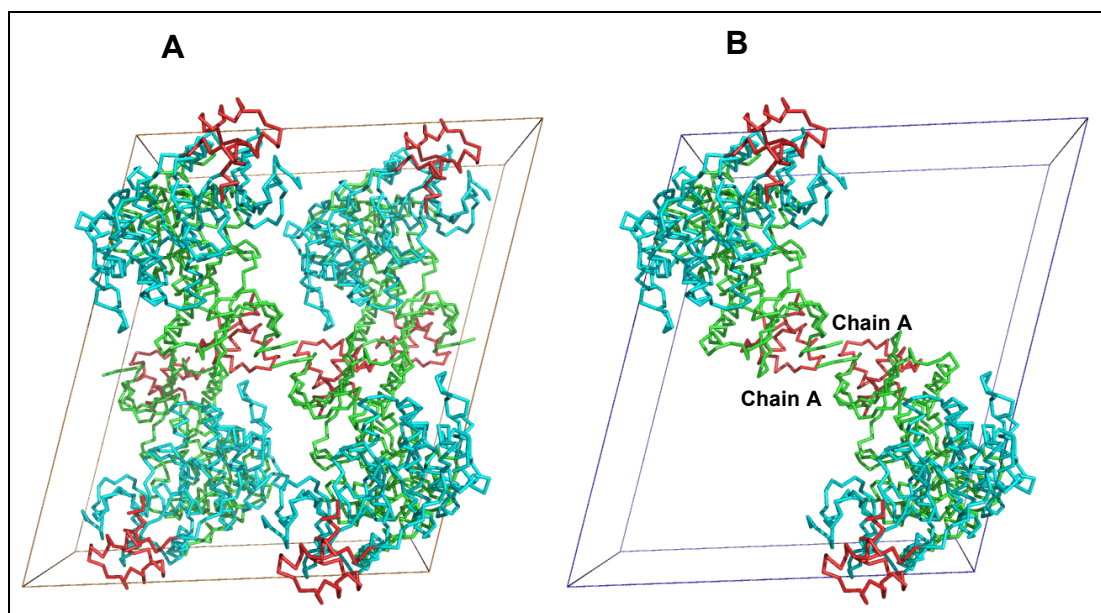
Figure 3.10: Crystal packing of MARK3. A. Arrangement of the molecules in the unit cell. Crystals are formed from dimers of the MARK3 molecules. The UBA domains are highlighted in red to show interactions with the adjacent UBA domains of other molecules. **B.** Similar molecules A interact through a β-sheet with their N-termini leading to stabilization of this region.

The molecules are arranged as symmetric dimers in the unit cell. The UBA domains of molecules A are in contact with UBA domains of another molecule A and a C-lobe of an adjacent molecule B. The general fold of the overall molecule and organization of the domains including the UBA domain are similar to MARK2.

3.5.2 Conformation of MARK3

The two molecules of MARK3 have similar global conformations. Most residues are completely modeled including the activation loop which was mostly disordered in MARK2 structures.

N-Lobe

The N-lobe is very similar in A and B molecules except the terminal two residues at the beginning of the sequence which fold in opposite directions. In molecule A, β-sheet interaction between molecules leads to stabilization of N-terminal residues thus one additional residue is seen in molecule A. The helix C swings out preventing the formation of the ion pair interactions between the conserved residues Lys85 in β-sheet 3 and Glu103 in

helix C, found in active kinases. Instead, these residues are stabilized by the new polar interactions (see below, section C-lobe) (Fig. 3.11).

C-lobe

Most of the structural parts of the C-lobe are visible including the activation loop but the activation loop is the region where most differences exist between molecules A and B. The Asp196 of the DFG motif is stabilized with a salt bridge with the Lys85 of the N-lobe which co-ordinates the α and β phosphates of the ATP. Phe199, the residue following the DFG motif seems to enter into the hydrophobic pocket of ATP. In molecule A, this residue is well defined and fixed conformation, however in molecule B, the conformation of this residue as calculated from the electron density maps seems to be compatible with a double conformer. The next residue, Ser200 forms a hydrogen bond with the conserved Glu103 of helix C (Fig. 3.11).

In the following part of the activation segment, a small stretch of residues have two different conformations with variation starting with Gly206 and ending at Cys213. This region starts with two glycines at residues 206 and 207 indicating that the loop is extremely flexible.
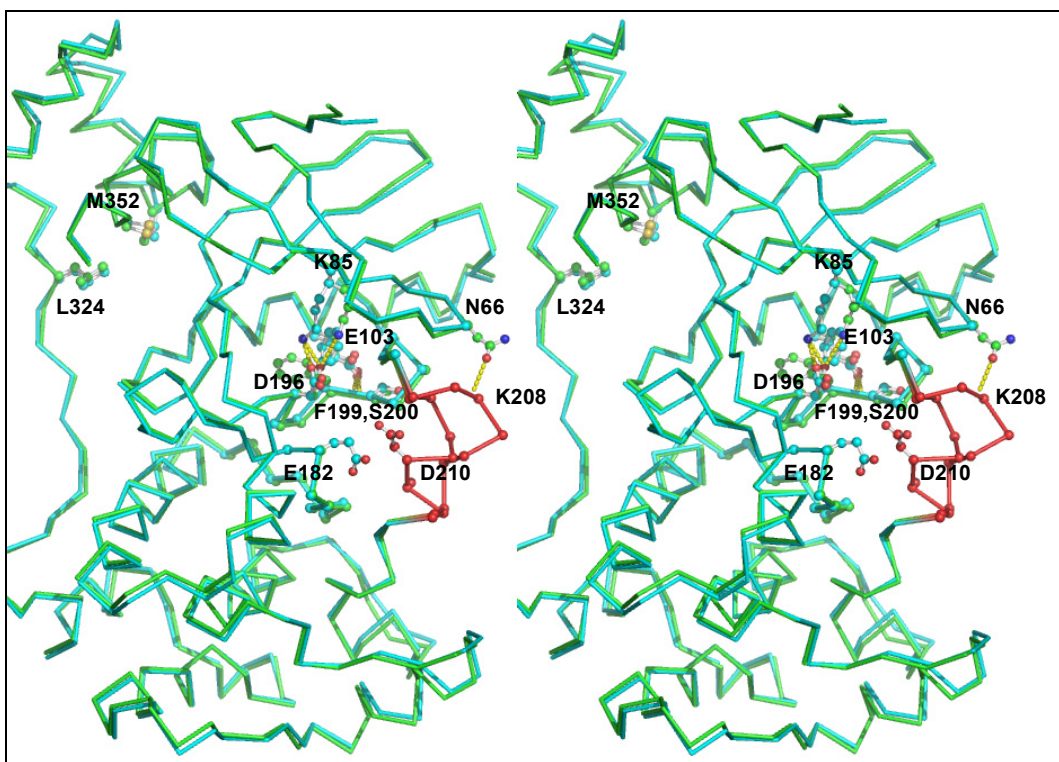
Figure 3.11: Overall conformation of the MARK3 structure. Stereo views of the different interactions present in the MARK3 crystal structure are shown. Lys85 which co-ordinates the ATP is hydrogen bonded to the Asp193 of the DFG motif, the conserved Glu103 of the helix C is hydrogen bonded to Ser200. Phe199 seems to enter into the hydrophobic pocket of the ATP. The conformation of activation loop (colored

red) which is different in both the molecules is stabilized by the local interactions. Leu324 of the UBA linker comes close to Met352 which is sandwiched between two lysine residues.

In molecule A, the variable region forms a stretched helix, whereas in molecule B, it forms an alpha helix of about two turns (Fig. 3.11 and 3.12). As a consequence of different conformations, a hydrogen bond is formed between the Asn66 of P-loop and amide of Lys 208 of the activation loop in molecule A, whereas in molecule B, the side chains of Asp210 and Glu182 come close to each other. It is not known if the change of conformation has any functional significance. In the most inactive kinase structures, this region is usually disordered and in active structures it adopts a extended conformation. It is possible that the helical form observed in our crystal structure represents a relatively stable conformation of this region corresponding to a local minimum of the energy and that the variable region toggles between helical and stretched conformation upon activation allowing access to the ATP or substrate.
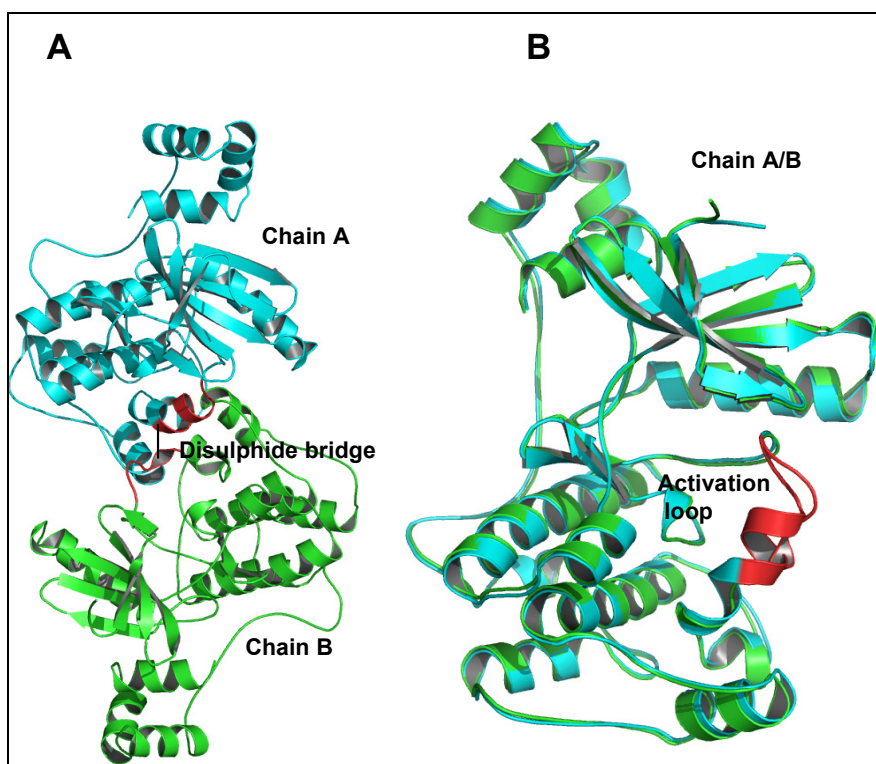
Figure 3.12: Arrangement and variability of molecules in MARK3 crystals. The variable parts of the activation loops depicted in red. **A.** The two molecules in the asymmetric unit are covalently linked by a disulphide bridge and arranged as dimers in the crystals. The activation loops and other structural elements near to it are in close contact. **B.** Superposition of the two molecules of the dimer shows that the activation loop is present in two different conformations.

Some of the features in MARK3 kinase domain are strikingly similar to the "autoinhibited" inactive form of c-Src kinases (Xu et al., 1999) (Fig. 3.13). These include,

1. The stabilization of the conserved Glu of helix C with an interacting residue from the activation loop.

2. The conformations of the activation loop are helical.

3. The polar interaction of the Asp of the DFG motif with the conserved Lys that is essential for the co-ordination of the ATP.

4. The conformation of the Asp and Phe of the DFG motif is similar to "DFG-in" configuration of c-Src (Levinson et al., 2006).
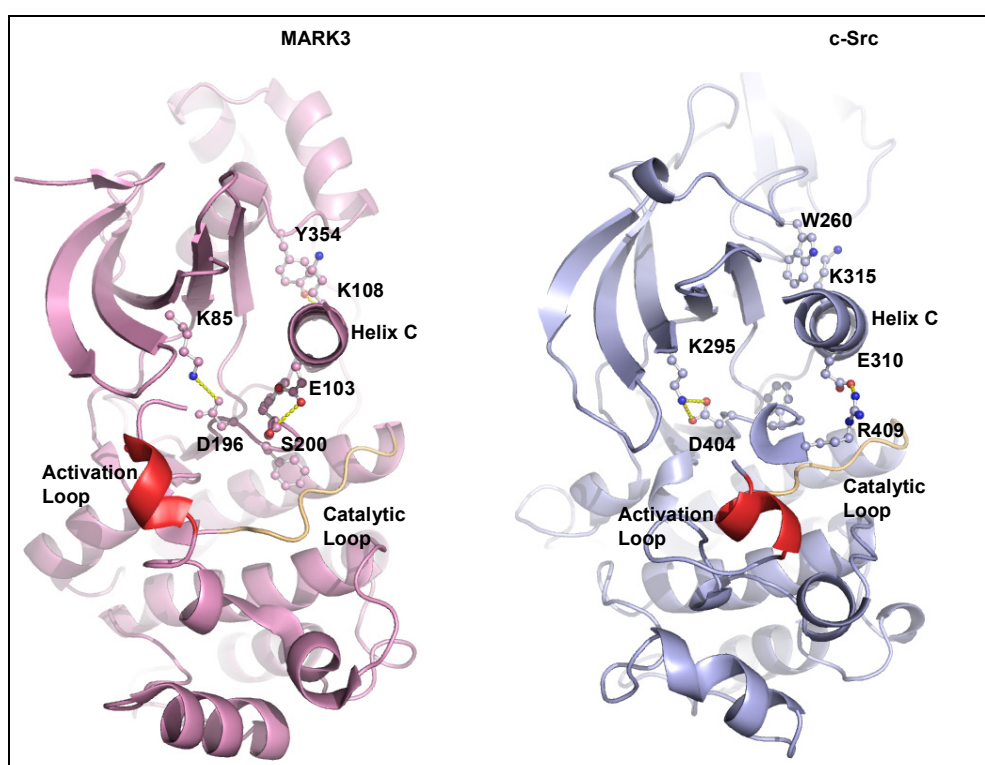
Figure 3.13: Conformation of MARK3 compared to autoinhibited c-Src. Both kinases have their helix C swung out, the catalytically important Asp (196 in MARK3, 404 in c-Src) of the DFG motif is hydrogen bonded to conserved Lys (85 in MARK3, 295 in c-Src) needed for co-coordinating the ATP, conserved Glu (103 in MARK3, 310 in c-Src) of helix C is hydrogen bonded to a residue from the activation loop. A bulky amino acid residue outside the catalytic domain interacts with helix C (in c-Src, src-linker residue, Trp260 interacts with the side chain of Lys315 similar to Tyr354 of the UBA domain with Lys108). The activation loops are in helical conformation (red). The catalytic loops also seem to be in similar conformation (yellow).

5. Interactions between side chains of Trp260 of the src linker and Lys315 of helix C which is similar to interactions between the side chain of Tyr364 of the UBA domain and amide of Lys108 of helix C (Fig. 3.13).

Conservation of the features of c-Src in MARK3 indicates that the conformation of MARK3 also seems to be locked in "Autoinhibited" form.

UBA domain

The UBA domain is tethered to the N-lobe through hydrophobic interactions. Met352 which is sandwiched between two lysines comes close to the Leu324 of the UBA linker. The amide of Lys108, located at the C-terminus of helix C forms a hydrogen bond interaction with the Tyr 354 located in the loop between the last two helices of the UBA domain (Fig. 3.12).
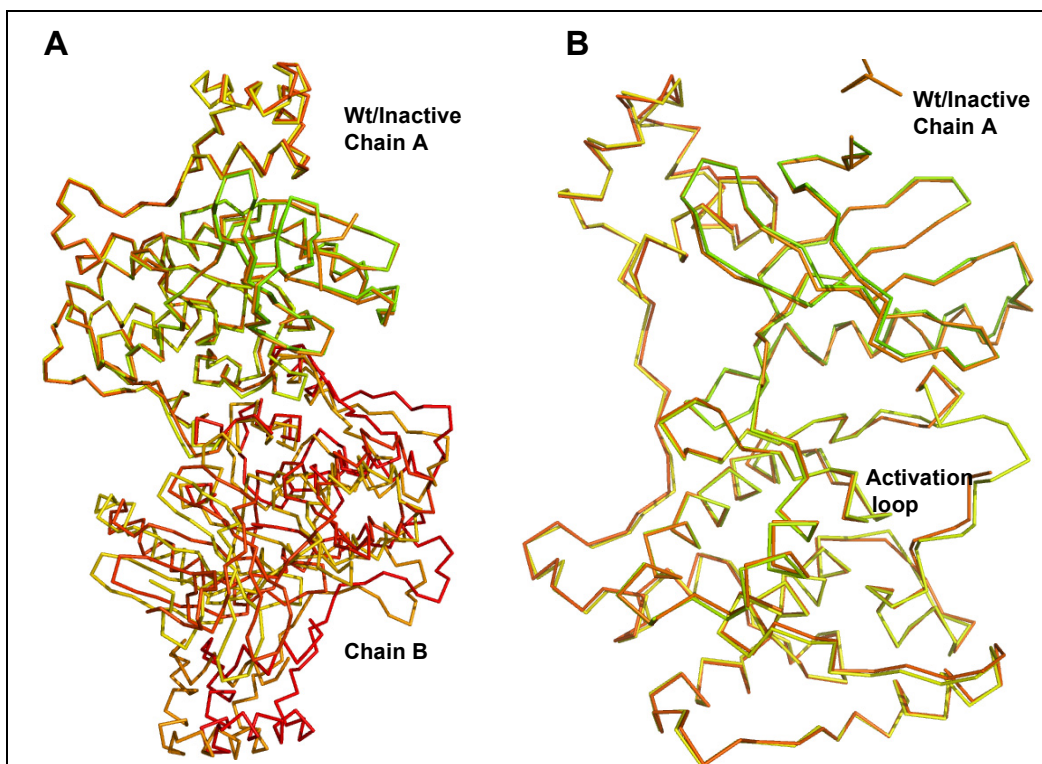
3.6 Comparison of wild type and inactive double mutant structures of MARK3

Wild type MARK3 (Murphy et al., 2007) crystallized in space group $P2_12_12_1$ with two molecules in the asymmetric unit. The inactive double mutant crystallized in space group C2 also with two molecules in the asymmetric unit. In the inactive mutant structure, the two molecules A and B correspond to molecules linked through a disulphide bridge. In the wild type structure, the disulphide bridge between the molecules A and B is not represented since non disulphide linked molecules are modeled in the structure. On rearranging the molecules of wild type structure similar to the inactive the double mutant dimer (Fig. 3.14A), the possibility of formation of disulphide bridge is present even in the wild type structure.

Other differences include the fact that the wild type construct has extra five residues at the N-terminus which do not belong to the kinase and three residues at the C-terminus which are invisible in the structure. On superimposing molecule A of the wild type structure with molecule A of the inactive structure, the conformation of the activation segment is similar in both the molecules (Fig. 3.14B). The activation segment from residues 205-207 is invisible in both molecules of the wild type structure.

The overall conformation of the UBA domain is also similar in both molecules. The reported π-π stacking interaction between Arg331 and Tyr361 which contributes to the stabilization of the hydrophobic core (Murphy et al., 2007) is also present in the inactive structure.

Figure 3.14: Comparison of wild type and inactive mutant of MARK3. A. Overlay of the ribbon diagrams of wild type (brown and red) and double inactive (shades of green) mutant structures of MARK3 shows that the arrangement and conformation of the molecules are similar. The molecule B of the wild type structure is slightly displaced with respect to molecule B of inactive double mutant. B. Overlay of the molecules A of both the structures shows that the wild type structure has extra non catalytic residues at the N-terminus and the activation loop is partly disordered in the wild type structure.

3.7 Comparison of MARK3 and MARK2

MARK2 crystallizes in space group $P6_1$ with one dimer per asymmetric unit. The arrangement of molecules in the MARK3 crystals is different, However, dimers which are formed by disulphide bridges are the basic building units in both types of crystals. The dimers in MARK2 have a proper two-fold symmetry (NCS), MARK3 possesses a similar NCS but with a slight distortion. The arrangement of the monomers, conformation and organization of the domains are also similar. To compare the conformations of the molecules, comparison is done between the molecule A of inactive double mutant structure of MARK2 (Panneerselvam et al., 2006) and the molecule A of inactive double mutant structure of MARK3. For the sake of simplicity of the comparison, MARK2 numbering is used. To convert to MARK3 numbering, add + 3 to MARK2 residue numbers.

3.7.1 N-lobe

The helix C of MARK3 swings out relative to C-lobe of MARK2. This results in substantial dislocation of the helix C, away from the C-lobe (Fig. 3.15).

3.7.2 C-Lobe

The activation segment was mostly disordered in MARK2 from residue 193 to 219. In the MARK3 structure, the main trace of the entire activation segment along with the activation loop is completely visible. The activation segment is nestled to helix C and the P-loop. The activation segment is stabilized through several interactions from the N-lobe. This could be one of the reasons why the activation segment is completely visible in MARK3. It is also possible that helix C swings out of the catalytic cleft to accommodate the activation segment thus leading to more open, inactive structure of MARK3. The C-terminal part of the activation segment which was visible in the MARK2 structure was in close contact with the activation segment of the other molecule of the dimer. This interaction and the other intermolecular contact zones which lead to stabilization of the MARK2 dimers are conserved in the MARK3 structure (Fig. 3.16). The conformation of the catalytic loop and other structural elements of the C-lobe are also similar to MARK2.
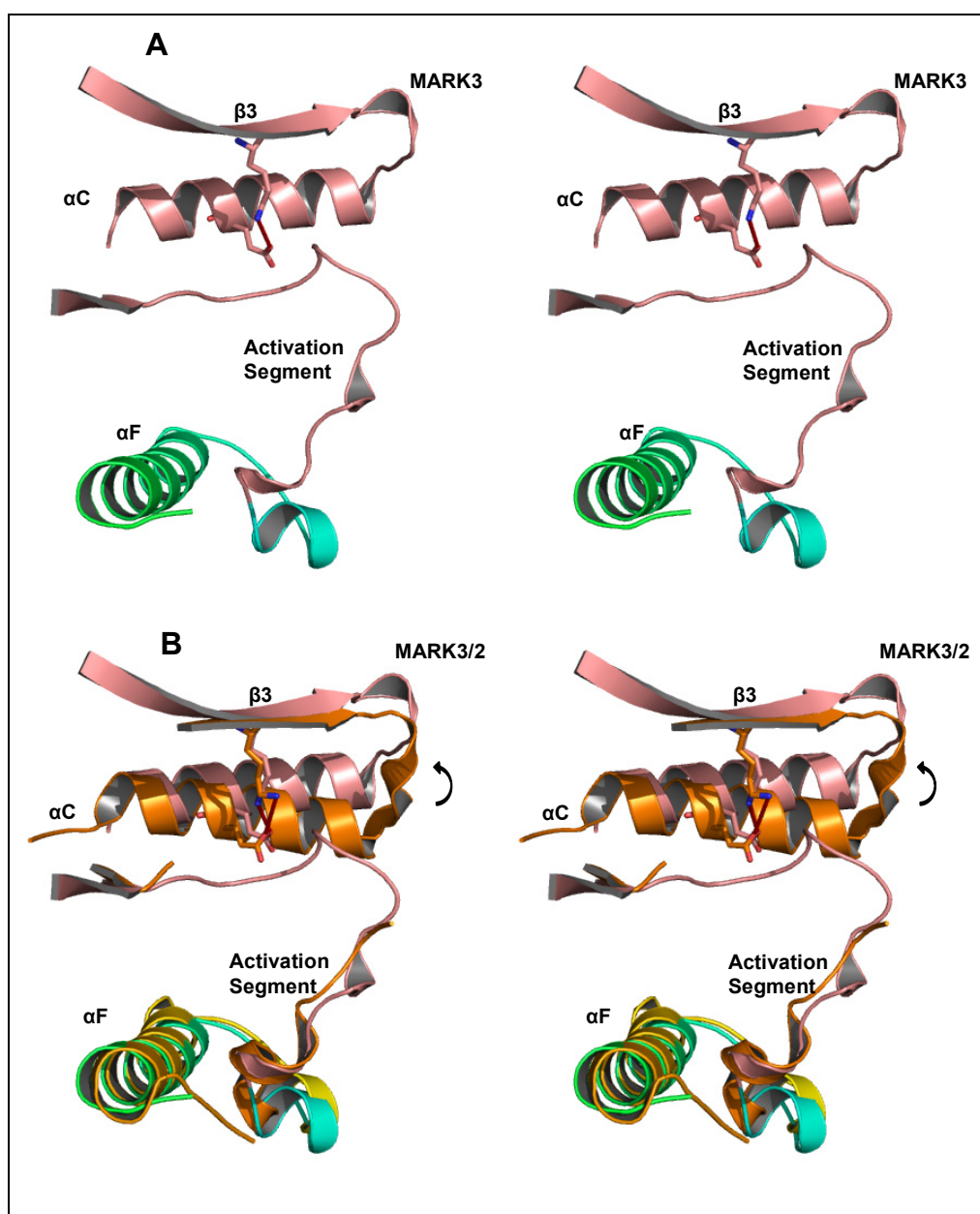
Figure 3.15 (stereo view): Helix C and activation segment of MARK3 and MARK2. The conserved polar interaction between Lys82 and Glu100 is shown in sticks. **A.** The activation segment of MARK3 is nested to helix C and is stabilized through several interactions from N-lobe. **B.** Superposition of MARK3 and MARK2 in the same region shows that helix C of MARK3 swings out as shown by an arrow mark, more than helix C of MARK2, relative to the C-lobe. Thus the MARK3 structure represents more open and inactive form of structure then MARK2.

3.7.3 UBA domain

The overall fold of the UBA domain is conserved with the UBA domain attaching at the same place in MARK2 structure with similar interactions despite the fact that the UBA domain contains the most amino acid differences between these two isoforms of MARK (Fig. 3.16).

3.7.4 Dimerization

MARK2 dimers are arranged in such a way that the two catalytic domains face each other with their active sites. The three interacting zones (zone1, 2 and 3) of interactions which stabilize the MARK2 dimer are also present in MARK3 but are slightly distorted due to non perfect NCS (Fig. 3.16). The activation loops are in contact, but their conformation is different as shown before (Fig. 3.11), in the short segment starting with tandem glycine residues. Helix G due to the slight distortion in NCS seems to induce different conformations of the activation loop in molecules A and B.
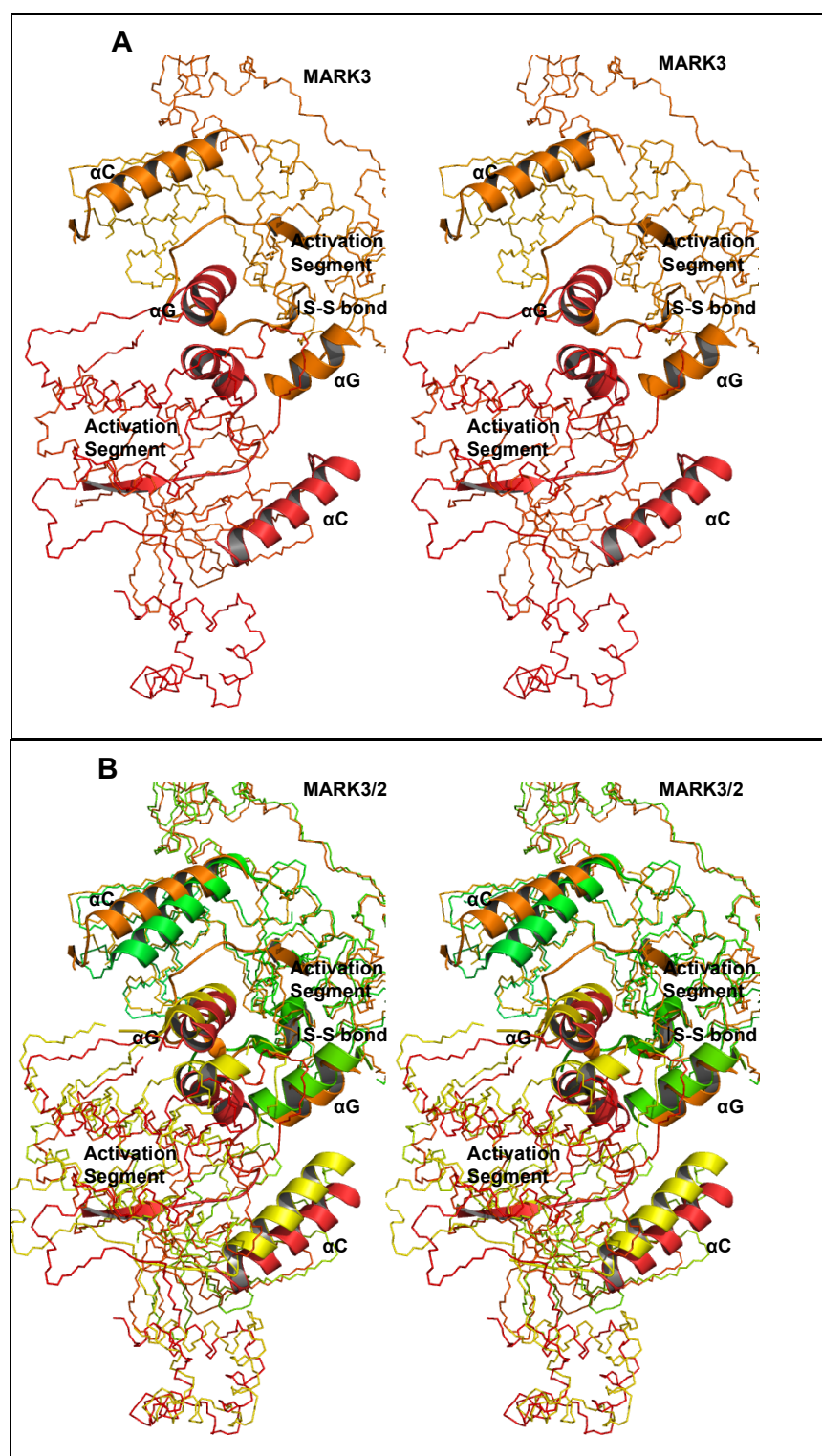
Figure 3.16 (stereo view): Structural elements involved in dimerization of MARK3 and MARK2. Ribbon diagram of the MARK structures highlighting the structural elements (shown as cartoons) involved in intermolecular contacts. **A.** Molecules of the dimer of MARK3 are linked by a disulphide bridge. The activation loops are in close contact with the activation loop of partner molecule of the dimer. Helix G plugs into the cleft formed by helix C and the activation segment. **B.** Overlay of MARK3 and MARK2 dimers shows that these interaction elements are similar to MARK2 dimer.

3.8 Structure of MARK1

3.8.1 Organization of the MARK1 crystal structure

MARK1 crystallizes in $P2_12_12_1$ space group with eight molecules per asymmetric unit. The molecules are packed as two lozenge-shaped "tetramers", bent across the short diagonal (molecules A, B, C, D, and molecules E, F, G, H). The UBA domains of the tetramers are in contact and are important elements of the crystal packing (Fig. 3.17). The overall fold of all the molecules is similar to MARK2.

3.8.2 Conformational variability of MARK1 molecules

The general fold of the eight molecules in the MARK1 crystal is similar except at regions of local interactions which lead to local and global variations. MARK1 crystal structure is numbered according to the numbering of MARK2. To reach MARK1 numbering; add +7 to MARK2 sequence numbering.

Among all the molecules, only molecules E and F are complete including the activation loop. Molecules D, G and H are largely affected by disorder.

To calculate superpositions and quantify the relative displacements, a structural core consisting of the core elements of N- and C-lobe are used. The structural core for the N-lobe was consisting of β strands 1,2, and 3, for the C-lobe was helices E and F. Due to small domain organization and relatively smaller size compared to N- and C-lobe, all the three helices of the UBA domain were used.

On superimposing the molecules using the structural core of the N-lobe, the C-lobe rotates upto 10° which results in shifts upto 7-8 Å (Fig. 3.18A). The UBA domain is relatively fixed compared to other domains which could be due to small domain organization and tight interactions with the N-lobe.

A

B
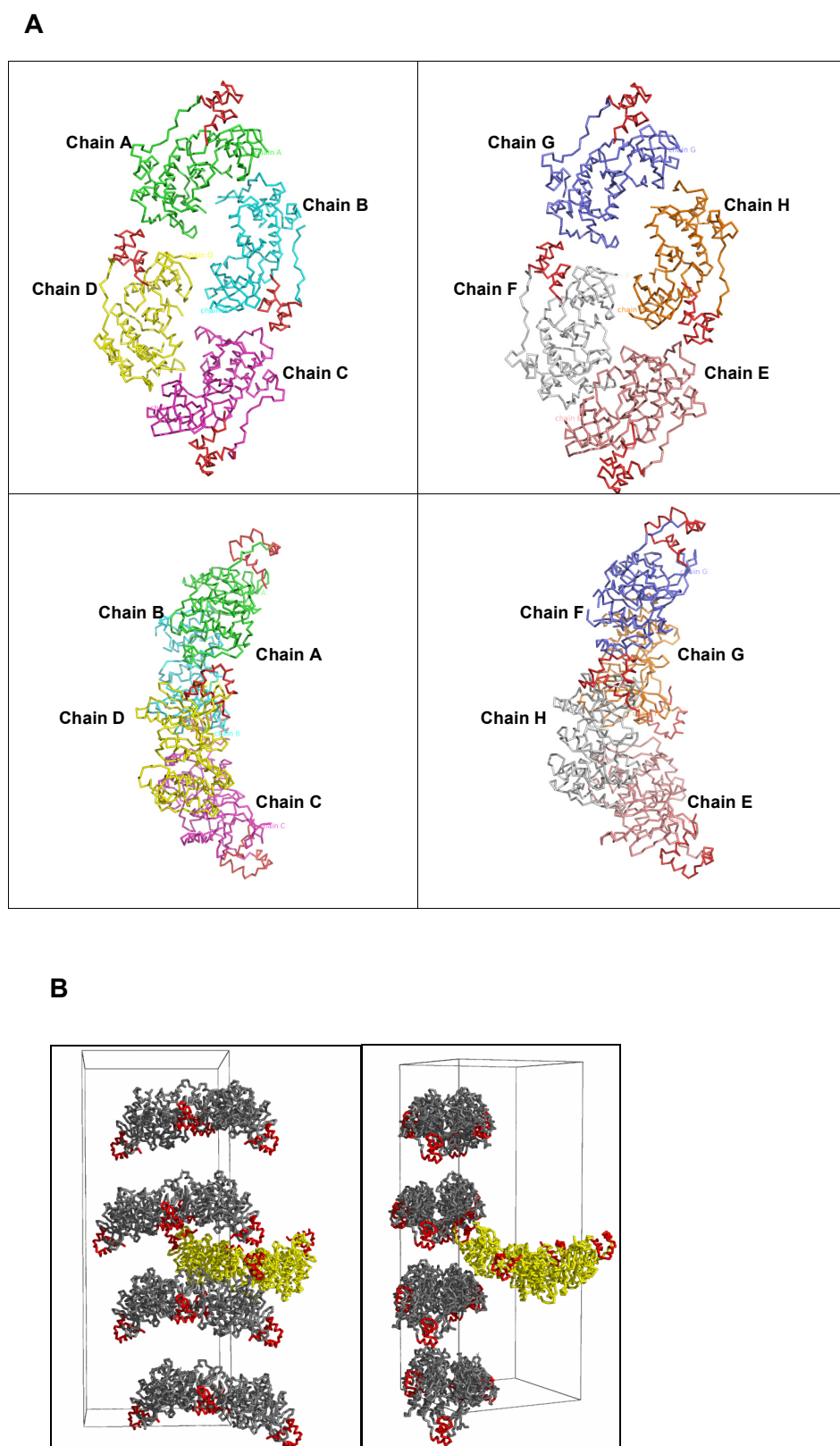
Figure 3.17: Crystal packing and arrangement of tetramers in MARK1. A. Front and side views (rotated by 90°) of tetramers formed by molecules A, B, C, D and E, F, G, H. **B.** Stacking of tetramers (grey) along the c-axis; only half the number of tetramers in the unit cell is shown. The same stack of tetramers as before, after rotation by 90°. One representative tetramer of another stack (yellow) is shown which illustrates the linkage of the grey tetramers with the remaining tetramers. The linkage relies heavily on the UBA-UBA interactions. In all panels, UBA domains are highlighted in red. Cα traces include structural elements that have been modeled tentatively.
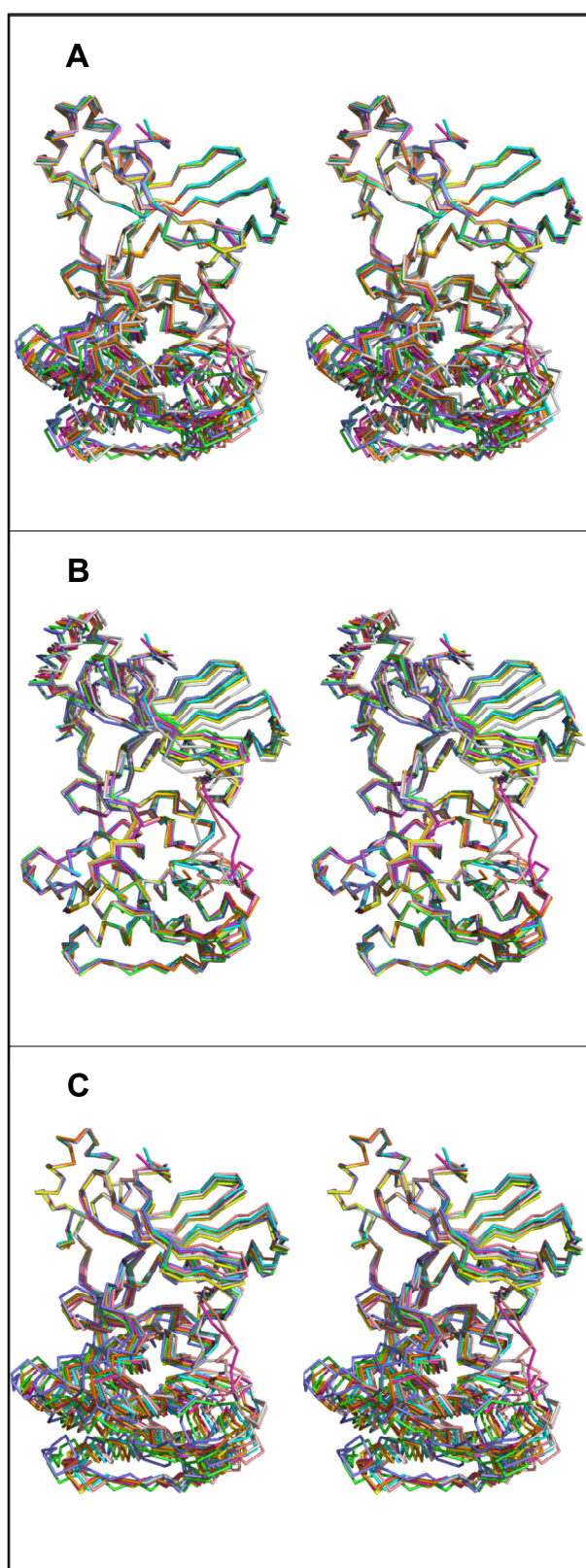
Figure 3.18 (stereo view): Conformational variability of MARK1. Overlay of Cα
traces with the eight molecules of MARK1. Superposition by RMS minimization of
deviations in Cα positions of core structural elements of the N-lobe (β1 to β3) (**A**), the
C-lobe (helix E and helix F) (**B**), and the UBA domain (complete) (**C**). For this overlay,
a model of the MARK1 crystal structure is used, with some ill defined regions of the
structure that are modeled tentatively. Variable regions in N-lobe include helix C and
loop preceding it, in the C-lobe include activation segment. The UBA domain is
relatively fixed due to interactions with the N-lobe.

One of the highly variable regions in the N-lobe consists of helix C and the loop preceding it (Fig. 3.18B). The C-lobe has high variability in the regions of activation loop, its C-terminal anchor and the N-terminus of helix F. The activation loop is visible only in two molecules, molecules E and F (Fig. 3.18B, 3.19). It is flexible and exhibits a variable conformation. The activation segment is stabilized by hydrogen bonds between Lys96 and conserved Glu100 of helix C to Ser197 of the activation segment, and Tyr170 of the catalytic loop to Phe194 of the DFG motif (Fig. 3.19). The C-terminal parts of the activation loops in molecules E and F are in contact similar to the symmetric dimers of MARK2. In the molecules D, G and H, major parts of the C-lobe like the C-terminal anchor, P+1 loop, helix E and helix G are highly disordered and thus invisible.

The UBA domains are well defined in all the molecules and adapt to the displacements of the C-lobe and the N-lobe (Fig. 3.18C). Tyr351 which is present in the loop between the last two helices of the UBA domain interacts with Lys105 of helix C.
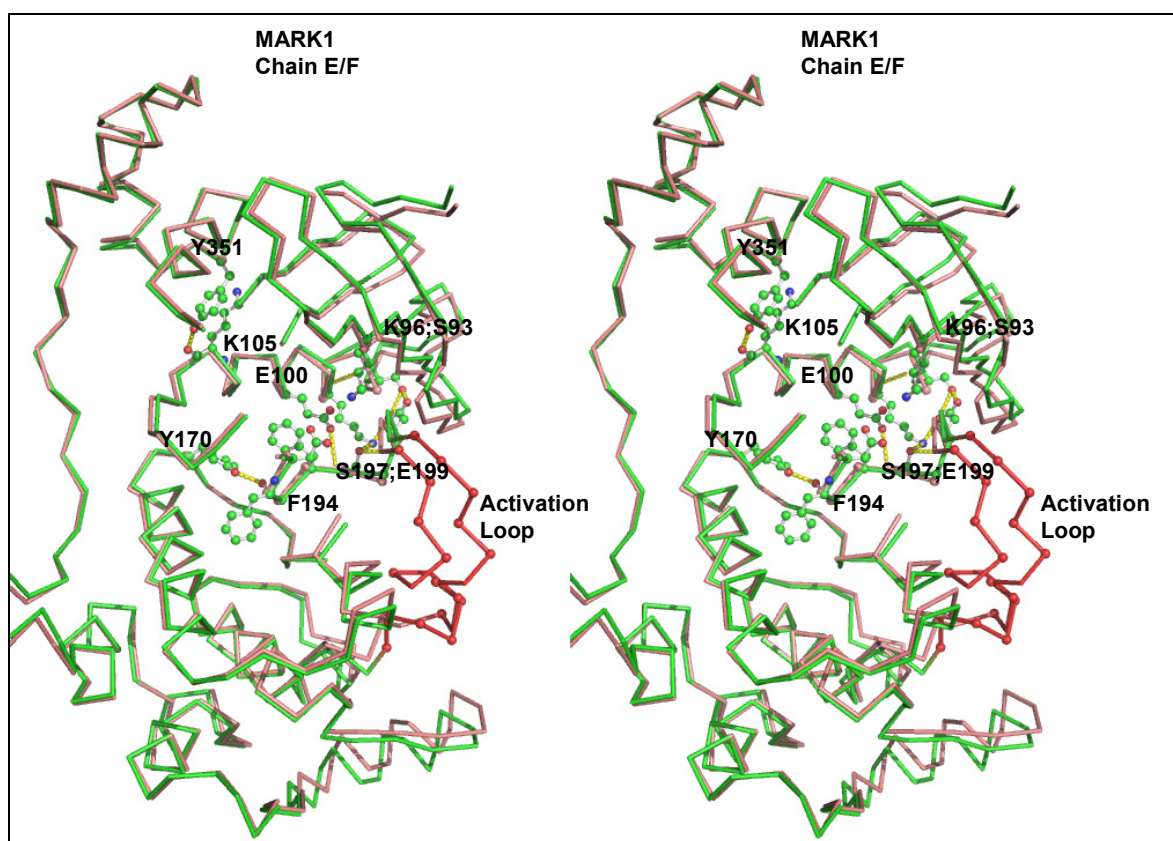
Figure 3.19: Conformation of the MARK1 structure. Stereo view of the MARK1 (molecules E and F) crystal structure. The activation segment is stabilized by several hydrogen bonds formed between the Lys96 and conserved Glu100 of helix C to the Ser197 of the activation segment, Tyr170 of the catalytic loop to Phe194 of the DFG motif. The conformation of the activation loop is variable (shown in red). Tyr351 of the UBA domain interacts with Lys105 of helix C. Some parts of the kinase structure are deleted to have unobstructed view of the interactions.

3.9 Comparison of MARK1 and MARK2

Comparisons are done between molecule E of MARK1 and molecule A of inactive double mutant of MARK2 (Panneerselvam et al., 2006).

3.9.1 N-lobe

Helix C of MARK1 performs a movement relative to MARK2 that consists of a small shift in axial direction combined with a tilt rotation of about 5°. This movement also extends to the adjacent loop and strands β4 and β5. The rotation of the N-lobe and the movement described before leads to a substantial dislocation of helix C farther away from the C-lobe (Fig. 3.20).

3.9.2 C-lobe

Most of the activation segment is disordered and invisible including the DFG motif in the MARK2 structure. Only the C-terminal part is traceable since it is stabilized by the interactions from the similar regions from the partner molecule of the dimer. In MARK1, the N-terminal part of the activation segment is well defined and similar in all the molecules. The activation loop is nestled to helix C and the P-loop. The activation segment is visible only in those molecules which are stabilized by hydrogen bond interactions from N- and C-lobe as described before. The C-terminal part of the activation segment forms a severely distorted helix in molecule E. The C-terminal end of the activation segment is similar in most of the MARK1 molecules. This region is well defined in MARK2 due to stabilization by interacting activation loops.

The catalytic loop of MARK1 assumes a different fold from that of MARK2. The change in conformation of the catalytic loop is due to change of residue 170 which is located at the end of helix E and beginning of the catalytic loop. In MARK2, this residue is Phe170 and its side chain points to the exterior of the molecule, whereas in MARK1, it is Tyr170 and is flipped towards the interior with its hydroxyl group forming a hydrogen bond with the oxygen of the Phe194 of the DFG motif. The inside flipping of Tyr170 causes an inverse flip of His173 (Fig. 3.21).
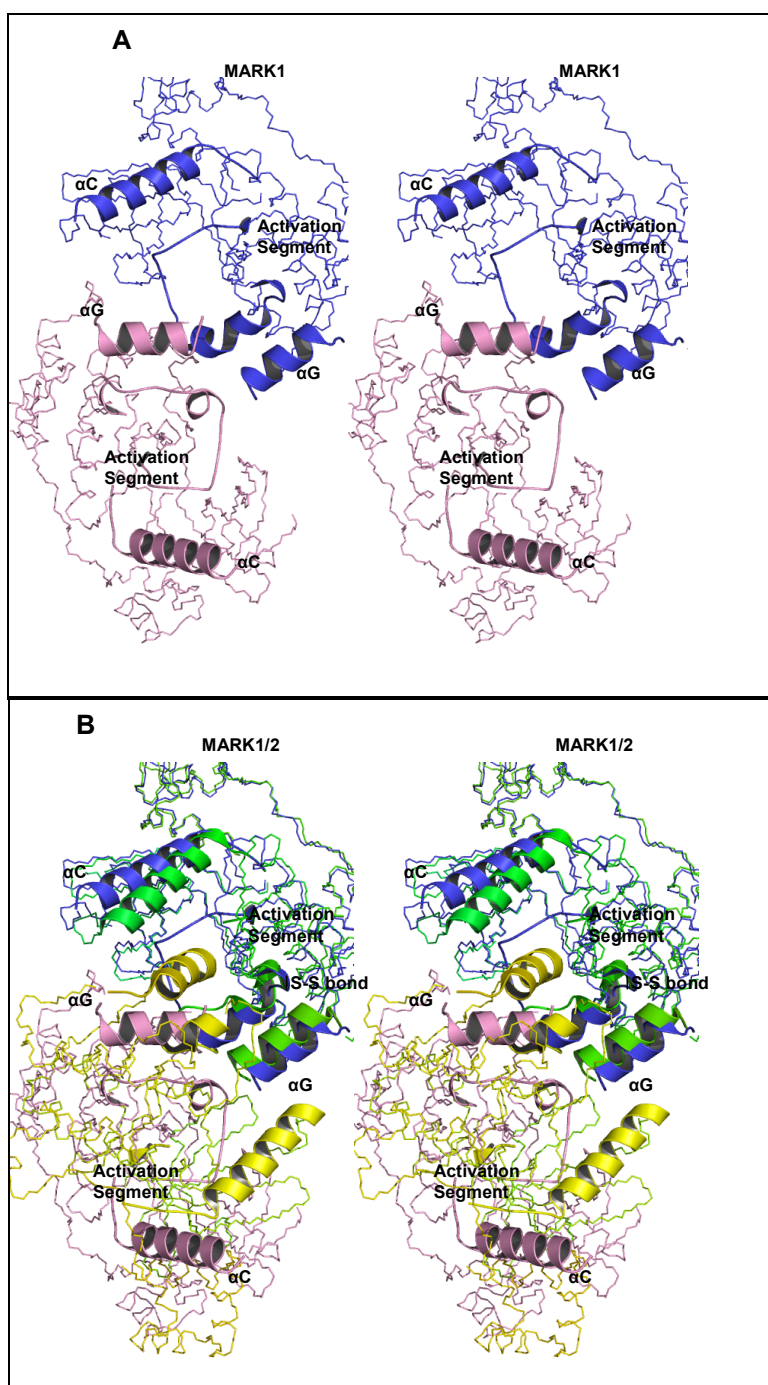
3.9.3 UBA domain

Most amino acid differences between MARK1 and MARK2 occur in the UBA domain. The changes are conserved and directed to the outside. Despite that, the overall fold and docking of the UBA domain to the N-lobe is similar to MARK2.
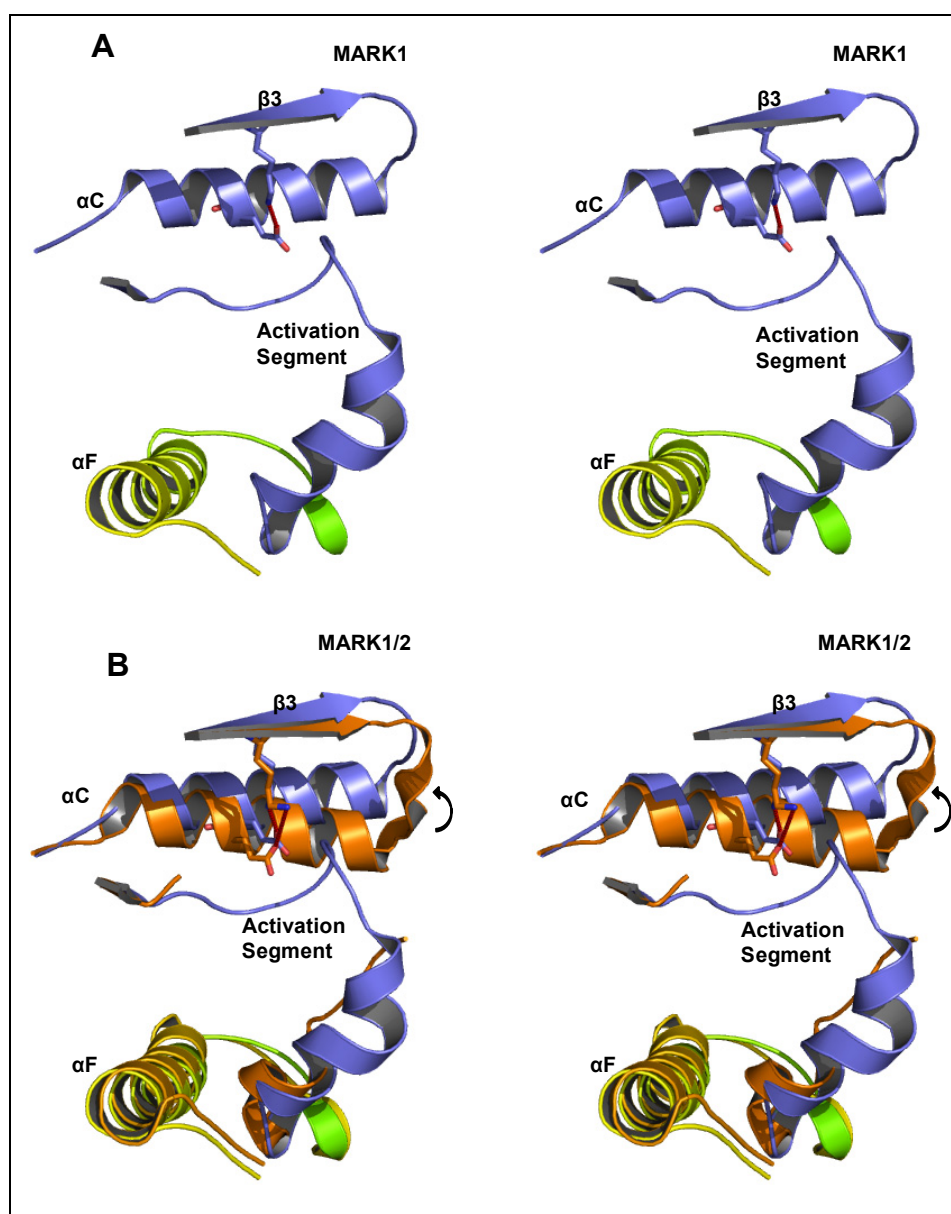
Figure 3.20 (stereo view): Helix C and activation segment of MARK1 and MARK2. The conserved polar interaction between Lys82 and Glu100 are shown in sticks. **A.** The activation segment in MARK1 (molecule E) is nestled to helix C and stabilized through hydrogen bonds from N- and C-lobe. **B.** Superposition of the MARK1 with MARK2 in the same region shows that helix C of MARK1 swings out more than helix C of MARK2, relative to the C-lobe as indicated by an arrow mark. Thus, the MARK1 structure represents more inactive and open form compared to MARK2.

Figure 3.21: Effect of the amino acid 170 on the conformation of the catalytic domain. (Stereo view) (Cartoon diagram). Residues 170, 173 and 194 are shown in stick model. In MARK1, the side group of Tyr170 is buried and forms a hydrogen bond with the carbonyl oxygen of Phe194 of the DFG motif, thus stabilizing the N-terminal anchor of the activation segment. The backbone flip by the side chain of Tyr170 in MARK1 results in an inverse flip of His173. **B.** Superposition of MARK1 and MARK2 shows that the side chain of the Phe170 is exposed and directed outside.

3.9.4 Intermolecular contacts and dimerization

The activation loops of the molecules of E and F of MARK1 are in contact similar to MARK2 dimer. The interaction elements involve helix G plugging into the cleft formed by helix C and the activation loop similar to interactions of the MARK2 dimer. Even tough there is no special symmetry between molecules E and F of MARK1, these molecules mimic the symmetric dimers of MARK2 in terms of its arrangement and stabilizing interactions (Fig. 3.22).

Figure 3.22 Structural elements involved in intermolecular contacts of MARK1 (molecules E and F) and MARK2. Ribbon diagram of the MARK structures highlighting the structural elements (cartoon diagram) involved in intermolecular contacts. **A.** Molecules E and F are involved in intermolecular contacts. The activation loops are in close contact with the interacting partner molecule. Helix G plugs into the cleft formed by helix C and the activation segment. **B.** Overlay of MARK1 (molecules E and F) with MARK2 dimer shows that the interaction elements of MARK1 are similar to the elements of dimer formation in MARK2.

3.10 Conformation of MARK in solution

One of the important features of MARK crystal structures is that the UBA domain attaches to the N-lobe of the kinase domain through hydrophobic interactions and to the C-lobe through the UBA linker. The UBA domains are named based on the similarity of these sequences to proteins binding to mono-or poly-ubiquitin. In MARK2 crystal structures, the presumed ubiquitin binding site (Ohno et al., 2005) is occluded on the MARK-UBA interface by binding of the UBA domain to the N-lobe (Panneerselvam et al., 2006). An important question arising from this observation is, if the UBA domain was constrained by the crystal lattice to bind to the N-lobe and it might detach from the N-lobe in solution state and certain states of regulation like activation. To study such effects, Small-Angle X-ray Scattering (SAXS) analysis was performed in collaboration with Efstratios Mylonas and Dr. Dmitri I. Svergun of EMBL, Hamburg on the wild type constructs of two different isoforms of MARK and a pseudophophorylation state of MARK2 mimicking the phosphorylation of the activation loop by MARKK (Timm et al., 2003).

The results of the scattering studies (Fig. 3.23) shows that scattering curves of wild type constructs of MARK1 (curve 1) and MARK2 (curve 2) were similar to each other within the experimental errors (R_g and D_{max} values of MARK1 are 23.4 ± 0.6 Å and 75 ± 5 Å, for MARK2 are 23.2 ± 0.6 Å and 75 ± 5 Å, respectively).

These values are in good agreement with the R_g value of 22.9 Å and D_{max} value of 73 Å computed from the crystal structures of MARK accounting for the hydration shell using the CRYSOL program (D. Svergun, 1995). This indicates that the UBA domain remains attached to the N-lobe even in solution, free of crystal constraints.

Calculating the R_g and D_{max} from scattering of the activation loop mutant (curve 3) (Fig. 3.23) gives a result of 23.7 ± 0.7 Å and 77 ± 6 Å respectively, indicating that there is no major change in conformation upon phosphorylation of the activation loop and the UBA domain still remains attached to the N-lobe. In summary, the SAXS data shows that in ground or activated state, there is no major re-arrangement occurring in the kinase domain.
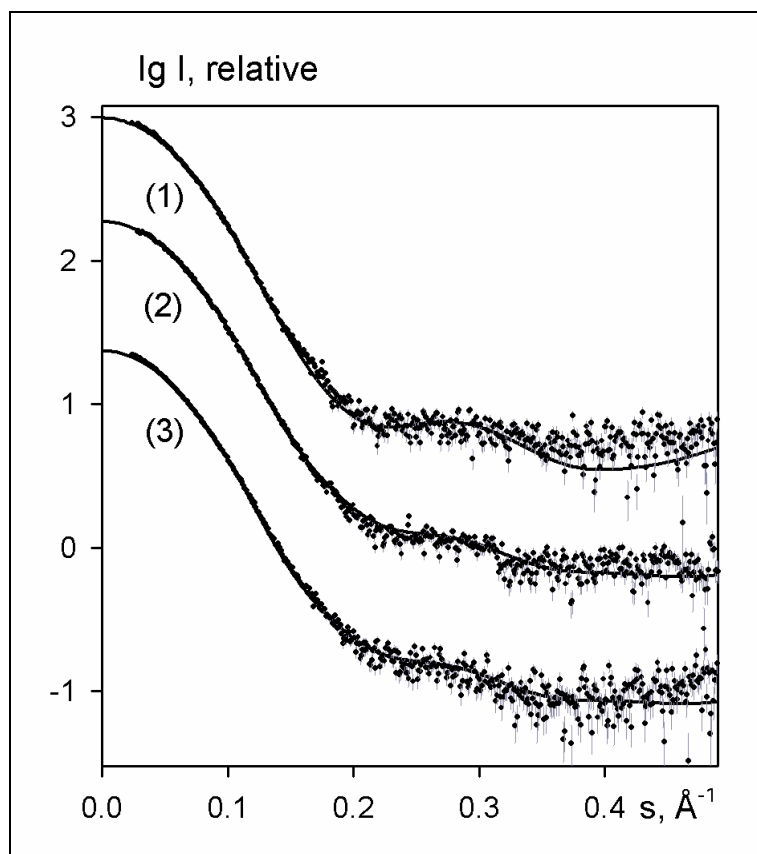
Figure 3.23: SAXS patterns from MARK1 and MARK2 isoforms. Plots (1-3) correspond to MARK1, wild type MARK2 and its T208E mutant, respectively (the T208E mimics the phosphorylation by MARKK or LKB1, active form of MARK2). The experimental data are displayed as dots with error bars, the fits from the crystallographic models computed by CRYSOL (Svergun et al., 1995) are displayed as solid lines. The logarithm of the scattering intensity (I) is plotted as a function of the momentum transfer s; the successive fits are appropriately displaced along the logarithmic axis for better visualization (Fig. 7 from Marx et al., 2006).

Supporting the SAXS data, additional evidence for binding of the UBA domain to the N-lobe of the kinase domain in solution comes from the MARK1 "UBA detachment mutant" which was designed to prevent interaction between the UBA domain and the N-lobe. Leu360 of the UBA domain inserts into the hydrophobic binding pocket formed by Val79 and surrounding residues. When the Val79 was mutated to Arg (Fig. 3.24) preventing the binding of Leu360 into the hydrophobic pocket thereby causing the detachment of the UBA domain from the N-lobe, the net result was that the exposure of the two hydrophobic surfaces leads to total insolubility of the protein. Thus attempts to study the "UBA detachment mutant" were not successful due to insolubility problems, but this result once again confirms indirectly that the UBA domain docks to the N-lobe of the catalytic domain even in solution thereby masking the hydrophobic surface patch and preventing aggregation.
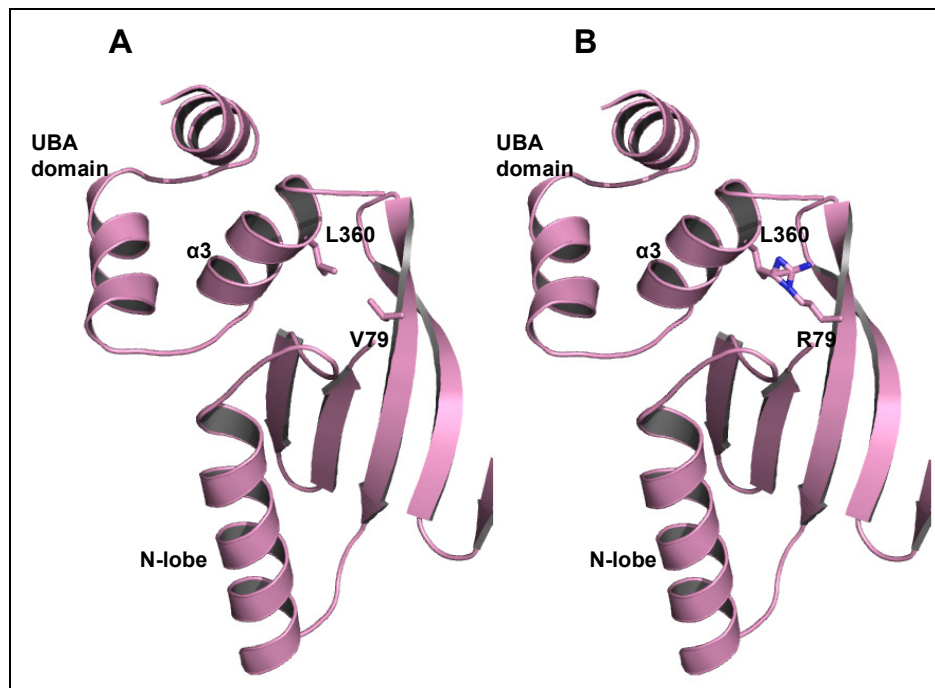
Figure 3.24: The UBA domain binds to the N-lobe of the kinase in solution. A.
Leu367 of the UBA domain inserts into the hydrophobic binding pocket formed by
Val79 and surrounding residues. **B.** Introducing Arg at position 79 results in a steric
clash with Leu360 thereby detaching the UBA domain from the catalytic domain. The
net result of this detachment is the exposure of the hydrophobic surfaces both from the
kinase and UBA domain leading to destabilization and insolubility of the protein.

3.11 Role of the UBA domain in kinase activity

The crystal structures of MARKs show that the kinase domain is present in an inactive and
open conformation and the UBA domain strongly binds at the N-lobe. This leads to the
hypothesis that the UBA domain might be pulling the N-lobe of the kinase, keeping it in a
open and inactive conformation. Thus to test if the UBA domain has any influence on the
kinase, kinase activities were tested using constructs in which the UBA domain was retained
or deleted. These constructs were tested further for activation by MARKK which activates
the MARK kinases by phosphorylating the activation loop threonine (Thr208 in MARK2)
(Timm et al., 2003). The results of the kinase assay was quantified using the TR1 peptide
which contains Ser262 of the tau protein, the main target of MARK kinases (Drewes et al.,
1998).

The results (Fig. 3.25) show that unphosphorylated MARK1 constructs with and without
UBA domain and full-length MARK1 and MARK2 have similar activities, about $0.01 -$
$0.05 \, \text{min}^{-1}$. The basal activity of the MARK2 construct without UBA domain was slightly
higher ($\sim 0.1 \, \text{min}^{-1}$). Phosphorylation by MARKK increases the activity of all constructs
including the full length proteins; however, the extent of activation is different. The activity

of the full-length kinases increases to about 0.25 min^{-1}. Activation by MARKK was highest for the constructs without UBA domain (0.9 min^{-1} for MARK1, 0.6 min^{-1} for MARK2). For the constructs with UBA domain, the activities were intermediate (0.5 min^{-1}, MARK1) or close to that of the full-length kinase (~0.15 min^{-1}, MARK2). Compared to the constructs without UBA domain, the activities of the constructs comprising the UBA domain are reduced by a factor of 2 (MARK1) to 4 (MARK2). Thus, the UBA domain has a moderate but significant inhibitory effect on the kinase activity of MARK1 and MARK2 after phosphorylation by MARKK.
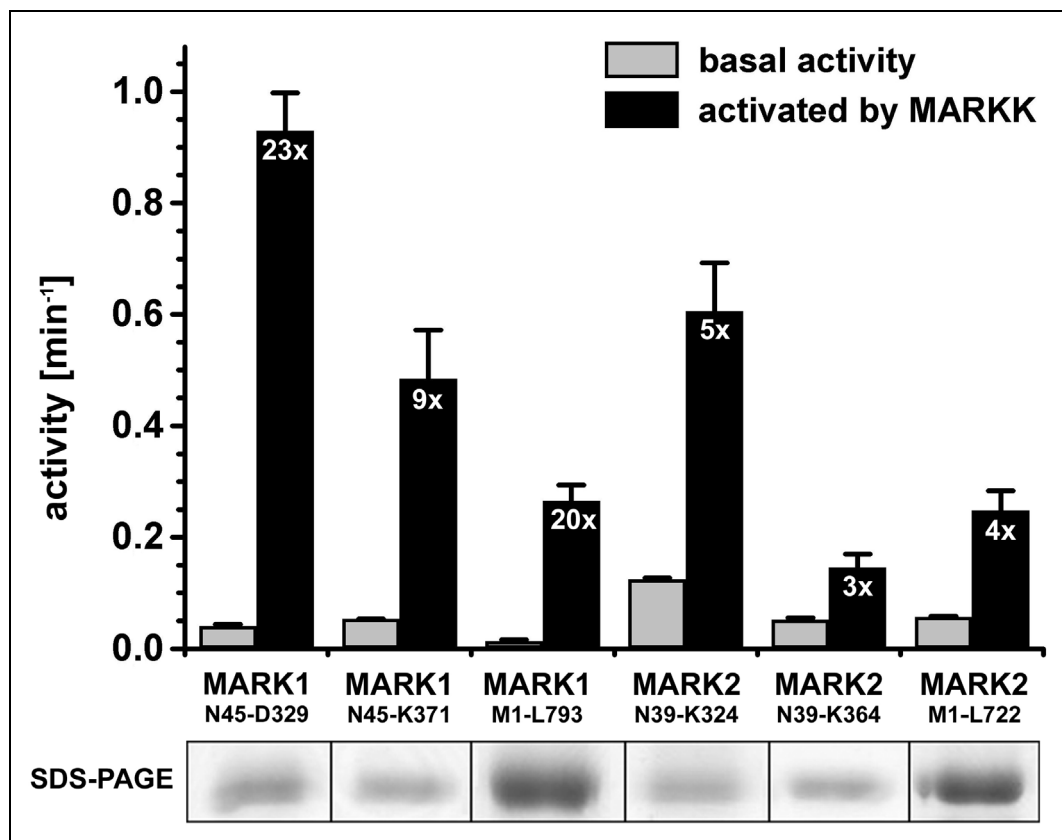

Figure 3.25: Kinase activities of constructs with and without UBA domain compared to full-length MARK1 and MARK2. All constructs have basal activities comparable to the full-length MARKs and can be activated by phosphorylation with MARKK. Constructs with the UBA domain, could not activated to the same extent as the constructs without the UBA domain by MARKK. Activities (expressed in moles of product per minute and moles of kinase) are averages of three independent measurements, error bars indicate s.e.m. values. Proteins were adjusted to the same molar concentrations by comparison with the full-length kinases (Fig. 8 from Marx et al., 2006).

4 Discussion

4.1 Effect of amino acid exchanges

All the MARK constructs used for crystallization were of the similar size, comprising the catalytic domain and the UBA domain. These isoforms differ mainly in the primary sequence of the UBA domain. About 50% of the UBA domain residues are different in all MARK isoforms. These exchanged residues of the UBA domain are conservative and are located at the loops or the termini of the helices. The overall result of change of residues is that they affect neither the folding of the UBA domain (Fig. 4.1) nor its interaction with the catalytic domain. The different crystal packing of the MARK isoforms could be due to the combined effect of amino acid exchanges in the catalytic domain and small variation in the length of the constructs. In MARK2 and MARK3, the UBA-UBA domain interactions are part of the interactions within the crystal but are of minor importance for crystal packing. In the case of MARK1, the UBA-UBA domains are the key elements in crystal packing.
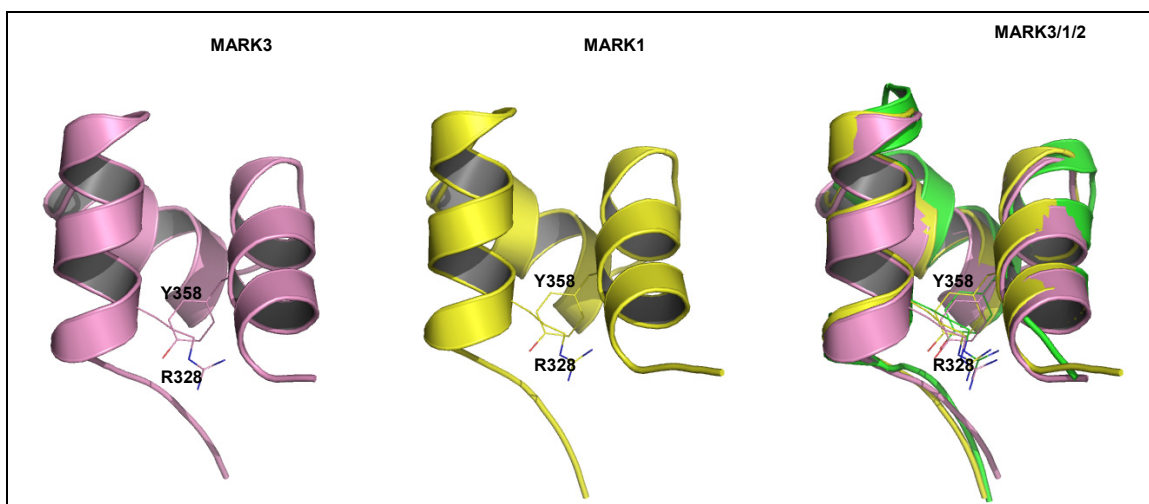

Figure 4.1: The UBA domain fold. The UBA domain folds are similar in all three MARK crystal structures (overlay of all three MARKs UBA domains) in spite of the many amino acid exchanges which are observed in this domain. The reported π-π interaction between Arg328 and Tyr358 which contributes to the stability and topology of the UBA domain reported in the wild type structure of MARK3 (Murphy et al., 2007) is present in all the available MARK crystal structures.

The catalytic domain is relatively more conserved and the variable amino acids are scattered across the kinase domain. One of the most important residues in the catalytic domains is the amino acid 170. This residue defines the end of helix E and beginning of the catalytic loop and is different in all the MARK isoforms. Compared to MARK2, hydrophobic Phe170 is changed to charged Arg170 in case of MARK3 which does not bring any effect on the conformation of the catalytic loop and thus this region is similar to MARK2 (Fig. 4.2) but in

case of MARK1, substitution by Tyr170 leads to a substantial change in the conformation of the catalytic domain. Tyr170 induces an unusual conformation of the catalytic loop where the side chain of Tyr is buried and forms a hydrogen bond with the carbonyl oxygen of Phe194 of the DFG motif (Fig. 4.2), stabilizing the N-terminal anchor of the activation loop. Owing to the importance of its location in catalytic loop, it is possible that this amino acid influences the catalytic activity, function or mechanism of action of the different isoforms of MARK *in vivo*.
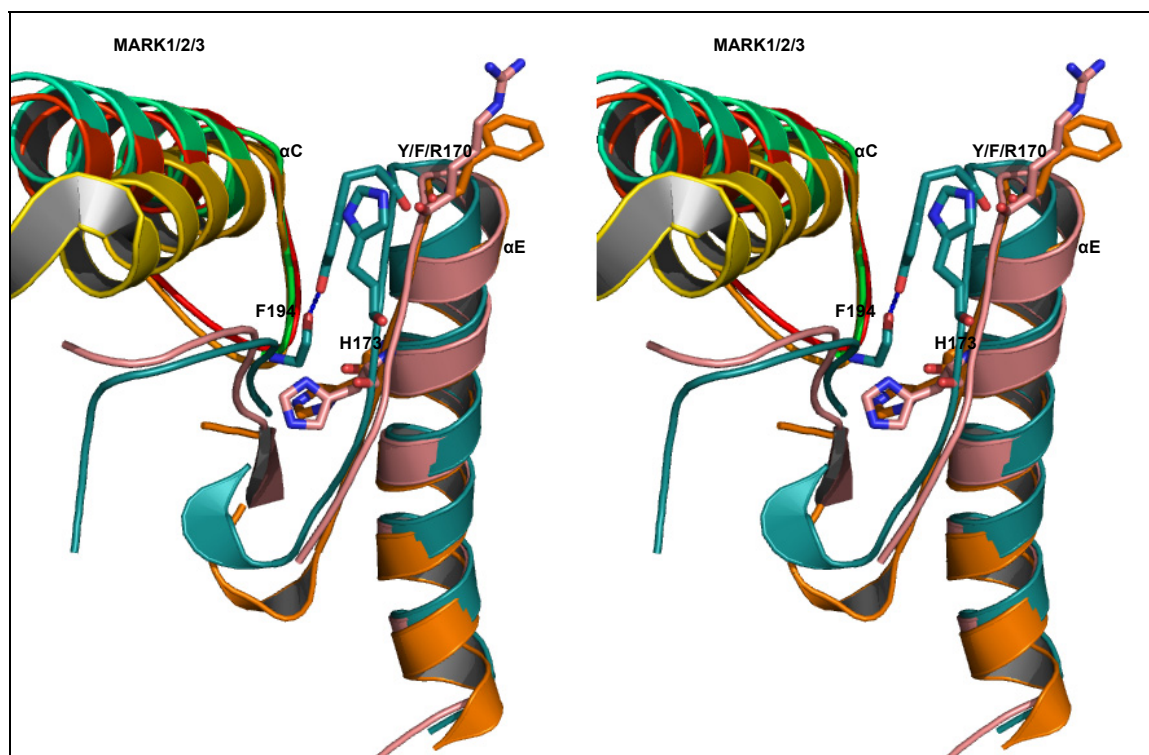
Figure 4.2: Effect of the amino acid 170 on the conformation of the catalytic domain. Stereo view of the superposition of all the three MARKs which were crystallized till now are shown as cartoons. Residues 170, 173 and 194 are shown in stick model. In MARK2, side chain of Phe170 is exposed and His173 is present on the inner side. In MARK1, the side chain of Tyr170 is buried and hydrogen bonded to Phe194 of the DFG motif, and stabilizes the N-terminal anchor of the activation segment. The inside flip of the side chain of Tyr170 results in an inverse flip of His173 and displacement of the backbone by about 6 Å. In case of MARK3, Arg170 does not bring any significant effects in the conformation of the catalytic loop as seen in the case of MARK1.

4.2 Dimerization and role of helix G in intermolecular interaction

The crystal structure of MARK2 was built from non-crystallographic symmetry dimers arranged in helical tubes. The MARK2 dimer exhibits two-fold symmetry with the catalytic sites facing each other in the center of the dimer. In MARK3, the catalytic domains are also facing each other in the centre of the dimer with their activation loops in contact. The non-

crystallographic symmetry observed in MARK3 crystals is slightly distorted compared to MARK2 but overall interactions observed between the molecules of MARK3 dimers are similar to MARK2. The slightly distorted non-crystallographic symmetry and helix G have influenced different conformations of the activation loop in MARK3. Nevertheless, the arrangement of molecules and interactions make it most similar to MARK2. In addition, N-terminal interactions between the similar molecules lead to more stabilization of the MARK3 dimer. On the other hand, the MARK1 crystal consists of tetrameric complexes interconnected by the UBA-UBA contacts. Within each tetramer, two pairs of molecules interact with each other with their activation loops and other structural elements, similar to the MARK2 dimer. These results indicate that the overall interaction elements required for the formation of the dimer are present in most of the MARK crystal structures.

The role of helix G and activation loop in forming dimers are also exemplified by the Snf1 kinase, similar to MARK2. Snf1 kinase was crystallized in two different space groups (Nayak et al., 2006; Rudolph et al., 2005) which have a different non-crystallographic symmetry but similar organization of the dimers. The helix G acts as a plug inserting into the cleft formed by the N- and C-lobe of the partner molecule in dimer. Thus, helix G and the preceding loop act as flexible docking sites in interacting with the similar molecules or interaction partners.

4.3 Conformation of MARK in solution

The UBA domain is one of the important domains involved in protein-protein interactions. Studies based on sequence comparison of proteins containing the UBA domains, which either bind or do not bind mono- or poly-ubiquitin (Raasi et al., 2004; Varadan et al., 2005), indicated that the UBA domains of MARK belong to the class of UBA proteins which do not bind to ubiquitin. Thus, the potential role of the UBA domains in MARK could be to regulate the kinase activity by small conformational rearrangements in certain states of regulation.

The results from the SAXS experiments and "UBA detachment mutant" strongly support the observations from the crystal structure that the UBA domain binds to the N-lobe even in the solution state and is not influenced by the crystal constraints. This concludes that binding of the UBA domain to the N-lobe is determined by the intrinsic nature of the hydrophobic interactions between the surfaces. The SAXS data also show that there is no major conformational rearrangement in the kinase in response to the pseudophosphorylation state of the activation loop.

The results reported from the SAXS experiment here are in contrast to the results obtained by Jaleel and coworkers (Jaleel et al., 2006). These authors used constructs of MARK2 and

MARK3 consisting of the kinase and the UBA domains which are similar in length to the constructs used in the study here (residues 39-364 of MARK2). These authors reported R_g value of 26.5 Å of the kinase in the non-phosphorylated state and R_g value of 22.7 Å upon phosphorylation by LKB1 complex. These results are interpreted as kinase molecule undergoing compaction by rearrangement of the UBA domain upon phosphorylation by LKB1 complex.

The R_g of the kinase measured from the non-phosphorylated state (26.5 Å) by these authors is compatible, neither with the R_g of the kinase calculated from the crystal structure (22.9 Å), nor with the R_g's calculated from the non-phosphorylated or the pseudophosphorylation state (both approximately 23Å), from the studies done here. The results obtained here also show that there is no compaction of the kinase on mimicking phosphorylation as interpreted by the Jaleel and co-workers. On the contrary, the R_g of the activated state of the kinase (22.7 Å) calculated by Jaleel and co-workers is in good agreement with the R_g of the MARK crystal structures. The reason for the discrepancy in the non-phosphorylated state is likely due to interference effects with the incrementing sample concentrations. MARK samples systematically gave a higher R_g (27 Å) at higher concentrations which indicates that the protein aggregates at higher concentrations. The R_g values calculated at lower concentrations from the studies here are always consistent with low R_g values and this value when extrapolated to infinite dilution gives scattering pattern fully compatible with the crystal structures.

Another reason for discrepancy in results could be due to MARK UBA model of Jaleel and co-workers. According to this model, the UBA domain is positioned at the bottom of the C-lobe, which is diametrically opposite to what is present in the crystal structure.

4.4 Kinase activity vs. UBA domain

Kinase activities were performed on different constructs of MARK to determine the influence of the UBA domain on activity. On comparing the kinase activities from various constructs, the results show that all constructs of MARK can be activated irrespective of the presence or absence of the UBA domain. Surprisingly, constructs with the UBA domain could not be activated to same extent as constructs without UBA domain. These results indicate that activation is not strongly pronounced in the presence of the UBA domain and that the presence of the UBA domain is actually inhibiting. These results once again are in contrast to the results of Jaleel and co-workers who reported that constructs with the UBA domain had enhanced kinase activity compared to constructs without the UBA domain. The reasons for the discrepancy are not understood as the constructs here and in the study of Jaleel and co-

workers are of similar length. The constructs used here were also tested for activation using LKB1 complex and AMARA peptide, which gave similar results to activation with MARKK. Taken together, the results presented here are consistent, irrespective of the activating kinase.

4.5 Regulatory functions of the UBA domain

The solution scattering studies and the kinase activity results presented here are fully consistent with all the crystal structures of MARK despite the fact that these crystals are packed in completely different crystal lattices. The UBA binds to the N-lobe of the kinase due to its intrinsic properties rather then the crystal constraints. Binding of the UBA domain masks the surface hydrophobic patches and increases the solubility of the protein. Disturbing the hydrophobic interactions or deleting the UBA domain has deleterious effects on the solubility of the protein. Thus the UBA domain plays an important role in maintaining the solubility status of the MARK kinases. Similarly, the UBA domain was shown to be important for MELK (Beullens et al., 2005) and other AMPK-related kinases (Jaleel et al., 2006).

The UBA domain binds at the distal side of the catalytic domain interacting with the N-lobe through hydrophobic contacts and to the C-lobe by a linker, enforcing an open, inactive conformation of the catalytic domain, similar to the SH3 domain and SH2-kinase linker (Young et al., 2001) of Src kinases. Tyrosine kinases of the Src family contain SH2 and SH3 domains (Src homology domains) at the N-terminus to the catalytic domain. These domains are responsible for binding of the Src kinases to proteins containing corresponding docking sites of phosphotyrosines and proline helices, respectively. The SH2 and SH3 domains also regulate the kinase activity. Src kinases like c-Src and Hck are regulated by phosphorylation of tyrosine residues in the activation segment (Tyr416 in chicken c-Src) and the C-terminal tail of the catalytic domain (Tyr527 in c-Src, (Schindler et al., 1999; Xu et al., 1999)). Phosphorylation of the Tyr of the activation loop is activating while phosphorylation at the tail inhibits the protein. The inhibitory effect depends on binding of the SH2 domain to the phosphotyrosine in the tail. This results in a clamped configuration of the kinase with the SH2 and SH3 domains tightly bound at the distal side of the catalytic domain (Fig. 4.3). The UBA domain is firmly attached to the N-lobe in MARK similar to the SH3 domain which attaches to N-lobe of Src. The SH2 and SH3 domains together form a rigid structure at the rear side of the catalytic domain which prevents breathing movements of the kinase that are required for substrate phosphorylation. The important structural element for this kind of inhibition is the linker between the SH2 and the SH3 domains which acts as a "snap lock" (Young et al., 2001). Extending the connector by addition of the glycine residues or

detachment of the SH3 domain by interaction with Nef a high-affinity ligand for SH3 (Moarefi et al., 1997), leads to activation.

The inhibitory mechanisms described for Src kinases, confirmed by extensive molecular dynamics calculations (Young et al., 2001), serves as a hypothetical illustration for the regulatory mechanism of MARK kinases by the UBA domain (Panneerselvam et al., 2006).

As shown in Figure 4.3, SH2 and SH3 domains form a solid structure that clamps Src kinase in open conformation. This solid structures acts as a lever arm to amplify the torque applied by the linker. In MARK, the corresponding linker is close to the hinge and thus the maximum torque exerted by MARK is comparatively lower than Src kinase. This explains the inhibitory effect of the UBA domain and lower activation of the constructs retaining the UBA domain.

Thus, the mechanism of kinase inhibition exemplified by Src kinases can also be relevant for MARK *in vivo*, where the kinase domain is complemented with other extra-catalytic domains and with upstream or downstream interaction partners, such as regulatory molecules binding to the UBA linker or to the CD domain; this could provide enough rigidity to the "connector" to efficiently suppress breathing movements of the kinase and thus, reduce kinase activity.

In conclusion, the comparison of the presently available MARK structures points to some regions of conformational variability which are likely to be important for the mechanism (catalytic loop, T-loop), regulation (helix C, G-loop), and interaction (helix G plug) of MARK. The most prominent feature, conserved in all MARK crystals structures till now is the UBA domain with its atypical fold (helix $\alpha 3$ inverted), which is tightly bound to the N-lobe and tethered through a extended linker to the C-lobe of the catalytic domain. This special configuration of the two domains suggests a role of the UBA domain in autoinhibition by restraining internal motions of the catalytic domain that may be required for enzymatic activity. Since the effects of the UBA domain on the *in vitro* kinase activities as here observed are rather weak, the UBA domain alone seems not sufficient for efficient down-regulation and may be assisted by regulatory binding partners of MARK *in vivo*.
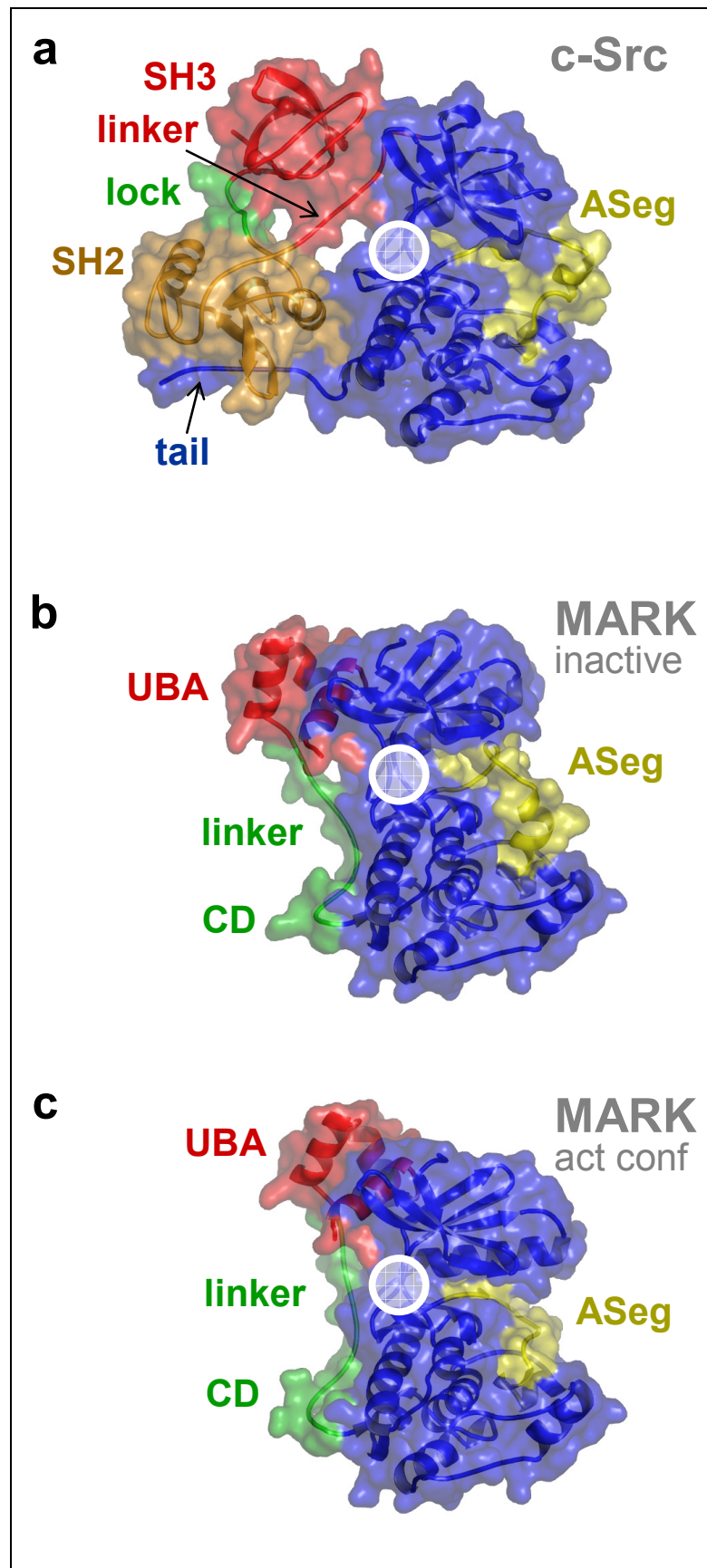
Figure 4.3: Inhibition by extra-catalytic domains in c-Src and MARK. Catalytic domains in blue with activation segments (A Seg) in yellow, hinge regions marked by white circles. All molecules are shown in the same orientation as determined by least squares fitting of helices E and F of the C-lobes. (a) Restrained (inactive) conformation of human c-Src (PDB-ID: 2SRC, (Xu et al., 1999)). The SH3 and SH2 domains of c-

Src are N-terminal to the catalytic domain. The SH3 domain and the linker between SH2 and catalytic domain bind together to the N-lobe and are shown in the same color (red). The SH2 domain binds to the tail of the catalytic domain via interaction with phosphotyrosine Tyr527. The connector between the SH3 and the SH2 domain ("lock", shown in green) is essential for inhibition of c-Src as it efficiently restricts breathing movements of the catalytic domain (Young et al., 2001). (b) MARK, represented by molecule E of the MARK1 crystal structure. (c) hypothetical active conformation of MARK, with activation segment and orientation of the N-lobe (and UBA domain) relative to the C-lobe modeled by comparison with Aurora-A, active conformation (PDB-ID: 1OL5; (Bayliss et al., 2003)). Rotation of the UBA domain in synchrony with the N-lobe is accomplished by unfolding the base of the linker (labeled "CD" in analogy to CD domains of MAP kinases; (Tanoue et al., 2000)). According to this model, efficient damping of the catalytic domain's breathing movements requires stabilization of the CD domain by binding of another interaction partner (Fig. 9 from Marx et al., 2006).

5 References

Angrand, P.O., Segura, I., Volkel, P., Ghidelli, S., Terry, R., Brajenovic, M., Vintersten, K., Klein, R., Superti-Furga, G., Drewes, G.*, et al.* (2006). Transgenic mouse proteomics identifies new 14-3-3-associated proteins involved in cytoskeletal rearrangements and cell signaling. Mol Cell Proteomics *5*, 2211-2227.

Bachmann, M., Hennemann, H., Xing, P.X., Hoffmann, I., and Moroy, T. (2004). The oncogenic serine/threonine kinase Pim-1 phosphorylates and inhibits the activity of Cdc25C-associated kinase 1 (C-TAK1): a novel role for Pim-1 at the G2/M cell cycle checkpoint. The Journal of biological chemistry *279*, 48319-48328.

Bachmann, M., Kosan, C., Xing, P.X., Montenarh, M., Hoffmann, I., and Moroy, T. (2006). The oncogenic serine/threonine kinase Pim-1 directly phosphorylates and activates the G2/M specific phosphatase Cdc25C. The international journal of biochemistry & cell biology *38*, 430-443.

Bayliss, R., Sardon, T., Vernos, I., and Conti, E. (2003). Structural basis of Aurora-A activation by TPX2 at the mitotic spindle. Mol Cell *12*, 851-862.

Beghini, A., Magnani, I., Roversi, G., Piepoli, T., Di Terlizzi, S., Moroni, R.F., Pollo, B., Fuhrman Conti, A.M., Cowell, J.K., Finocchiaro, G.*, et al.* (2003). The neural progenitor-restricted isoform of the MARK4 gene in 19q13.2 is upregulated in human gliomas and overexpressed in a subset of glioblastoma cell lines. Oncogene *22*, 2581-2591.

Benton, R., Palacios, I.M., and St Johnston, D. (2002). Drosophila 14-3-3/PAR-5 is an essential mediator of PAR-1 function in axis formation. Developmental cell *3*, 659-671.

Bertolaet, B.L., Clarke, D.J., Wolff, M., Watson, M.H., Henze, M., Divita, G., and Reed, S.I. (2001a). UBA domains mediate protein-protein interactions between two DNA damage-inducible proteins. Journal of molecular biology *313*, 955-963.

Bertolaet, B.L., Clarke, D.J., Wolff, M., Watson, M.H., Henze, M., Divita, G., and Reed, S.I. (2001b). UBA domains of DNA damage-inducible proteins interact with ubiquitin. Nature structural biology *8*, 417-422.

Bessone, S., Vidal, F., Le Bouc, Y., Epelbaum, J., Bluet-Pajot, M.T., and Darmon, M. (1999). EMK protein kinase-null mice: dwarfism and hypofertility associated with alterations in the somatotrope and prolactin pathways. Developmental biology *214*, 87-101.

Beullens, M., Vancauwenbergh, S., Morrice, N., Derua, R., Ceulemans, H., Waelkens, E., and Bollen, M. (2005). Substrate specificity and activity regulation of protein kinase MELK. The Journal of biological chemistry *280*, 40003-40011.

Biernat, J., Wu, Y.Z., Timm, T., Zheng-Fischhofer, Q., Mandelkow, E., Meijer, L., and Mandelkow, E.M. (2002). Protein kinase MARK/PAR-1 is required for neurite outgrowth and establishment of neuronal polarity. Molecular biology of the cell *13*, 4013-4028.

Bjorbaek, C., and Kahn, B.B. (2004). Leptin signaling in the central nervous system and the periphery. Recent progress in hormone research *59*, 305-331.

Bohm, H., Brinkmann, V., Drab, M., Henske, A., and Kurzchalia, T.V. (1997). Mammalian homologues of C. elegans PAR-1 are asymmetrically localized in epithelial cells and may influence their polarity. Curr Biol *7*, 603-606.

References

Bourenkov, G.P., and Popov, A.N. (2006). A quantitative approach to data-collection strategies. Acta crystallographica *62*, 58-64.

Bradford, M.M. (1976). A rapid and sensitive method for the quantitation of microgram quantities of protein utilizing the principle of protein-dye binding. Analytical biochemistry *72*, 248-254.

Brajenovic, M., Joberty, G., Kuster, B., Bouwmeester, T., and Drewes, G. (2004). Comprehensive proteomic analysis of human Par protein complexes reveals an interconnected protein network. The Journal of biological chemistry *279*, 12804-12811.

Brunger, A.T., Adams, P.D., Clore, G.M., DeLano, W.L., Gros, P., Grosse-Kunstleve, R.W., Jiang, J.S., Kuszewski, J., Nilges, M., Pannu, N.S.*, et al.* (1998). Crystallography & NMR system: A new software suite for macromolecular structure determination. Acta Crystallogr D Biol Crystallogr *54 (Pt 5)*, 905-921.

Chen, L., and Madura, K. (2002). Rad23 promotes the targeting of proteolytic substrates to the proteasome. Molecular and cellular biology *22*, 4902-4913.

Chen, Y.M., Wang, Q.J., Hu, H.S., Yu, P.C., Zhu, J., Drewes, G., Piwnica-Worms, H., and Luo, Z.G. (2006). Microtubule affinity-regulating kinase 2 functions downstream of the PAR-3/PAR-6/atypical PKC complex in regulating hippocampal neuronal polarity. Proceedings of the National Academy of Sciences of the United States of America *103*, 8534-8539.

Cohen, D., Brennwald, P.J., Rodriguez-Boulan, E., and Musch, A. (2004a). Mammalian PAR-1 determines epithelial lumen polarity by organizing the microtubule cytoskeleton. The Journal of cell biology *164*, 717-727.

Cohen, D., Rodriguez-Boulan, E., and Musch, A. (2004b). Par-1 promotes a hepatic mode of apical protein trafficking in MDCK cells. Proceedings of the National Academy of Sciences of the United States of America *101*, 13792-13797.

Cooper, D.R., Boczek, T., Grelewska, K., Pinkowska, M., Sikorska, M., Zawadzki, M., and Derewenda, Z. (2007). Protein crystallization by surface entropy reduction: optimization of the SER strategy. Acta crystallographica *63*, 636-645.

D. Svergun, C.B.a.M.H.J.K. (1995). CRYSOL - a program to evaluate X-ray solution scattering of biological macromolecules from atomic coordinates. Journal of Applied Crystallography *28*, 768-773.

Dale, S., Wilson, W.A., Edelman, A.M., and Hardie, D.G. (1995). Similar substrate recognition motifs for mammalian AMP-activated protein kinase, higher plant HMG-CoA reductase kinase-A, yeast SNF1, and mammalian calmodulin-dependent protein kinase I. FEBS letters *361*, 191-195.

de Leng, W.W., Jansen, M., Carvalho, R., Polak, M., Musler, A.R., Milne, A.N., Keller, J.J., Menko, F.H., de Rooij, F.W., Iacobuzio-Donahue, C.A.*, et al.* (2007). Genetic defects underlying Peutz-Jeghers syndrome (PJS) and exclusion of the polarity-associated MARK/Par1 gene family as potential PJS candidates. Clin Genet.

Dequiedt, F., Martin, M., Von Blume, J., Vertommen, D., Lecomte, E., Mari, N., Heinen, M.F., Bachmann, M., Twizere, J.C., Huang, M.C.*, et al.* (2006). New role for hPar-1 kinases

References

EMK and C-TAK1 in regulating localization and activity of class IIa histone deacetylases. Molecular and cellular biology *26*, 7086-7102.

Drewes, G. (2004). MARKing tau for tangles and toxicity. Trends in biochemical sciences *29*, 548-555.

Drewes, G., Ebneth, A., and Mandelkow, E.M. (1998). MAPs, MARKs and microtubule dynamics. Trends in biochemical sciences *23*, 307-311.

Drewes, G., Ebneth, A., Preuss, U., Mandelkow, E.M., and Mandelkow, E. (1997). MARK, a novel family of protein kinases that phosphorylate microtubule-associated proteins and trigger microtubule disruption. Cell *89*, 297-308.

Elbert, M., Cohen, D., and Musch, A. (2006). PAR1b promotes cell-cell adhesion and inhibits dishevelled-mediated transformation of Madin-Darby canine kidney cells. Molecular biology of the cell *17*, 3345-3355.

Elbert, M., Rossi, G., and Brennwald, P. (2005). The yeast par-1 homologs kin1 and kin2 show genetic and physical interactions with components of the exocytic machinery. Molecular biology of the cell *16*, 532-549.

Emsley, P., and Cowtan, K. (2004). Coot: model-building tools for molecular graphics. Acta Crystallogr D Biol Crystallogr *60*, 2126-2132.

Espinosa, L., and Navarro, E. (1998). Human serine/threonine protein kinase EMK1: genomic structure and cDNA cloning of isoforms produced by alternative splicing. Cytogenetics and cell genetics *81*, 278-282.

Garman, E.F., and Schneider, T.R. (1997). Macromolecular Cryocrystallography. In Journal of Applied Crystallography, pp. 211-237.

Goransson, O., Deak, M., Wullschleger, S., Morrice, N.A., Prescott, A.R., and Alessi, D.R. (2006). Regulation of the polarity kinases PAR-1/MARK by 14-3-3 interaction and phosphorylation. Journal of cell science *119*, 4059-4070.

Guo, S., and Kemphues, K.J. (1995). par-1, a gene required for establishing polarity in C. elegans embryos, encodes a putative Ser/Thr kinase that is asymmetrically distributed. Cell *81*, 611-620.

Guo, S., and Kemphues, K.J. (1996). A non-muscle myosin required for embryonic polarity in Caenorhabditis elegans. Nature *382*, 455-458.

Gustke, N., Steiner, B., Mandelkow, E.M., Biernat, J., Meyer, H.E., Goedert, M., and Mandelkow, E. (1992). The Alzheimer-like phosphorylation of tau protein reduces microtubule binding and involves Ser-Pro and Thr-Pro motifs. FEBS letters *307*, 199-205.

Gustke, N., Trinczek, B., Biernat, J., Mandelkow, E.M., and Mandelkow, E. (1994). Domains of tau protein and interactions with microtubules. Biochemistry *33*, 9511-9522.

Hooft, R.W., Vriend, G., Sander, C., and Abola, E.E. (1996). Errors in protein structures. Nature *381*, 272.

Hurov, J., and Piwnica-Worms, H. (2007). The Par-1/MARK family of protein kinases: from polarity to metabolism. Cell cycle (Georgetown, Tex *6*, 1966-1969.

References

Hurov, J.B., Huang, M., White, L.S., Lennerz, J., Choi, C.S., Cho, Y.R., Kim, H.J., Prior, J.L., Piwnica-Worms, D., Cantley, L.C.*, et al.* (2007). Loss of the Par-1b/MARK2 polarity kinase leads to increased metabolic rate, decreased adiposity, and insulin hypersensitivity in vivo. Proceedings of the National Academy of Sciences of the United States of America *104*, 5680-5685.

Hurov, J.B., Stappenbeck, T.S., Zmasek, C.M., White, L.S., Ranganath, S.H., Russell, J.H., Chan, A.C., Murphy, K.M., and Piwnica-Worms, H. (2001). Immune system dysfunction and autoimmune disease in mice lacking Emk (Par-1) protein kinase. Molecular and cellular biology *21*, 3206-3219.

Hurov, J.B., Watkins, J.L., and Piwnica-Worms, H. (2004). Atypical PKC phosphorylates PAR-1 kinases to regulate localization and activity. Curr Biol *14*, 736-741.

Illenberger, S., Zheng-Fischhofer, Q., Preuss, U., Stamer, K., Baumann, K., Trinczek, B., Biernat, J., Godemann, R., Mandelkow, E.M., and Mandelkow, E. (1998). The endogenous and cell cycle-dependent phosphorylation of tau protein in living cells: implications for Alzheimer's disease. Molecular biology of the cell *9*, 1495-1512.

Jaleel, M., Villa, F., Deak, M., Toth, R., Prescott, A.R., Van Aalten, D.M., and Alessi, D.R. (2006). The ubiquitin-associated domain of AMPK-related kinases regulates conformation and LKB1-mediated phosphorylation and activation. The Biochemical journal *394*, 545-555.

Jenne, D.E., Reimann, H., Nezu, J., Friedel, W., Loff, S., Jeschke, R., Muller, O., Back, W., and Zimmer, M. (1998). Peutz-Jeghers syndrome is caused by mutations in a novel serine threonine kinase. Nature genetics *18*, 38-43.

Johnson, G.V., and Stoothoff, W.H. (2004). Tau phosphorylation in neuronal cell function and dysfunction. J Cell Sci *117*, 5721-5729.

Kato, T., Satoh, S., Okabe, H., Kitahara, O., Ono, K., Kihara, C., Tanaka, T., Tsunoda, T., Yamaoka, Y., Nakamura, Y.*, et al.* (2001). Isolation of a novel human gene, MARKL1, homologous to MARK3 and its involvement in hepatocellular carcinogenesis. Neoplasia (New York, NY *3*, 4-9.

Kemphues, K.J., Priess, J.R., Morton, D.G., and Cheng, N.S. (1988). Identification of genes required for cytoplasmic localization in early C. elegans embryos. Cell *52*, 311-320.

Kosuga, S., Tashiro, E., Kajioka, T., Ueki, M., Shimizu, Y., and Imoto, M. (2005). GSK-3beta directly phosphorylates and activates MARK2/PAR-1. The Journal of biological chemistry *280*, 42715-42722.

Laemmli, U.K. (1970). Cleavage of structural proteins during the assembly of the head of bacteriophage T4. Nature *227*, 680-685.

Laskowski, R.A., MacArthur, M.W., Moss, D.S., and Thornton, J.M. (1993). PROCHECK: a program to check the stereochemical quality of protein structures. J Appl Crystallogr *26*, 283-291.

Lee, V.M., Goedert, M., and Trojanowski, J.Q. (2001). Neurodegenerative tauopathies. Annual review of neuroscience *24*, 1121-1159.

References

Levinson, N.M., Kuchment, O., Shen, K., Young, M.A., Koldobskiy, M., Karplus, M., Cole, P.A., and Kuriyan, J. (2006). A Src-like inactive conformation in the abl tyrosine kinase domain. PLoS biology *4*, e144.

Lizcano, J.M., Goransson, O., Toth, R., Deak, M., Morrice, N.A., Boudeau, J., Hawley, S.A., Udd, L., Makela, T.P., Hardie, D.G.*, et al.* (2004). LKB1 is a master kinase that activates 13 kinases of the AMPK subfamily, including MARK/PAR-1. The EMBO journal *23*, 833-843.

Mandelkow, E., Song, Y.H., Schweers, O., Marx, A., and Mandelkow, E.M. (1995). On the structure of microtubules, tau, and paired helical filaments. Neurobiol Aging *16*, 347-354.

Mandelkow, E.M., and Mandelkow, E. (1998). Tau in Alzheimer's disease. Trends in cell biology *8*, 425-427.

Mandelkow, E.M., Thies, E., Trinczek, B., Biernat, J., and Mandelkow, E. (2004). MARK/PAR1 kinase is a regulator of microtubule-dependent transport in axons. The Journal of cell biology *167*, 99-110.

Manning, G., Whyte, D.B., Martinez, R., Hunter, T., and Sudarsanam, S. (2002). The protein kinase complement of the human genome. Science (New York, NY *298*, 1912-1934.

Marx, A., Nugoor, C., Muller, J., Panneerselvam, S., Timm, T., Bilang, M., Mylonas, E., Svergun, D.I., Mandelkow, E.M., and Mandelkow, E. (2006). Structural variations in the catalytic and ubiquitin-associated domains of microtubule-associated protein/microtubule affinity regulating kinase (MARK) 1 and MARK2. The Journal of biological chemistry *281*, 27586-27599.

Matenia, D., Griesshaber, B., Li, X.Y., Thiessen, A., Johne, C., Jiao, J., Mandelkow, E., and Mandelkow, E.M. (2005). PAK5 kinase is an inhibitor of MARK/Par-1, which leads to stable microtubules and dynamic actin. Molecular biology of the cell *16*, 4410-4422.

Matsudaira, P.T., and Burgess, D.R. (1978). SDS microslab linear gradient polyacrylamide gel electrophoresis. Analytical biochemistry *87*, 386-396.

Moarefi, I., LaFevre-Bernt, M., Sicheri, F., Huse, M., Lee, C.H., Kuriyan, J., and Miller, W.T. (1997). Activation of the Src-family tyrosine kinase Hck by SH3 domain displacement. Nature *385*, 650-653.

Mueller-Dieckmann, J. (2006). The open-access high-throughput crystallization facility at EMBL Hamburg. Acta crystallographica *62*, 1446-1452.

Mueller, T.D., and Feigon, J. (2002). Solution structures of UBA domains reveal a conserved hydrophobic surface for protein-protein interactions. J Mol Biol *319*, 1243-1255.

Muller, J., Ory, S., Copeland, T., Piwnica-Worms, H., and Morrison, D.K. (2001). C-TAK1 regulates Ras signaling by phosphorylating the MAPK scaffold, KSR1. Molecular cell *8*, 983-993.

Muller, J., Ritt, D.A., Copeland, T.D., and Morrison, D.K. (2003). Functional analysis of C-TAK1 substrate binding and identification of PKP2 as a new C-TAK1 substrate. The EMBO journal *22*, 4431-4442.

Murphy, J.M., Korzhnev, D.M., Ceccarelli, D.F., Briant, D.J., Zarrine-Afsar, A., Sicheri, F., Kay, L.E., and Pawson, T. (2007). Conformational instability of the MARK3 UBA domain

References

compromises ubiquitin recognition and promotes interaction with the adjacent kinase domain. Proceedings of the National Academy of Sciences of the United States of America *104*, 14336-14341.

Murshudov, G.N., Vagin, A.A., and Dodson, E.J. (1997). Refinement of macromolecular structures by the maximum-likelihood method. Acta Crystallogr D Biol Crystallogr *53*, 240-255.

Nayak, V., Zhao, K., Wyce, A., Schwartz, M.F., Lo, W.S., Berger, S.L., and Marmorstein, R. (2006). Structure and dimerization of the kinase domain from yeast Snf1, a member of the Snf1/AMPK protein family. Structure *14*, 477-485.

Ohno, A., Jee, J., Fujiwara, K., Tenno, T., Goda, N., Tochio, H., Kobayashi, H., Hiroaki, H., and Shirakawa, M. (2005). Structure of the UBA domain of Dsk2p in complex with ubiquitin molecular determinants for ubiquitin recognition. Structure *13*, 521-532.

Ohno, S. (2001). Intercellular junctions and cellular polarity: the PAR-aPKC complex, a conserved core cassette playing fundamental roles in cell polarity. Current opinion in cell biology *13*, 641-648.

Ossipova, O., Dhawan, S., Sokol, S., and Green, J.B. (2005). Distinct PAR-1 proteins function in different branches of Wnt signaling during vertebrate development. Developmental cell *8*, 829-841.

Otwinowski, Z., Minor, W., and Charles W. Carter, Jr. (1997). [20] Processing of X-ray diffraction data collected in oscillation mode. In Methods in Enzymology (Academic Press), pp. 307-326.

Panneerselvam, S., Marx, A., Mandelkow, E.M., and Mandelkow, E. (2006). Structure of the catalytic and ubiquitin-associated domains of the protein kinase MARK/Par-1. Structure *14*, 173-183.

Pellettieri, J., and Seydoux, G. (2002). Anterior-posterior polarity in C. elegans and Drosophila--PARallels and differences. Science (New York, NY *298*, 1946-1950.

Peng, C.Y., Graves, P.R., Ogg, S., Thoma, R.S., Byrnes, M.J., 3rd, Wu, Z., Stephenson, M.T., and Piwnica-Worms, H. (1998). C-TAK1 protein kinase phosphorylates human Cdc25C on serine 216 and promotes 14-3-3 protein binding. Cell Growth Differ *9*, 197-208.

Raasi, S., Orlov, I., Fleming, K.G., and Pickart, C.M. (2004). Binding of polyubiquitin chains to ubiquitin-associated (UBA) domains of HHR23A. Journal of molecular biology *341*, 1367-1379.

Raasi, S., Varadan, R., Fushman, D., and Pickart, C.M. (2005). Diverse polyubiquitin interaction properties of ubiquitin-associated domains. Nature structural & molecular biology *12*, 708-714.

Riechmann, V., and Ephrussi, A. (2004). Par-1 regulates bicoid mRNA localisation by phosphorylating Exuperantia. Development (Cambridge, England) *131*, 5897-5907.

Rudolph, M.J., Amodeo, G.A., Bai, Y., and Tong, L. (2005). Crystal structure of the protein kinase domain of yeast AMP-activated protein kinase Snf1. Biochemical and biophysical research communications *337*, 1224-1228.

References

Saadat, I., Higashi, H., Obuse, C., Umeda, M., Murata-Kamiya, N., Saito, Y., Lu, H., Ohnishi, N., Azuma, T., Suzuki, A.*, et al.* (2007). Helicobacter pylori CagA targets PAR1/MARK kinase to disrupt epithelial cell polarity. Nature *447*, 330-333.

Sanger, F., Nicklen, S., and Coulson, A.R. (1977). DNA sequencing with chain-terminating inhibitors. Proceedings of the National Academy of Sciences of the United States of America *74*, 5463-5467.

Schaar, B.T., Kinoshita, K., and McConnell, S.K. (2004). Doublecortin microtubule affinity is regulated by a balance of kinase and phosphatase activity at the leading edge of migrating neurons. Neuron *41*, 203-213.

Schindler, T., Sicheri, F., Pico, A., Gazit, A., Levitzki, A., and Kuriyan, J. (1999). Crystal structure of Hck in complex with a Src family-selective tyrosine kinase inhibitor. Molecular cell *3*, 639-648.

Segu, L., Pascaud, A., Costet, P., Darmon, M., and Buhot, M.C. (2006). Impairment of spatial learning and memory in ELKL Motif Kinase1 (EMK1/MARK2) knockout mice. Neurobiology of aging.

Shulman, J.M., Benton, R., and St Johnston, D. (2000). The Drosophila homolog of C. elegans PAR-1 organizes the oocyte cytoskeleton and directs oskar mRNA localization to the posterior pole. Cell *101*, 377-388.

Storoni, L.C., McCoy, A.J., and Read, R.J. (2004). Likelihood-enhanced fast rotation functions. Acta crystallographica *60*, 432-438.

Studier, F.W., and Moffatt, B.A. (1986). Use of bacteriophage T7 RNA polymerase to direct selective high-level expression of cloned genes. Journal of molecular biology *189*, 113-130.

Sun, T.Q., Lu, B., Feng, J.J., Reinhard, C., Jan, Y.N., Fantl, W.J., and Williams, L.T. (2001). PAR-1 is a Dishevelled-associated kinase and a positive regulator of Wnt signalling. Nature cell biology *3*, 628-636.

Suzuki, A., Hirata, M., Kamimura, K., Maniwa, R., Yamanaka, T., Mizuno, K., Kishikawa, M., Hirose, H., Amano, Y., Izumi, N.*, et al.* (2004). aPKC acts upstream of PAR-1b in both the establishment and maintenance of mammalian epithelial polarity. Curr Biol *14*, 1425-1435.

Svergun, D.I., Barberato, C., and Koch, M.H.J. (1995). Crysol - a program to evaluate x-ray solution scattering of biological macromolecules from atomic coordinates. Journal of Applied Crystallography *28*, 768-773.

Tanoue, T., Adachi, M., Moriguchi, T., and Nishida, E. (2000). A conserved docking motif in MAP kinases common to substrates, activators and regulators. Nat Cell Biol *2*, 110-116.

Tanoue, T., and Nishida, E. (2003). Molecular recognitions in the MAP kinase cascades. Cell Signal *15*, 455-462.

Tassan, J.P., and Le Goff, X. (2004). An overview of the KIN1/PAR-1/MARK kinase family. Biology of the cell / under the auspices of the European Cell Biology Organization *96*, 193-199.

References

Terabayashi, T., Itoh, T.J., Yamaguchi, H., Yoshimura, Y., Funato, Y., Ohno, S., and Miki, H. (2007). Polarity-regulating kinase partitioning-defective 1/microtubule affinity-regulating kinase 2 negatively regulates development of dendrites on hippocampal neurons. J Neurosci *27*, 13098-13107.

Timm, T., Li, X.Y., Biernat, J., Jiao, J., Mandelkow, E., Vandekerckhove, J., and Mandelkow, E.M. (2003). MARKK, a Ste20-like kinase, activates the polarity-inducing kinase MARK/PAR-1. The EMBO journal *22*, 5090-5101.

Timm, T., Matenia, D., Li, X.Y., Griesshaber, B., and Mandelkow, E.M. (2006). Signaling from MARK to tau: regulation, cytoskeletal crosstalk, and pathological phosphorylation. Neuro-degenerative diseases *3*, 207-217.

Tochio, N., Koshiba, S., Kobayashi, N., Inoue, M., Yabuki, T., Aoki, M., Seki, E., Matsuda, T., Tomo, Y., Motoda, Y.*, et al.* (2006). Solution structure of the kinase-associated domain 1 of mouse microtubule-associated protein/microtubule affinity-regulating kinase 3. Protein Sci *15*, 2534-2543.

Towbin, H., Staehelin, T., and Gordon, J. (1979). Electrophoretic transfer of proteins from polyacrylamide gels to nitrocellulose sheets: procedure and some applications. Proceedings of the National Academy of Sciences of the United States of America *76*, 4350-4354.

Trinczek, B., Brajenovic, M., Ebneth, A., and Drewes, G. (2004). MARK4 is a novel microtubule-associated proteins/microtubule affinity-regulating kinase that binds to the cellular microtubule network and to centrosomes. The Journal of biological chemistry *279*, 5915-5923.

Uboha, N.V., Flajolet, M., Nairn, A.C., and Picciotto, M.R. (2007). A calcium- and calmodulin-dependent kinase Ialpha/microtubule affinity regulating kinase 2 signaling cascade mediates calcium-dependent neurite outgrowth. J Neurosci *27*, 4413-4423.

Vaccari, T., Rabouille, C., and Ephrussi, A. (2005). The Drosophila PAR-1 spacer domain is required for lateral membrane association and for polarization of follicular epithelial cells. Curr Biol *15*, 255-261.

Varadan, R., Assfalg, M., Raasi, S., Pickart, C., and Fushman, D. (2005). Structural determinants for selective recognition of a Lys48-linked polyubiquitin chain by a UBA domain. Molecular cell *18*, 687-698.

Xu, W., Doshi, A., Lei, M., Eck, M.J., and Harrison, S.C. (1999). Crystal structures of c-Src reveal features of its autoinhibitory mechanism. Molecular cell *3*, 629-638.

Young, M.A., Gonfloni, S., Superti-Furga, G., Roux, B., and Kuriyan, J. (2001). Dynamic coupling between the SH2 and SH3 domains of c-Src and Hck underlies their inactivation by C-terminal tyrosine phosphorylation. Cell *105*, 115-126.

6 Appendix

6.1 Abbreviations

(v/v)   Volume per volume

(w/v)   Weight per volume

Å   Angstrom (0.1 nm)

ADP   Adenosine- 5'- diphosphate

AI   Arabinose inducible

AIEX   Anion exchange chromatography

Amp   Ampicillin

APP   Amyloid precursor protein

ATP   Adenosine- 5'- triphosphate

A_x UV Absorbance at x nm

CaMKII   Calmodulin dependent protein kinases II

cAMP   3'5' cyclic Adenosine monophosphate

CCD   Charge coupled devise

CCP4   Collaborative computer project number 4

Cdc25C   Cell division cycle 25C

CHK1   Check point kinase 1

CD   Common docking domain

cDNA library   Complementary DNA library

CIEX   Cation exchange chromatography

C-TAK1   Cdc25C-associated kinase 1

DESY   Deutsches elektronen synchrotron

DNA   Deoxyribonucleic acid

DNTP   Deoxynucleotide triphosphate

DORIS   Double storage ring (Doppelring-Speicher)

DLS   Dynamic light scattering

DTT	Dithiothreitol
ECL	Electro chemical luminescence
EDTA	Ethylendiaminetetraacetate
EGTA	Ethylenglycol-bis-(2-aminoethylether)-N, N, N', N'-tetra acetic acid
EMBL	European molecular biology laboratory
EMK	ELKL motif kinase
GST	Glutathione-S-transferase
GSK-3	Glycogen synthatase kinase-3
HASYLAB	Hamburger sychrotron laboratory
HDAC	Class IIa histone deacetylases
HEPES	N-2-Hydroxyethyl-piperazine-N-2-ethanesulfonic acid
X his-tag	X x Histidine tag
IEX	Ion exchange chromatography
IMAC	Immobilized metal chelating chromatography
IPTG	Isopropyl-D-β-galactopyranoside
KA1	Kinase associated domain 1
Kan	Kanamycin
kDa	Kilodalton(s)
krpm	1000 revolutions per minute
KSR1	Kinase suppressor of ras 1
LB	Luria-bertani
MAP	Microtubule-associated protein
MARK	MAP/microtubule affinity regulating kinase
MARKK	MAP/microtubule affinity regulating kinase kinase
MIR	Multiple isomorphous replacement
MR	Molecular replacement
MPG	Max planck gesellschaft (Society)

Appendix

HHR23A	Human homologue of RAD23 A
MT	Microtubules
NCS	Non crystallographic symmetry
Ni-NTA	Nickel-nitrilotriacetic acid
NMR	Nuclear magnetic resonance spectroscopy
OD_x	Optical density at x nm
PCR	Polymerase chain reaction
PAGE	Polyacrylamide gel electrophoresis
PAK5	p21 activated kinase 5
PAR	Partitioning defective
PDB	Protein data bank
PEG	Polyethyleneglycol
PKA	Protein kinase A
PVDF	Poly vinylidene difluoride
PMSF	Phenylmethylsulfonylfluoride
RNA	Ribonucleid acid
SAXS	Small angle x-ray scattering
SDS	Sodium dodecyl sulphate
SH	Src homology domain
TCA	Trichloro acetic acid
TCEP	Tris (2-Carboxyethyl) phosphine hydrochloride
TE	Tris-EDTA
TEV	Tobacco etch virus
T_m	Melting temperature
Tris	Tris- (Hydroxylmethyl)-aminomethane
Tween 20	Polyoxyethylen-sorbitanmonolaurate 20
UBA	Ubiquitin-associated domain

Appendix

6.2 List of figures

6.3 Oligonucleotides

MARK1 Primers

hMARK1 wt _F (Primerwith TEV)

5'-CAT ATG GAA AAC CTG TAT TTT CAG GGC AAC TCC ATT ACG TCA GCA ACA GAT-3'

hMARK1 wt _R (CterPrimer)

5'-GGA TCC TTA   TTT TCT ACC TAG AAG AAT ATA AGT AGC CAT -3'

hMARK1 wt _F (Primer for MARK1 Kinase only)

5'-GGA TCC TTA ATC CGG ATC AGG CTC AGT ATA TG-3'

hMARK1 K89R_F

5'-GCT GAG TTT TGT CTA TTA TGC GCA CAG CAA CCT CTC TAC CAG -3'

hMARK1 K89R_F

5'-CTG GTA GAG AGG TTG CTG TGC GCA TAA TAG ACA AAA CTC AGC-3'

hMARK1 T215A S219A_F

5'-CAG CAT AGG GTG GCG CTC CAC AAA ACG CGT CCA ATT TGT T-3'

hMARK1 T215A S219A_R

5'-AAC AAA TTG GAC GCG TTT TGT GGA GCG CCA CCC TAT GCT G-3'

hMARK1 T215E_F

5'-AGG GTG GGC TTC CAC AAA ATT CGT CCA ATT TGT TCC CAA CTG TA-3'

hMARK1 T215E_R

5'-TAC AGT TGG GAA CAA ATT GGA CGA ATT TTG TGG AAG CCC ACC CT-3'

hMARK1 V86R_F

5'-TGT CTA TTA TTT TCA CAG CGC GCT CTC TAC CAG TTA GAA CGT G-3'

hMARK1 V86R_R

5'-CAC GTT CTA ACT GGT AGA GAG CGC GCT GTG AAA ATA ATA GAC A-3'

hMRK1I4G_ F

5'-GTG TCA TTG AAA TCC GGA CCA CCA CCA CCA TCA GGC TCA GTA TAT G-3'

hMRK1I4G_R

5'-CAT ATA CTG AGC CTG ATG GTG GTG GTG GTC CGG ATT TCA ATG ACA C-3'

hMRK1Fl_F

5'-CGT GTC CCG CTC GTT CAC CGT CGG CAA TGG CGT CCG GGC CGA CAT-3'

hMRK1Fl_CterHis

5'-CAT CAA AAA TAG CAA ATG AGC TTA AGC TCG AGC ACC A-3'

hMRK1_seq1

5'-CTG TGA AAA TAA TAG ACA AAA-3'

hMRK1_seq2

5'-GAA AGA GAA AGA GGC C-3'

hMRK1_seq3

5'-GAG TCT GGG CG TCA T-3'

hMRK1_seq4

5'-AGC CAT ATA CTG AGC CT -3'

MARK3 Primers

hMARK3 CD WT F

5'-CAT ATG GAA AAC CTG TAT TTT CAG GGC GCA GAT GAA CAA CCT CAC ATC GG-3'

hMARK3 CD WT R

5'-GCC GGA TCC TTA TTT TCT CCC CAA -3'

hMARK3CD 47-370 F

5'-GTT AGC AGC CGG ATC CTT ACT CGC TGC TTT TTC TCC CCA ATA AC-3'

hMARK3CD 47-370 R

5'-GTT ATT GGG GAG AAA AAG CAG CGA GTA AGG ATC CGG CTG CTA AC-3'

hMARK3CD K85R F (NS3)

5'-CAA TTA TTT TTA TTG CAA CCT CTC TGC CTG CAA TTA TTT TTA TTG CAA CCT CTC TGC CTG-3'

hMARK3CD K85R R (NS4)

5'-CAG GCA GAG AGG TTG CAA TAA AAA TAA TTG CAG GCA GAG AGG TTG CAA TAA AAA TAA TTG-3'

hMARK3 CD T90D F

5'-GAC TTG TTG GAT TCA ACT GGT CTT TGT CAA TTA TTT TTA TTG CAA CCT CTC TGC C-3'

hMARK3 CD T90D R

5'-GGC AGA GAG GTT GCA ATA AAA ATA ATT GAC AAA GAC CAG TTG AAT CCA ACA AGT C-3'

hMARK3 CD T90A F

5'-GAC TTG TTG GAT TCA ACT GCG CTT TGT CAA TTA TTT TTA TTG CAA CCT CTC TG-3'

hMARK3 CD T90A R

5'-CAG AGA GGT TGC AAT AAA AAT AAT TGA CAA AGC GCA GTT GAA TCC AAC AAG TC-3'

hMARK3 CD T211, S215A F (NS5)

5'-GCG TAT GGA GGA GCG CCA CAA AAC GCG TCA AGC TTA CCG C-3'

hMARK3 CD T211,S215A R (NS6)

5'-GCG GTA AGC TTG ACG CGT TTT GTG GCG CTC CTC CAT ACG C-3'

hMARK3 CD T211, S215A C213A F

5'-GCG TAT GGA GGA CTG CCA CAA AAC GTG TCG AGT TTA CCG CC-3'

hMARK3 CD T211, S215A C213A R

5'-GGC GGT AAA CTC GAC ACG TTT TGT GGC AGT CCT CCA TAC GC-3'

hMARK3 CD T211E F (NS9)

5'-CTG TTG GCG GTA AGC TTG ACG AGT TTT GTG GCA GTC C-3'

hMARK3 CD T211E R (NS10)

5'-GGA CTG CCA CAA AAC TCG TCA AGC TTA CCG CCA ACA G-3'

hMARK3 CD K351,353A F

5'-GTG ATT TCA TCG TAC GCC ATC GCA CTA AGA GAT TCT TGA ATT TCT TC-3'

hMARK3 CD K351,353A R

5'-GAA GAA ATT CAA GAA TCT CTT AGT GCG ATG GCG TAC GAT GAA ATC AC -3'

hMARK3 Y354A F

5'-GTA GCT GTG ATT TCA TCG GCT TTC ATC TTA CTA AGA GAT TCT TG-3'

hMARK3 Y354A R

5'-CAA GAA TCT CTT AGT AAG ATG AAA GCC GAT GAA ATC ACA GCT AC-3'

hMARK3 CD ONLY F

5'-CGG GCT TTG TTA GCA GCC GGA TCC TTA CCT GTC CTT CAT GAT TTG CTC TAG AGT GCC -3'

hMARK3 CD ONLY F

5'-GGC ACT CTA GAG CAA ATC ATG AAG GAC AGG TAA GGA TCC GGC TGC TAA CAA AGC CCG -3'

6.4 Purification buffers

All Purification buffers were done in the absence of reducing agents. When used, the concentration was of β-Mercapitoethanol or DTT were 5-10 mM.

Cell lysis Buffer:

50 mM Hepes- NaOH pH 7.2 , 300 mM NaCl, 5% Glycerol

Ni-NTA Buffer A:

50 mM Hepes- NaOH pH 7.2 at RT, 300 mM NaCl, 5% Glycerol

Ni-NTA buffer B:

50 mM Hepes- NaOH pH 7.2 at RT, 300 mM NaCl, 1000 mM Imidazole, 5% Glycerol

Dialysis Buffer for TEV protease cleavage:

50 mM Hepes- NaOH pH 7.2 at RT, 250 mM NaCl,5% Glycerol, 1 mM EGTA,

5mM β-Mercapitoethanol

Dilution Buffer:

50 mM Hepes- NaOH pH 7.2 at RT, 5% Glycerol

MonoS buffer A:

50 mM Hepes- NaOH pH 7.2 at RT, 100 mM NaCl, 5% Glycerol

MonoS buffer B:

50 mM Hepes- NaOH pH 7.2 at RT, 1000 mM NaCl, 5% Glycerol

Gel filtration buffer:

50 mM Bis-TRIS SO_4 pH 6.5 at RT, 250 mM NaCl, 5% Glycerol or

50 mM Hepes pH 7.5 at RT, 250 mM NaCl, 5% Glycerol

6.5 PDB

The atomic co-ordinates are deposited with the following PDB IDs.

2HAK- Crystal structure of MARK1: wild type structure numbered according to MARK2.

3BH5- Crystal structure of MARK3: T11A, S215A, inactive double alanine mutant structure.

6.6 Acknowledgements

Chanakya Nugoor

European Molecular Biology Laboratory
Laboratoire Européen de Biologie Moléculaire
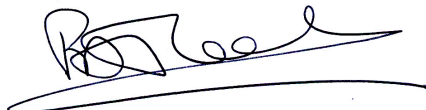**Europäisches Laboratorium für Molekularbiologie**

Dr. P.A. Tucker

EMBL

Hamburg 26th February 2008

To whom it may concern:

This letter is to certify that, as a native English speaker, I have read the Ph.D. thesis entitled **"Structural variations in catalytic and ubiquitin-associated domains of Human protein kinase MARK1 and MARK3"** This thesis is to be submitted to the University of Hamburg by Chanakya Nugoor.

Yours Sincerely,

Dr. P. A. Tucker (Group Leader)

c/o DESY   Notkestrasse 85
D22603 Hamburg   Germany
Telephone: (+49) 40 89902 0   (via exchange)
                    (+49) 40 89902 129   (direct)
Telex: 461613 (embl d)
Telefax: (+49) 40 89902 149
Network address: tucker@embl-hamburg.de